TAMPEREEN TEKNILLINEN YLIOPISTO
TAMPERE UNIVERSITY OF TECHNOLOGY

Suvi Santa-aho

Barkhausen Noise Method for Hardened Steel Surface Characterization – The Effect of Heat Treatments, Thermal Damages and Stresses

Julkaisu 1080 • Publication 1080

Tampere 2012

Tampereen teknillinen yliopisto. Julkaisu 1080
Tampere University of Technology. Publication 1080

Suvi Santa-aho

Barkhausen Noise Method for Hardened Steel Surface Characterization – The Effect of Heat Treatments, Thermal Damages and Stresses

Thesis for the degree of Doctor of Science in Technology to be presented with due permission for public examination and criticism in Festia Building, Auditorium Pieni Sali 1, at Tampere University of Technology, on the 9th of November 2012, at 12 noon.

Tampereen teknillinen yliopisto - Tampere University of Technology
Tampere 2012

ISBN 978-952-15-2926-9 (printed)
ISBN 978-952-15-2947-4 (PDF)
ISSN 1459-2045

ABSTRACT

This work concentrates on the non-destructive magnetic Barkhausen noise (BN) method. The BN method can be utilized in the detection of altered material properties such as changes in microstructure and stress. Method can be used e.g. in detection of grinding burns from hardened and ground gears. One challenge in the BN utilization is the lack of standardized quantification processes and varying guidelines for the use of the method.

One of the aims of this study was to manufacture calibration samples for BN device to be used in quality control. The calibration samples must be characterized properly (microstructure, residual stress, surface condition) in order to use them. Then, the calibration samples can be used directly to verify the readings of the measurement device. In addition, these samples allow a more thorough analysis of the BN signal. The verification of the Barkhausen noise readings will give more confidence to the quality control. Two possible methods, induction heating and laser processing were studied for creation of controlled thermal damages. Laser processing was found to be more suitable method for producing these controlled thermal damages.

One of the current topics of BN method development is its application to case-depth measurements of hardened components. The non-destructive detection of hardened layer thickness would be useful in detection of layer left for re-grinding and verification of case-depths of hardening heat treatments. This study presents also results of the utilization of commercial Rollscan equipment to case-depth analysis. Method presented here is based on magnetizing voltage sweeps generated from the hardened samples. Calculated slope from magnetizing voltage sweep and division of these measured slopes using varying frequencies can give information about the sample with composition gradients and microstructure gradients related to case-depth value.

The relation between BN and stress is not yet well understood. This study also concentrates on this part of BN phenomenon. Here elastic stress was applied to case-hardened steel samples to examine the effect of elastic stress to BN responses. The stress sensitivity was found to be different in test bars with different hardness values obtained with tempering. The results revealed a linear behaviour of the reciprocal RMS value as a function of the applied stress. The stress sensitivity of the RMS value was noticed to depend on the surface hardness of the specimen.

PREFACE

This work was carried out at the Department of Materials Science (DMS) of Tampere University of Technology (TUT) during the years 2008-2012. The research work presented in this thesis was started as a part of Academy of Finland funded research project INTELBARK and the research continued as TEKES funded research project NOVEBARK. Doctoral Programme of TUT's President, the Finnish Foundation for Technology Promotion (TES), Emil Aaltonen Foundation and Walter Ahlström Foundation are acknowledged for financial support.

First and foremost, I want to thank my supervisors Prof. Toivo Lepistö and Dr. Minnamari Vippola for the guidance, support, new ideas and comments on my work. I express my sincere gratitude to Dr. Mari Lindgren for the guidance thought out the years concerning Barkhausen noise. Both research projects were consortium projects with collaboration of Control Engineering Laboratory at University of Oulu and industrial partners Stresstech Oy, Moventas Wind Oy, Takoma Gears Oy and Katsa Oy. I want to thank the personnel of the project members for providing the opportunity to carry out the work and for all of the resources and comments during the projects. Especially M.Sc. Aki Sorsa from University of Oulu and Lasse Suominen, Juha Siiriäinen and Merja Hakanen from Stresstech Oy are thanked for the valuable support, collaboration and discussions. M.Sc. Jyrki Latokartano from Laboratory of Production Engineering, Tampere University of Technology is greatly acknowledged for the help with the laser processing. In addition, I want to thank my past and present colleagues at DMS and especially at the Laboratory of Materials Characterization. Foremost Dr. Mari Honkanen is thanked for advises and help with the microscopes and M.Sc. Matti Isakov is thanked for the comments and help with the mechanical testing. Thanks also go to the inspiring people around our coffee table and research assistants who helped with the specimen preparations.

Finally, I want to thank my dear Tuomo for all the encouragement, fruitful conversations and critical comments during the years. I wouldn't have been able to finish this thesis without your care and support. Also I want to thank all my friends and mother for support during the years.

Tampere, September 2012

Suvi Santa-aho

TABLE OF CONTENTS

LIST OF ORIGINAL PUBLICATIONS

This thesis is based on the original experimental work presented in detail in the following six publications. They are referred in the text as Publications I-VI.

I Suvi Santa-aho, Minnamari Vippola, Aki Sorsa, Kauko Leiviskä, Mari Lindgren, Toivo Lepistö, Utilization of Barkhausen noise magnetizing sweeps for case-depth detection from hardened steel, *NDT&E International*, 52 (2012) 95-102.

II Suvi Santa-aho, Minnamari Vippola, Aki Sorsa, Jyrki Latokartano, Mari Lindgren, Kauko Leiviskä, Toivo Lepistö, Development of Barkhausen noise calibration blocks for reliable grinding burn detection, *Journal of Materials Processing Technology*, 212(2) (2012) 408-416.

III Suvi Santa-aho, Minnamari Vippola, Aki Sorsa, Mari Lindgren, Jyrki Latokartano, Kauko Leiviskä, Toivo Lepistö, Optimized laser processing of calibration blocks for grinding burn detection with Barkhausen noise, *Journal of Materials Processing Technology*, 212(11) (2012) 2282-2293.

IV Aki Sorsa, Kauko Leiviskä, Suvi Santa-aho, Minnamari Vippola, Toivo Lepistö, A study on laser-processed grinding burn simulation and analysis based on Barkhausen noise measurement, *Insight*, 52(6) (2010) 293-297.

V Suvi Santa-aho, Minnamari Vippola, Toivo Lepistö, Mari Lindgren, Characterisation of case-hardened gear steel by multiparameter Barkhausen noise measurements, *Insight*, 51(4) (2009) 212-216.

VI Suvi Santa-aho, Minnamari Vippola, Tuomo Saarinen, Matti Isakov, Aki Sorsa, Mari Lindgren, Kauko Leiviskä, Toivo Lepistö, Barkhausen noise characterisation during elastic bending and tensile-compression loading of case-hardened and tempered samples, *Journal of Materials Science, 47 (2012) 6420-6428*.

AUTRHOR'S CONTRIBUTION

In the publications I-III and V-VI Suvi Santa-aho was the main researcher and author. She planned and organized the experiments, did the Barkhausen noise and XRD measurements and the sample preparation. In publication IV Suvi Santa-aho carried out the measurements and helped M.Sc. Aki Sorsa with the manuscript. The supervisors Prof. Toivo Lepistö and Dr. Minnamari Vippola, gave advises on the experimental part and commented the manuscripts I-VI. Dr. Mari Lindgren and Prof. Kauko Leiviskä commented the manuscripts for publications I-VI. M.Sc. Tuomo Saarinen and M.Sc. Matti Isakov gave advises and commented on the manuscript for publication VI. M.Sc. Matti Isakov helped with the loading tests for publication VI.

In the publications I-VI M.Sc. Aki Sorsa carried out the modelling and part of the data analysing together with Suvi Santa-aho.

Suvi Santa-aho carried out the microscope studies in publications II and V. Dr. Mari Honkanen carried out the FESEM microscope characterizations in publications III and VI.

M.Sc. Jyrki Latokartano carried out the laser processing experiments in publications II, III and IV, gave advises and commented the manuscript in publications II and III.

LIST OF SYMBOLS AND ABBREVIATIONS

BN	Barkhausen noise
CCD	Composite experimental design
CHD	Case hardness depth for carburized parts
DP	Dual-phase
EDM	Electric discharge machining
EN	European standard
Emf	Electromotive force
FESEM	Field emission scanning electron microscope
FWHM	Full width at half maximum value of peak in XRD and BN studies
FTT	Fast Fourier Transformation, Frequency spectra
HV_1	Vickers hardness measured with 1 kg load
LD	Loading direction (0°)
MAPS	Magnetic anisotropy and permeability system
MBN	Magnetic Barkhausen noise
MVS	Magnetizing voltage sweep
NDC	Non-destructive characterization
NDE	Non-destructive evaluation
NDT	Non-destructive testing
Nd:YAG	Yttrium aluminium garnet doped laser with neodymium ions
Nht	Case hardness depth for nitrided parts
OTM	Over-tempered martensite
PHD	Pulse height distribution
PM	Powder metallurgically manufactured sample
PSD	Power spectral density
Rht	Case hardness depth for induction hardened parts
RMS	Root mean square value calculated from the voltage of the BN signal
RS	Residual stress
SEM	Scanning electron microscope
SRS	Surface residual stress
TEM	Transmission electron microscope
TD	Transverse direction (90°)
VG	Vibratory ground
XRD	X-ray diffraction

A	Cross-sectional area of sample
$\mathbf{B}$	Magnetic flux density
$\mathbf{B_r}$	Remanence
C	Calibration coefficient in strain measurements
C_v	Calibration output voltage in strain measurements
$d\mathbf{B}/t$	The rate of change of the magnetic flux
d_{hkl}	Distance between hkl lattice planes
d	Lattice spacing in stressed specimen
d_0	Lattice spacing in stress-free calibration powder
E	Young's modulus
f	Frequency
F	Load
g	Gage factor

H	Magnetic field
$\mathbf{H_c}$	Coercivity
l	Penetration depth of magnetic field
m	Slope obtained from d vs. $\sin^2\psi$ curve
$\mathbf{M_s}$	Saturation magnetization
n	Integer constant (1,2..)
No	Number of BN events per magnetization cycle
R	Frequency ratio
R_a	Surface roughness
u	Measured voltage in strain measurements
$\mathbf{V_{pp}}$	Voltage from peak-to-peak
ε	Strain
ε	Epsilon carbide
θ	Bragg angle
λ	Magnetostriction coefficient
λ	Wavelength of the X-ray diffraction
μ	Permeability
μ_o	Permeability of vacuum
μ_r	Relative permeability
ν	Poisson's ratio
σ	Conductivity
σ	Stress
φ	Rotation angle in X-ray diffraction
χ	Susceptibility
ψ	Tilt angle, the angle between the normal of the sample and the normal of the diffracting plane

1. INTRODUCTION

Renewable energy sources have recently gained importance due to an increased energy consumption and the regulations for limiting greenhouse emissions. One of the most important sources of renewable energy is wind. More wind turbines are being built all over the world due to the booming wind energy markets and with increased investment support for renewable energy solutions. In other fields too, such as the transportation industry, the need to reduce energy and raw material consumption by improving the manufacturing process is recognised. Due to the increasing demands in the manufacturing industry, requirements for long-lasting and reliably working gear components have emerged. In order to produce reliable and functional gearing, for example for wind turbine and heavy industry applications, the requirements for the production and, especially, the quality control and non-destructive testing of parts are critical. One aspect of quality control in gears is to detect possible material defects arising from heat treatment, grinding, milling and turning. In wind turbine gear manufacturing, grinding burn and quench crack detection is important. The fabrication process may cause changes in material properties, such as microstructure and texture. In addition to this, residual stresses may be created within the material due to inhomogeneous plastic deformation or thermal gradients during manufacturing. Macroscopic residual stresses prevail in the work piece over at distance comparable to the component size while microscopic residual stresses occur on a smaller scale within and between different phases and grains around dislocation structures. Stresses may be beneficial or detrimental to the component depending upon the nature of the stresses, compressive or tensile.

Non-destructive evaluation (NDE) is performed to gain confidence in the structural integrity of components. A calibration procedure performed with a known reference or calibration block is normally required prior to non-destructive testing. However, if the measurement technique is rather new and has not been in use for long, then there is a lack of personnel qualification schemes or calibration standards. In these situations, the need to demonstrate both the accepted and rejected material status is relevant. Usually, some flawless calibration blocks are used but the signal should also be verified with rejection level pieces. Signal level detection also confirms the proper and functional usage of the measurement equipment itself. Furthermore, the degradation and wear of the sensor equipment can be estimated by comparing accepted and rejected signals.

One option for demonstrating the rejected status is to produce an inspection test piece which mimics the components in question and contains deliberately produced defects such as decreased surface hardness and internal stresses in the case of grinding burn detection. Usually industrial NDE inspections require a realistic test piece that is manufactured from the same material as that normally inspected and has the same geometry as the inspected part in order to perform the calibration in the same manner as the actual inspection.

This work concentrates on the non-destructive magnetic Barkhausen noise (BN) method. The BN method is utilized in the detection of altered material properties such as changes in microstructure and stress. The method is widely used for the detection of grinding burns in hardened and ground gears. The challenges for the utilization of this method include e.g. the lack of a standardized quantification process and varying user guidelines. This work tackles these challenges using several different approaches.

2. NON-DESTRUCTIVE EVALUATION

Non-destructive testing (NDT) or non-destructive evaluation (NDE) is characterized as the examination of an object with technology without affecting the future usefulness of the inspected component [1]. Usually the term NDT refers only to the actual test itself whereas NDE refers to the testing and the role of testing in the process [1]. One branch of NDT is the non-destructive characterization (NDC) methods that can be performed to investigate the properties of materials and their fitness for use in predictive maintenance procedures and process monitoring [2]. The main advantage of an NDT method compared with destructive detection methods, such as hardness testing and microscopy techniques, is that the tested component can be used after the NDT inspection. Generally, destructive testing such as mechanical testing and metallographic examination requires test samples to be taken from the production line and sectioned into suitable pieces. The results from these destructive tests are quantitative e.g. hardness values or tensile strengths, while non-destructive testing often provides qualitative information e.g. visualizing the flaw but not obtaining detailed dimensions or indications of the seriousness of the flaw.

The physical phenomena behind NDT inspection methods may vary from magnetism-based methods such as magnetic flux leakage measurement, magnetic particle inspection and Barkhausen noise (BN), to transmission of different signals including ultrasound, acoustic emission, thermography and X-rays. NDT measurements can be carried out, for example, in the quality control of components. In addition, NDT can be performed in failure analysis and in-situ measurements of installed components to ensure safe and efficient operation e.g. in power plants such as nuclear power plants. For all cases, prior to use inspection and in-situ inspection of structures, economic and safety issues dictate that possible flaws need to be detected at the earliest stage and in components prior to assembly. Therefore, various NDT methods are needed to provide a means to detect possible flaws.

NDT inspection can be carried out in various ways. The simplest way is to use the naked eye together with assisting tools. This visual inspection is the most common quality control method. Often the inspected component prescribes the proper method and procedure to be used [1]. Also the selection of the appropriate inspection method is determined by the type of flaws expected or the anticipated material property changes. For example, ferromagnetic materials can be inspected using magnetic methods. In addition, the feedback method depends on the selection of the potential technique; radiographic inspection supplies an image of the location and size of the flaw, whereas the magnetic Barkhausen noise method provides an electrical signal whose characteristics are related to the properties of the component. This signal can be used as such or processed and further analyzed. The processed data can be compared to the rejection limit and the acceptance of the component is based on the pre-adjusted rejection limit. One challenge related to NDT methods is the extent of the testing. Often the integrity of a component must be ensured with minimal inspection efforts with an acceptable risk level. After this, factors like cost effectiveness, speed of measurement, the sensitivity and robustness of the technique and equipment come into consideration. Sooner or later, the ultimate question needs to be stated: how to apply the feedback from the NDT method to the process. The operators of NDT techniques need to interpret large amounts of inspection data. Some automatic signal classification systems could be used to do this.

While comparing destructive and non-destructive measurements, the benefits of destructive measurements lie in the quantitative results. Non-destructive measurements usually give only qualitative results. One example of an NDT method supplying generally qualitative results is

Barkhausen noise. However, Barkhausen noise has huge potential in the field of NDT because it can notice changes in the properties of a component, in microstructural properties, as well as stress changes. On the other hand, the simultaneous dependence of BN on microstructure and stress render the interpretation of the signal challenging. As in other NDT methods, for the BN method, the competence and experience of the inspector are crucial in analysing the obtained data.

In order to develop non-destructive testing measurements in a more quantitative direction, test specimens with artificial well-defined defects must be developed. For example, in the use of the remote field testing method, artificial discontinuities in standard test blocks have been prepared in order to obtain accurate quantitative data from the measurements [3]. The recent studies concerning the BN method have also raised the question of modifying the method itself into a more quantitative NDT method with artificially produced flaws in the calibration procedure.

2.1. Material defect inspection

NDT techniques are used to locate flaws, to size them and to characterize material conditions such as the presence of tensile residual stresses in the material. Firstly, the defects need to be detected. Secondly, the dimensions can be determined and, finally, the evaluation of the defects, based on the acceptance criteria, must be performed [4]. Defects studied using NDT methods can be divided into different groups depending on the appearance of the flaw itself and on the location of the flaw with respect to the studied volume. Basically this means division into surface and volumetric flaws. Discontinuities such as surface cracks located on the surface and open to the surface of the inspected component can be detected by liquid penetrant inspection, eddy current inspection and magnetic particle inspection. On the other hand, volumetric flaws (voids, delamination, porosity, slag inclusions) located in the interior or volume of a material can be inspected by ultrasonic inspection, acoustic emission and radiography methods. Various near surface or subsurface flaws can be detected using the eddy current method and magnetic particle inspection to some depth from the surface [1, 4].

The NDC methods can be performed to investigate the properties of the materials [2]. These changes in the physical properties of the material can be detected among others by the eddy current measurement, ultrasonic inspection, X-ray diffraction and micro-magnetic analysis methods such as the magnetic Barkhausen noise (MBN) method [1, 4]. For example, the BN method can be used to detect a changed microstructural and stress state in a ferromagnetic material. The X-ray diffraction (XRD) method can be utilized to quantify and describe the residual stresses non-destructively from all crystalline materials. In the XRD method, the lattice spacing between the crystal lattices acts as a strain gauge changing its dimension depending on the stress. The stress can be determined via the measured strain in crystal lattice utilizing the elastic constants. A diffracted X-ray beam can be employed to study the shift in the position of the diffracted beam and also the broadening of the diffracted peak [5].

One example of the utilization of non-destructive characterization methods is the detection of grinding burns formed during grinding. This can be performed using the Barkhausen noise method [6, 7]. Usually high-performance gears are carburized case-hardened and tempered. After heat treatment, various manufacturing processes are utilized. Grinding removes the heat treatment distortion and ensures the attainment of the final tolerances [8]. The localized contact pressures between the abrasive grinding wheel and work piece, frictional heating, high sliding speed and the fact that most of the energy input is converted to heat, can generate high temperatures between the wheel and the work piece [9]. Grum [10] concluded the causes of the heat input due to the grinding conditions to be as follows: the contact surface between the grains

and the work piece increases due to the blunting of the grinding grains. This further causes increased mechanical effects and higher heat input in the surface layer of the ground piece [10]. The above mentioned deleterious conditions may generate a local degradation in material properties, which is known as grinding burn. Grinding burns reduce the wear resistance and the fatigue strength of the component. The component may then fail prematurely and unpredictably in service. Thus, grinding burns need to be detected during the quality control of the gear.

Thermal damage that occurs in grinding can be divided into several categories, such as: softening and the formation of temper burns, formation of rehardening burns, formation of unfavourable residual stresses and formation of grinding cracks [11]. If the surface temperature in grinding exceeds the original tempering temperature, it leads to thermal damage called temper burn. The temperature rise between the grinding wheel and the ground surface produces softening near the surface due to the coarsening of the carbide cementite (Fe_3C). The produced softened layer consisting of coarsened cementite is called over-tempered martensite (OTM) [11]. The degree of softening depends on the temperature and the time of the interaction. Softening occurs due to carbon diffusion within the surface layer. Higher temperatures or a longer time period cause more softening [12].

The thermal damage known as rehardening burn occurs when the temperature in grinding increases into the austenitizing temperature range [11]. A new layer of martensite is formed when the surface of the ground part is quenched by grinding coolant or cooled by the bulk material after the surface temperature during grinding exceeds the austenitizing temperature. This new, untempered, martensite layer is very brittle and hard [13].

In addition, if enough heat is generated in the grinding process, the temperature will also relax the compressive residual stresses achieved in the hardening process [13]. The primary origins of tensile residual grinding stresses are thermally-induced plastic deformation and thermal phase transformations. In these, due to a temperature rise and the heating and cooling cycles between the grinding wheel and the work piece, some expansion of the surface layer is relieved by plastic flow. Additionally, a volume decrease in the surface layer also induces tensile residual stresses [11, 14]. Also, the grinding parameters have an effect on the magnitude of the residual stresses besides the physical and mechanical properties of the material [15].

2.2. Calibration of non-destructive measurements

Calibration refers to actions that are accomplished in order to evaluate and adjust the precision and the accuracy of the measuring equipment [16]. The use of calibration processes and reference or master calibration samples ensures stable, consistent and reproducible measurements over time. These reference standards are created in order to establish a general level of uniformity in NDT measurements. The calibration of the NDT technique consists of the measurement equipment and validation of the test setup to the desired level of precision and accuracy. This procedure is done in order to validate the setup to provide similar results over time and to validate similar results produced with different measurement systems [16]. It has also been stated that the calibration procedure should be accomplished in conditions similar to those in which the actual measurements are performed. The ambient temperature conditions and surrounding conditions, for example at the factory, have an impact on measurements. The results may vary when the testing is performed by a different device or a different inspector. Hence, the information acquired by NDT inspection is only qualitative, as mentioned earlier.

For the NDT methods that are used for detecting surface or subsurface flaws, calibration procedures are often used to determine the size and location of the flaw. One example of this is ultrasonic inspection calibration with a certain calibration block. For inspection methods that produce qualitative results such as the BN method, the calibration itself is not as straightforward as with ultrasonic inspection. For ultrasonic inspection, several types of calibration or reference blocks manufactured from different materials exist. These test blocks are standardized, for example [17], the standard for calibration block No. 2 gives detailed knowledge about the manufacturing and utilization of the calibration block. The calibration blocks for ultrasonic inspection can be used for the calibration of the distance scale in the measurement, the sensitivity settings of the equipment, to evaluate the near surface resolution and to evaluate the flaw size and depth sensitivity of the equipment. In addition, calibration blocks exist with different step sizes for thickness measurement verification [18]. When comparing the measuring results with the reference test block, the irrelevant information can be found and ignored. In the calibration procedure, the information acquired in NDT measurement is compared with the information yielded on the reference specimen.

For the radiographic inspection of weldments, the system resolution calibration of the equipment can be performed with a step wedge manufactured from the same material as that tested in order to detect the contrast sensitivity. The wedge is produced with 100 %, 99 %, 98 % and 97 % of the thickest and thinnest sections to be inspected [19].

As mentioned above, it is generally known that almost all NDT inspections carried out are relative, not absolute measurements. Thus, the raw data that the NDT instruments provide cannot be utilized unless it is compared with a reference specimen with known properties. As with most NDT methods, the BN method also requires a calibration procedure. At the moment, the exact calibration procedure has not been determined for Barkhausen noise measurements. The inspectors at facilities utilizing the BN method perform the calibration procedure in different ways; usually adhering to the internal guidelines of the institution. One example of internal guidelines has been presented by Kvist and Lundin [20]. They [20] discussed the mastering and calibration procedure for the BN measurements of camshafts at the heavy engine manufacturer Scania. Scania has been using BN since the end of the 1990's in the quality control of the grinding process. Nowadays, BN measurement is performed in a fully automated production cell mainly for camshafts to detect local soft and thermally damaged areas generated in both case hardening and grinding. The lobes of the camshafts are inspected with four BN sensors at once and a total of 300 measuring points from each lobe are registered. They [20] found a certain rejection limit for the annealed camshaft, which corresponded to a hardness value of HRC 59. It was claimed that altogether the rejection limit and the studied shape of the measured curves gave good indications of the errors that had occurred in both the hardening and grinding processes [20]. The calibration was performed with the daily production master roller sample, which was verified from super master roller results. Both production and super master rollers were manufactured by cutting samples from a normal production camshaft and annealing them to the relevant hardness. The samples were located in one area of the annealing oven close to the oven wall in order to produce a local softer area due to increased temperature. This generated a higher BN value compared with the mean value of the roller. Thus, a BN curve produced from this sample created both the basic level and a higher BN output for sensor verification [20].

In addition, a special magnetic calibration coil can also be used in the calibration procedure of BN devices [21]. In this case, calibration is performed by introducing a special calibration coil into the BN sensor. During the calibration, a short electrical pulse, simulating the movement of domain walls, is supplied and this magnetic field induces an electrical voltage. By carrying out

calibration in this way, BN measurements conducted with different sensors may be compared and the magnetic field waveform on the surface of a specimen can be reconstructed [21].

The BN apparatus can also be calibrated in terms of stress with specially made samples. The samples are stress relieved and strained in tension and compression within elastic limits by using tensile testing equipment while simultaneously monitoring the strain and the BN signal. In this way calibration curves for the BN – stress relation can be obtained for various materials [22].

2.3. Artificial flaw manufacturing

One way to check the reliability of in-service NDT inspections is the production of artificial flaws that mimic the flaws to be detected. The artificial flaws are introduced to the reference specimen on purpose so their exact properties are known. Artificially produced flaws, should closely resemble the actual flaw. Such reference samples with artificially produced flaws for example in ultrasonic inspection, can be used to estimate the size of the flaws. In general, the artificial flaw reference samples should have equivalent physical and chemical properties to the inspected component [23].

The traditional way to produce an NDT calibration flaw is by machining e.g. drilling, milling, or electrical discharge machining, EDM. Artificial flaws can be manufactured also with grinding [24]. The grinding process may produce many types of defects and the control of the grinding process can be challenging. Therefore repeatable and controllable production of the flaws with grinding is difficult. Calibration of ultrasonic equipment can be carried out with a drilled piece of inspected material. The different diameters of the holes can be used to determine the flaw characteristics. However, it is stated [16] that most drilled holes produced in the ultrasonic reference blocks do not represent the actual flaws exactly because they are better sound reflectors with their flat and smooth edges than actual flaws. Therefore, these artificially produced holes may produce larger indications than a similar real flaw. On the other hand, the utilization of a calibration sample for BN inspection requires knowledge of the reference condition and the rejection limit. The rejection limit for defects can also be estimated from these calibration samples.

One common ultrasonic inspection target is the cracks in steel materials that are used in power plants. As a result, several studies by Kemppainen and Virkkunen [25, 26, 27] have been carried out to produce realistic cracks to imitate stress corrosion cracking for ultrasonic inspection. This need has grown because of NDT inspections that have found some atypical flaws in specific components. The crack production technique represented in [25, 26, 27] is reportedly capable of producing true cracks that are representative of service-induced cracks. The method for stress corrosion crack production involves thermal fatigue loading cycles for which different heating rates and cooling times were used. Results showed that the flaw location and size could be controlled accurately [25].

Artificial surface cracks have also been produced for the eddy current inspection procedure by Helifa *et al.* [28]. The EDM cracks were introduced with different crack widths of 0.14-0.35 mm on different steel materials up to a depth of 3 mm. Drill saw machining was used to introduce cracks with a depth greater than 3 mm [28].

2.3.1. Artificial thermal damage production by laser irradiation

In order to vary the sample surface stress state and microstructure, controlled heating should be performed. One method to produce controlled heating of metal surfaces is laser processing. As stated in the literature [29, 30, 31], it is possible to create artificial thermal damage with laser processing for non-destructive testing methods, which is why it is introduced here more comprehensively. Laser processing is based on the transformation of the optical energy of the electromagnetic radiation of the laser into thermal energy. The material absorbs part of the light of the irradiated laser beam and as a result, the temperature increases in the beam-material interaction volume [32]. Publications by Klocke and Gorgels, and Klocke *et al.* [29, 30] and Lomaev *et al.* [31] report the use of laser processing in order to produce test samples for non-destructive testing using BN. The study of Lomaev *et al.* [31] concentrated on the laser quench layers measured using the BN method to determine the quench layer thickness. Klocke and Gorgels [29] first compared two different methods to produce thermal damage: laser and grinding. Later on, they performed a study of the load-carrying capacity of rollers in which laser heating was performed to generate different degrees of thermal damage. Laser stripes were manufactured on the rollers with three different laser power values. The thermal damage was also analysed using BN prior to the actual load carrying tests and it was noticed that the relative magnetoelastic parameter increased to a certain point with increasing laser power. No further information about the other laser parameters or the equipment, laser interaction time and repeatability of the tests used were given [30].

Usually laser processing is used for hardening processes, but it can also be used for minor heat treating, such as surface tempering. Laser heating is followed by a rapid cooling as the heat produced in the surface is transported by thermal conduction to the deeper layers of the material. Different laser-processing parameters provide different peak temperatures on the surface of the treated part, which then have a different effect on the microstructure and the residual stress state of the processed sample. By using low laser power values, heat conduction is the predominant heat transport phenomenon. Wang *et al.* [33] stated that the surface temperature control of laser processing could be done by adjusting the laser parameters: the beam power, laser beam traverse rate and the diameter of the laser beam. Of course, the properties of laser-processed materials such as thermal conductivity, density, heat capacity and thermal diffusivity also affect heat conduction into the material. The reflectivity of machined metal surfaces is high, which means that little of the incident laser light is absorbed by the material. The laser-material interaction is influenced by many factors, some of which are briefly discussed below.

Absorptance, which refers to the fraction of incident laser light absorbed by a surface, is dependent on multiple factors. Several authors [34, 35] have reported that laser properties such as the wavelength and also the metal surface properties: temperature, roughness and oxide layers, have an effect on the absorptance of a surface to laser light [32, 34]. Kwon *et al.* [35] studied the effect of the absorptance of two different wavelength lasers at various temperatures on metal surfaces and noticed that a laser beam with a wavelength of 1.07 µm was absorbed better by polished metal surfaces than a laser beam with a wavelength of 10.6 µm. However, the elevation of the surface temperature increased the absorptance values for polished stainless steel samples only at high temperatures above 700 °C [35]. According to several authors [36, 37, 38], surface-oxidized metal surfaces have also been reported to have higher absorptance values. Oxide layers may produce multiple reflections of laser light. Surface contamination with higher absorptance can also produce different absorption behaviour than a plain metal surface [34].

One method for reducing the reflectivity of metal surfaces and gaining better absorptance is to coat the surface with a high absorption coating, such as a graphite coating [32]. Also other surface treatments such as roughening of the surface, e.g. by sand blasting or shot peening, can be performed to make the surface less reflective and to increase the absorption of the metal surface [38]. However, Kwon and Yoh [39] found that the steepness of the peaks and valleys and the spatial frequency of the peak-to-valley on the surface also have an effect, together with surface roughness, on the reflectance of the metal surface due to the multi-reflections. Bommi *et al*. [40] worked on the surface modification of the steel surfaces prior to laser hardening. They used sand blasted surfaces for laser hardening. Their results showed that in all studied laser scanning speeds, sand blasted surfaces had better properties than black painted surfaces.

Surface roughness, according to Murty [41], is defined as the deviation from the nominal surface texture that forms the surface pattern and irregularities in the surface texture that originate from processing. Surface roughness plays an important role because the peaks can consequently create multiple absorption transactions. Thus, a rough surface can increase absorption [32]. However, the surface roughness value itself can sometimes be misleading; surfaces with identical roughness values may have different frequencies of roughness peaks or different peak-to-valley lengths [32]. Therefore, the surface must be carefully characterized in order to make conclusions about it. For example Kwon and Yoh [39] noticed that a lapped metal surface with a smaller surface roughness value produced multi-reflections and increased absorption when compared to an electro-polished surface with a higher surface roughness value. This was due to the steeper peaks and valleys of the lapped surface. In addition, it can be concluded that the surface is optically smooth if the average surface roughness is smaller than the wavelength of the laser light [32]. However, mechanical surface finish processes such as grinding may produce surface directionality in the surface that influences the polarized reflectance of metals [39].

The repeatability of the laser processing method is good, as long as the laser absorption of the metal surface is constant. Therefore, a surface treatment that makes the surface even looking and less reflective is detrimental prior to laser processing. The treatment also needs to be reproducible. With proper selection of laser beam parameters, an adjustment can be made so that the maximum temperature is limited below the Ac1 temperature (referring to the temperature at which austenite begins to form on heating). This is done to avoid re-hardening of the sample surface if only restricted elevated temperatures are demanded for generating temper thermal damage.

2.4. Qualification of non-destructive measurements

Standardization refers to the unifying of modes of operation [42]. The standardization of NDT testing methods started in the 1950s with national standards. At the same time as the standardization of the NDT methods, attempts also began to create certification systems. Nowadays, national or international certification schemes exist for visual testing, radiography, ultrasonic methods, magnetic particle methods, penetrant methods, eddy current methods and leak detection [4].

Inspection qualification is usually used to verify the capability of NDT inspection to fulfill the expectation of locating flaws. This procedure is used e.g. in the nuclear industry [43]. The methodology of general NDT inspection guidelines [44] has been introduced to explain and guide how the inspection qualification needs to be carried out.

Usually, inspectors carrying out NDT inspection need a qualification which ensures that they have the competence to do the inspection. These personal schemes comprise both theoretical and practical work to test the inspector on different levels of certification [45]. In addition, while performing the inspection procedure, a written procedure for the particular method and component can also be made. Additionally, the auditing of NDT inspection in a company is one way to ensure confidence in the quality of NDT inspections [45]. The European Committee for Standardization has published a standard for the qualification of NDT tests applicable to all industries that carry out NDT [44]. This European standard (EN) methodology presents the NDT qualification phases from pre-NDT qualification to the implementation of qualified NDT. At the moment, for example, there is no code or standard or relevant personnel certification for Barkhausen noise inspection [46]. Also, most facilities that use BN in NDT inspection have their own regulations or guidelines for the inspections. Thus, the Barkhausen noise qualification procedure and guidelines for the measurement itself are under development in Europe [46]. The guidelines are being compiled by gathering existing knowledge from BN method users (what is tested, testing conditions, equipment and environmental conditions for tests) as well as from the testing device producers [46]. In addition to the guidelines of the measurement itself a protocol for calibration also needs to be established. Qualification procedures should also include flaw production techniques to produce representative defects. Thus, there is a need to develop a method for producing realistic and representative grinding burn marks that could be used in training NDT inspectors and also for the certification of the method.

3. BASIS OF THE MAGNETIC BARKHAUSEN NOISE METHOD

The Barkhausen noise (BN) method is a non-destructive inspection technique for ferromagnetic materials. In the BN method, the irreversible motion of the magnetic domain walls in ferromagnetic materials causes measurable changes in the magnetization values [47, 48]. A ferromagnetic material consists of small magnetic regions called domains. First introduced by Weiss in 1907, these are small areas in the crystal structure of a ferromagnetic material with uniformly oriented magnetic moments in the unmagnetized state. In each domain, the magnetic moments tend to align along certain crystallographic axes called the easy axis. Transition layers, referred to as the domain walls, exist between the magnetic domains where the magnetic moments undergo a reorientation and this layer separates adjacent domains [47]. For iron-based alloys, the domain walls can be separated into 180° walls and 90° domain walls [49, 50]. These two kinds of domain walls are presented in Fig. 1.

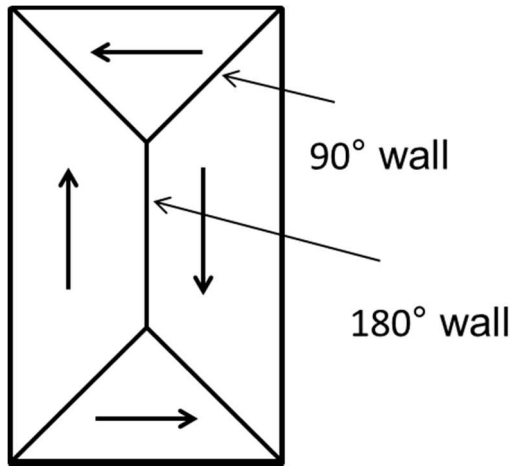

Figure 1. *Diagram showing examples of 90° domain wall and 180° domain wall.*

The magnetization of a piece of iron is a process in which the domains are rearranged and reoriented. The result of the magnetization process is a hysteresis curve produced by alternating the applied magnetic field **H** from negative to positive field strength whilst measuring the magnetic flux density **B**. Examples of hysteresis curves are presented in Fig. 2. A slow increase in the magnetic field applied to a ferromagnetic material will cause the material to become magnetized in a series of small steps as illustrated in Fig. 2 a). During the magnetization process, the domain walls move in the material discontinuously and this leads to discrete changes in magnetization that can be detected. These discontinuous changes in the magnetic flux density **B** are known as the Barkhausen effect, as the applied magnetic field is changed continuously [47].

Fig. 2 a) introduces the different changes that occur during the magnetization process for a soft magnetic material. The movement of domain walls is reversible when the applied magnetic field is small. With a small applied field, the domains oriented along the magnetic field can grow at the expense of non-optimally oriented domains by the motion of the domain walls. In order to move a domain wall, the domain located on one side of the wall has to expand in size while the other domain on the opposite side of the domain wall has to shrink. The result of this domain wall motion is a change in the overall magnetization of the sample. When the small field is returned to zero, the domains can return to their original position. For larger applied magnetic fields, the domain movement becomes irreversible. Domain rotation can take place if the magnetic field is further increased. At the saturation magnetization $\mathbf{M_s}$ state only one large domain exists with magnetic moments aligned in parallel. $\mathbf{M_s}$ is also the maximum magnetization achieved by the applied magnetic field. Remanence $\mathbf{B_r}$ is the magnetization observed from a fully magnetized sample at a zero applied magnetic field, as shown in Fig. 2 b). Coercivity is defined as the reverse field $\mathbf{H_c}$ which is the field required to reduce the magnetization to zero after the sample has been fully magnetized [48].

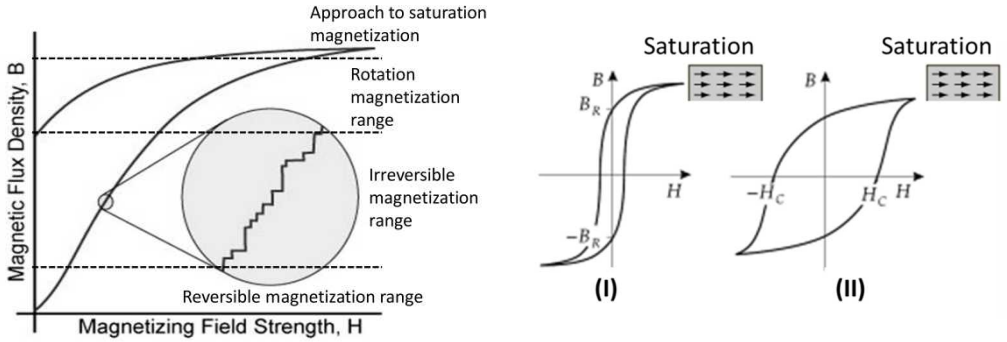

a) b)

Figure 2. *a) Hysteresis curve with large magnification produced by alternating the applied magnetic field **H** as a function of magnetic flux density **B** [51]. b) Hysteresis curve [modified from 52] for magnetically soft (I) and magnetically hard material (II).*

From the hysteresis curve presented in Fig. 2 b); a few basic quantities can be introduced. The response of a material to the applied magnetic field strength **H** can be determined by two quantities; susceptibility χ and permeability μ. Susceptibility χ expresses the response of a material to the applied magnetic field. Susceptibility is defined as the ratio of the magnetization **M** and the magnetic field strength **H**. It is given by equation (1)

$$\chi = \frac{\mathbf{M}}{\mathbf{H}} \quad (1)$$

As magnetic field strength **H** is applied to a medium, a magnetic flux density is introduced within this medium. Magnetic flux density **B** is given by

$$\mathbf{B} = \mu_0(\mathbf{H} + \mathbf{M}) \quad (2)$$

where μ_0 is the permeability in a vacuum, **H** is the magnetic field strength representing the externally applied field and magnetization **M** describes the ability of the material to be magnetized. Magnetization **M** is defined as the magnetic moment per unit volume. The unit for **B** is tesla, and for **H** and **M** the unit is A/m.

Permeability μ is defined as the ratio of the magnetic flux density **B** to the applied magnetic field strength **H**. It is defined as the capability of the material to conduct magnetic flux and is given by

$$\mu = \frac{\mathbf{B}}{\mathbf{H}} \quad (3)$$

The different permeabilities are related to relative permeability μ_r which is given by

$$\mu = \mu_0(\chi+1) = \mu_0\mu_r \quad (4)$$

In a vacuum the magnetization **M** is zero and the relative permeability μ_r is one, thus the equation (2) can be rewritten as equation (3) in a vacuum.

The electromotive force (emf) induced in a BN pick-up coil is proportional to the rate of change of the magnetic flux **B** through the pick-up, d**B**/dt. This effect is strongest on the steepest part of the magnetization curve, the irreversible magnetization range [53].

The magnetic hysteresis loop parameters such as coercivity $\mathbf{H}_c$ and remanence $\mathbf{B}_r$ can also be used to characterize the ferromagnetic material because they are reported to be structure sensitive [54]. In the literature, coercivity is typically related to hardness [55, 56]. Coercivity is used to distinguish hard and soft magnetic materials [54] as shown in Fig. 2 b). In addition, the coercive field has been observed to have a linear relationship to stress [57]. Many studies [58, 59, 60] have found that coercivity and permeability show changes as the case-depth of hardened samples change because the surface layer and the bulk have different magnetic properties. Jiles [54] has reported a dependence of remanence on stress. Some controversial observations have been noted, e.g. Makar *et al.* [57] observed that remanence shows a non-linear and monotonic behaviour as a function of stress.

Barkhausen noise measurement system

BN measurement is performed by creating a changing controlled magnetic field with a magnetizing yoke that is fed with an alternating current and recording of the magnetic flux changes in the studied material with an electromagnetic probe or a pick-up coil. The obtained signal can be amplified, recorded and processed by computer-aided software. Both laboratory-made BN equipment [61, 62, 63, 64, 65] and commercial BN equipment systems [20, 61, 66, 67, 68] have been used in the BN studies. One example of a commercial BN sensor is presented in Fig. 3 a) and a schematic example of external coil BN equipment is shown in Fig. 3 b). Grum

and Pecnik [69] concentrated on comparing different BN units, both compact sensors (internal coil and integrated internal coil) and a sensor unit with an external detection coil on cold-rolled specimens. They concluded that the signals captured with a compact sensor provided more reliable BN signals than those with an external coil, due to better contact with the sample surface, providing a smaller air gap and a better geometrical relationship between the magnetic yoke and the internal detection coil [69].

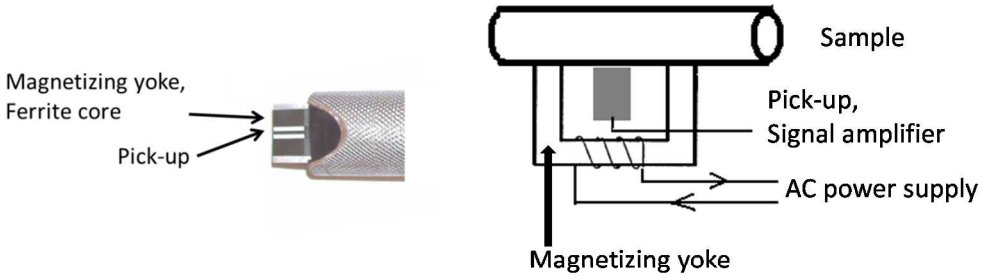

a) b)

Figure 3. *a) Example of a commercial BN coil. b) Schematic presentation of external detection coil BN measurements.*

The BN signal measurement depth depends on the frequency used and the permeability and conductivity of the tested material [53]. The adjustment of the magnetizing and analysing frequency can be used to vary the depth from which the BN signal information comes. To study only the surface layer of the component, high frequencies are utilized. One example of the high frequency BN method is the detection of grinding burns from hardened and ground components [7]. With high frequency BN measurements, the analysing frequency range from 20 to 1000 kHz can be used to study depths between 150 to 20 µm below the surface in a case carburized steel [70]. Usually low frequency measurements are described as having a magnetizing excitation frequency of less than 1 Hz [61]. The typical signal analysing frequency range is 0.1-100 kHz for low frequency measurements [61]. The 1 kHz analysing frequency was reported to have a skin-depth value of 635 µm [61].

By utilizing a low magnetization frequency in BN measurement, the penetration of the magnetic field into the specimen can be increased. The BN measurement depth, related closely to the penetration depth of eddy current measurements, can be calculated from the following equation [71]

$$l = \sqrt{\frac{1}{\pi \mu \sigma f}} \tag{5}$$

where l is penetration depth, µ is permeability of material, σ is conductivity of the material and f is the frequency of the BN signal. The problem in the low frequency BN studies is that the BN signal is attenuated exponentially as a function of the distance travelled inside the material due to the eddy current damping that depends on the frequency of the magnetized signal [61, 72]. In addition, measurement sensor properties such as distance between the magnetizing pole pieces and the sensitivity of the coil, will affect the low-frequency BN measurement depth estimations [61].

One example of a typical Barkhausen noise signal is shown in Fig. 4. The BN signal consists of a collection of voltage pulses of varying amplitude. Two BN bursts are formed during an increasing and decreasing magnetization cycle. The signal observed is affected by various BN events, their magnitude and duration. Different features are calculated from the BN signal. The most typical parameter calculated from the signal is the root mean square (RMS) value of the voltage signal, which is given by

$$RMS = \sqrt{\frac{1}{n}\sum_{i=1}^{n} x_i^2} \tag{6}$$

The RMS value gives information about the maximum Barkhausen activity. A reduced RMS value is typically formed when pinning of the domain walls slows down the moving domain walls in a high hardness material or when domain walls move under compressive stress. Lattice defects such as dislocations, precipitates and grain boundaries hinder the domain wall movement and decrease the RMS value. High hardness is an indication of high pinning sites and cause a lower RMS value. A BN burst for one half of the magnetization cycle can also be plotted as a function of time or magnetic field strength as shown in Fig. 4 b). The envelope profile that is created provides information about the BN peak height, peak position and the full width half maximum (FWHM) value of the burst. The envelope has been used in calculating various features [70, 73, 74]. Table 1. summarizes the behaviour of the different BN envelope features reported in the literature.

As mentioned above, the height and position of the peak can be used to evaluate the material properties. The BN peak height has been reported to decrease with increasing hardness [55, 75]. In addition, over-tempering has been shown to increase the peak height of hardened samples [70]. Nevertheless, it has been claimed that the peak or peak height conveys the same information as the RMS value [55, 76]. The peak position moves to higher magnetic field strengths with high hardness samples because a higher magnetic field is required to detach the domain walls from the pinning sites [75]. In the case of over-tempering [70], the peak position was observed to move to lower magnetic field strengths. Also, pulse height distribution is one way to describe a BN signal [50]. The voltage signal consists of different voltage pulses that have varying amplitude. This describes the magnetization process and the magnetic behaviour of the studied piece. Magnetic Barkhausen noise energy, MBN energy, is also used, referring to the area of the squared voltage pulse [77].

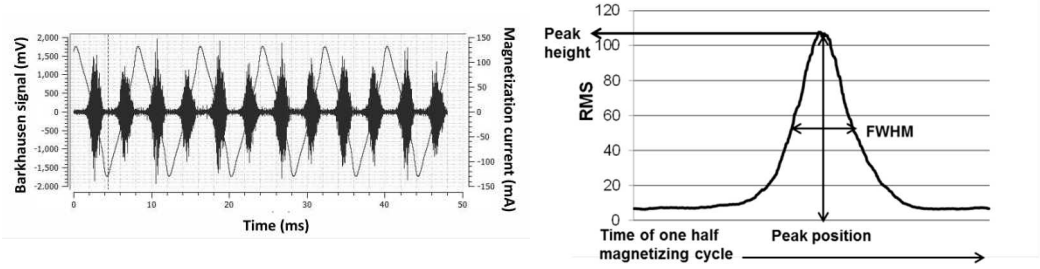

a) b)

Figure 4. *a) Typical Barkhausen noise signal. b) Barkhausen noise envelope profile showing parameters; peak height, peak position and full width half maximum values.*

Table 1. Typical BN envelope features used in BN studies.

Envelope feature	Effect/Behaviour/dependence on	Sensitive to	Refs.
RMS, BN activity, Vrms (Average of BN activity), RMS voltage	Decrease with increasing hardness	-Number of pinning sites (dislocation density) - Microstructure	Cullity1972 [53], Mitra *et al.* 1995 [78]
	Increase with tensile stress in the measurement direction parallel to load direction in steels with positive magnetostriction	Stress	Cullity1972 [53]
MBN energy, BN energy	Similar to RMS	Similar to RMS	Stefanita *et al.* 2000 [77], Kim *et al.* 1992 [79]
1/MBN(RMS)	Linear relationship between hardness	Number of pinning sites (e.g. dislocation density)	O'Sullivan *et al.* 2004 [56]
1/RMS	Linear relationship between stress	Stress	Mierzcak *et al.* 2011 [65], Gariketapati et al. 1988 [80]
Peak height, peak (referring to maximum value of the running average of signal)	Decrease with increasing hardness	-Number of pinning sites (e.g. dislocation density) - Number of domain walls moving -The mean free path of domain wall displacement	Moorthy *et al.* 1997 [75], Davut and Gür 2007, Moorthy *et al.* 1998 [81]
	Increase with tensile stress in the measurement direction parallel to load direction in steels with positive magnetostriction	Stress	Stewart *et al.* 2004 [74]
Vm, maximum amplitude	Increase with increasing austempering time	- Microstructure, varies with heat treatment parameters	D'Amato *et al.* 2003 [82]
Peak position, the magnetizing current at which the peak value is achieved	High hardness moves peak position to larger magnetic field strengths	Sensitive to average pinning strength of given type of barriers	Moorthy *et al.* 1997 [75]
N_o, Number of BN events per magnetization cycle	N_o was compared to threshold voltage of BN measurement and showed different behaviour for base material and weld	Microstructure	Mitra *et al.* 1995 [78], Mitra *et al.* 1997 [83]
V_{pp}, peak-to-peak voltage, The difference between largest positive and negative voltage pulse during one magnetizing cycle	V_{pp} was found to be sensitive to creep assisted damages on Cr-Mo steel	-Indicative of BN signal strength generated during domain wall movement and the amplitude depends on distance between pinning sites or strength of pinning sites	Mitra *et al.* 1997 [83]
MBN_p, peak-to-peak voltage, R, frequency ratio	R= ratio of the MBN_p measured with two magnetizing frequencies	MBN_p was found to be sensitive to stress	Chen *et al.* 2011 [84]
BN count (each point above predicted threshold)	BN count was found to have a linear relationship with residual stresses	Residual stress	Vashista and Paul 2011 [85]
BN event (peaks of signal above predicted threshold)	BN event was found to have a linear relationship with residual stresses	Residual stress	Vashista and Paul 2011 [85]
PHD, Pulse height distribution	As-quenched martensite produced larger number of pulses compared to tempered martensite	Microstructure	Mitra *et al.* 1995 [78], Davut and Gür 2007 [55], Zhu *et al.* 2001 [86]
FTT, Frequency spectra	Used as an analysing algorithm for grain size estimation, ratio of two frequency components was noticed to estimate grain size [87]	High frequency components diminish as the correlation length increases (range of interaction of domain wall with pinning sites) [72], different pinning site density [86]	Zhu *et al.* 2001 [86], Yamaura *et al.* 2001 [87], Jiles 2000 [72], Zerovnik *et al.* 2010 [88]
PSD, power spectral density	Used as an analysing algorithm on high amplitude regime	High frequency components diminish as the correlation length increases (range of interaction of domain wall with pinning sites)	Zhu *et al.* 2001 [86], Jiles 2000 [72]
Amplitude spectrum area	Analysis done with certain frequency band	Stress, increasing compression stress reduces the area of amplitude spectrum	Desvaux *et al.* 2004 [89]

3.1. Factors influencing Barkhausen noise

Although it is generally known that BN is simultaneously influenced by both the microstructure of the material and the stress state, the relationship to both is still not completely understood and contradictory results exist. During external magnetization, the signal registered with a BN pick-up coil is influenced by the pinning of domain walls due to microstructural barriers. These hindrances slow down the velocity of the moving domain wall, shorten the mean free path and an increased magnetic field strength is required in order to overcome some of the obstacles. The further increased magnetic field strength causes the domain walls to be released abruptly and create voltage pulses. The interfaces that are present in the material, for example between the matrix and the precipitate or changes in the micro residual stress, limit the mean free path of the moving domain wall. This, in turn, has an influence on the Barkhausen noise. More hindrances to domain wall motion create a greater number of individual BN events, but they have been observed to have smaller amplitude [72]. When there are not many hindrances present and the resistance to the movement of the domain walls is small, a smaller number of BN events are observed [72] and the Barkhausen noise burst is obtained from lower magnetic field values. When the moving domain wall confronts many obstacles, i.e. the density of pinning sites is increased, the growing applied magnetic field will provide the energy for domain wall to go past the hindrances. In this situation, the Barkhausen noise burst is observed with higher magnetic field values.

Due to the different pinning power of the various obstacles, a BN signal distribution is created with changes in amplitude of the pulses, which is generally referred to as the pulse height distribution. The domain wall motion is influenced by the density of obstacles, such as dislocations. It is generally known that harder materials have a higher dislocation network and thus hardness has a major effect on the BN signal. The Barkhausen noise level continuously decreases in microstructures characterized by increasing hardness. The same microstructural properties that hinder the motion of the dislocations also affect the movement of the domain walls [53]. Furthermore, stress also changes the number of BN events and their relative magnitude [90].

Residual stress fields have an effect on the magnetic field that is needed to move and rotate the domains. If the tensile stress that the domains are experiencing is increased, an increase is also required in the magnetic field strength to make the domains move [48]. Cullity [53] roughly divided pinning sites into two categories; second-phase particles and residual microstresses, such as dislocations. Second-phase particles can be further classified as precipitates, inclusions or impurities that have different spontaneous magnetization than the surrounding material [53].

Residual microstresses also affect domain wall motion. Residual microstresses in a material consisting of only one-phase are caused by crystal imperfections like dislocations in the material. A local stress field emerges around the dislocations that produce inhomogeneous microstrains on the material. The higher the dislocation density in the material, the greater is the resistance to the movement of domain walls [91]. The stress-induced change in the BN signal can be understood from the basis of the changes in the magnetic domain wall configuration and the mobility of the domain walls. They also show that the BN phenomenon itself is complex and that interpretation of the results is challenging.

Next, the effect of stress on Barkhausen noise is discussed. Further on in the Chapter 3.1.2. , the relationship between BN and microstructure is introduced.

3.1.1. The effect of stress

The BN signal is affected by many microstructural features and also by applied or residual stress. The fundamentals of the relation between BN and stress are relatively well understood as illustrated in Fig. 5. Ferromagnetic materials experience the magnetostriction phenomenon depending on the magnetic field and stress state. For ferromagnetic materials, such as steels and cobalt, which have a positive magnetostriction coefficient λ, the BN signal shows an increasing trend in the direction of the applied elastic tensile stress. On the other hand, an applied elastic compressive stress will decrease the magnetization in materials with positive magnetostriction. Materials with negative magnetostriction coefficient show the reverse effect [53].

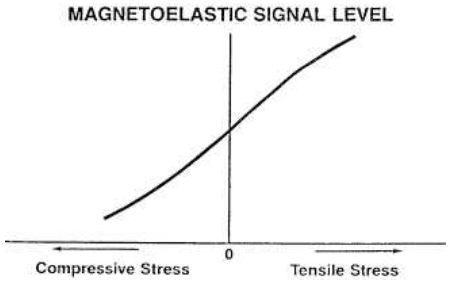

Figure 5. *Barkhausen noise response to tensile and compressive stress [22].*

When a load is exerted on a ferromagnetic piece of steel, it becomes slightly magnetic in the direction of the loading. Without loading, a ferromagnetic material with positive magnetostriction elongates towards the magnetization direction in order to minimize magnetoelastic energy [50]. This kind of behaviour is observed in iron and cobalt, whereas nickel, which has a negative magnetostriction coefficient, will experience the opposite behaviour. Due to these different interactions between magnetostriction, magnetization and stress, the behaviour of a ferromagnetic material under stress is not easily described [53].

It is generally known that the stress response of a material to BN measurements is determined by the microstructure of the ferromagnetic steel. The composition and heat treatment have an effect on the observed BN-stress sensitivity [90, 92, 93]. Usually mild steel specimens have been used when studying the effect of applied loading on the BN phenomenon [50, 77, 94, 95]. However, in some studies hardened (and tempered) steel grades have also been tested [93, 96, 97, 98]. Usually the hardened steel grades are more difficult to study because the microstructure is more complex in nature and the observed BN signal is weaker. The hard martensite structure also requires a greater applied load for plastic deformation to take place in the material. It is, however, still important to study these materials because they are commonly used in components subjected to loading, e.g. gears.

The BN signal is observed to show angular dependence towards the stress direction [99]. This is generally reported as being caused by magnetic anisotropy meaning that the magnetic properties depend on the measuring direction. High BN emissions are measured parallel to the tensile elastic stress direction [50]. This occurs due to the reorientation of domains into the direction within the family of [100] which is closest to the applied stress direction [72]. The anisotropy energy of the domain walls is the lowest if they lie parallel to the easy axis of magnetization [48].

Besides the uniaxial stress, the BN method has been used to study the biaxial stress response [100, 101]. For the practical point of view, the biaxial stress state is the common stress acting on components. The biaxial stress behaviour of the BN means that the BN in one direction also depends on the stress in another direction. Thus the quantitative BN measured outcome is dependent on the fact that the BN-stress calibration should be carried out also with a biaxial stress state. For example, with the MAPS system, referring to Magnetic Anisotropy and Permeability System, calibration maps can be identified where the magnetic parameters are mapped as a function of the biaxial stress [101]. This can be performed by making the measurements whilst the probe itself is rotated on its axis whilst collecting data [101].

Elastic and plastic deformation

Strain is the relative deformation caused by applied forces. Strain can be either elastic or plastic. Elastic and plastic deformation represents different deformation mechanisms. Elastic deformation is described by changes in the atomic spacing of the crystals. A material behaves elastically when the stress acting on a specimen is smaller than the yield strength. Thus the deformation state is reversible [102]. Prior to reaching the actual macroscopic elastic limit or yield strength, early states of plastic deformation, referred to as microyielding, may occur. This is characterized as dislocation formation that has commenced in some favourably oriented grains.

Plastic deformation, characterized as loading greater than yield strength, affects the generation of defects such as dislocations, twins and shear bands [77]. When the plastic region is reached the macroscopic elastic strain remains constant, but plastic deformation occurs through slip processes that increase the number of pinning sites such as dislocation tangles and cell boundaries. Also, the development of crystallographic texture (easy axis alteration) and the work hardening process occur [77]. It has been observed that plastic deformation creates anisotropic behaviour with respect to stress direction and this leads to both 180° and 90° domain wall interactions instead of just 180° domain wall interactions [57].

The effect of elastic and plastic deformation can be studied with mechanical loading such as tensile and compressive testing. In addition bending can be utilized. In tensile testing, a uniform uniaxial load is applied to the sample cross-sectional area, whereas in bending the sample configuration differs from the tensile tensing. In bending, depending on the mode of the bending, a stress gradient is formed from tensile on the bend surface to compression on the opposite surface.

The elastic strain caused by stress has been noticed [77] to have more effect on the BN average MBN energy response than the plastic strain caused by stress. Plastic deformation causes only minor changes to the average MBN energy values [77, 95]. This is explained by the different deformation mechanisms occurring during elastic and plastic deformation. [77] Moreover, the relationship between the magnetic hysteresis parameters, such as remanence induction $\mathbf{B}_r$, permeability and coervitity, and plastic strain have been studied. With increasing plastic strain in a pearlite pipe steel, Birkett *et al.* [103] observed that remanence induction $\mathbf{B}_r$ and permeability μ decreased. Coercivity $\mathbf{H}_c$ increased with increasing plastic strain [103]. In addition, plastic deformation can cause changes to the pulse height distribution of the BN amplitudes. Plastic deformation was observed to increase the number of larger BN pulses due to the alteration of the pinning site energy [50].

Tensile and compressive loading

Tensile stress increases the BN emissions and increases the observed RMS value and compressive stress decreases them when a material with a positive magnetostiction coefficient is studied. Tensile stress creates a magnetic easy axis in the direction of the applied stress to which the domains in the sample try to rotate. The same phenomenon is observed with compressive stress applied to the direction perpendicular to the applied magnetic field. However, in some cases the BN measurement stress sensitivity is observed to behave non-symmetrically during tension and compression [74]. It has been reported that stress sensitivity is higher both in tension [92] and in compression [74, 104]. This phenomenon can be seen in Fig. 6. This different stress sensitivity observed in BN responses may be due to the different steel composition, heat treatment and BN measuring equipment used. Some studies report that the stress versus BN behaviour is saturated at some point of stress level.

In addition to the saturation of BN as a function of stress, a decrease in the BN amplitude with applied high tensile stress, after the saturation point can also be observed [74, 104, 105] Therefore, the BN signal saturation needs to be taken into account when utilizing the BN method to residual stress measurements. This complicated phenomenon, illustrated in Fig. 6, can be explained in many ways according to Cullity [53]. The main issue influencing this behaviour is the fact that tensile stress affects the magnetostrictive coefficient changing it to negative and, thus, influencing the BN amplitude. Both the applied magnetic field strength and applied stress induces the magnetostriction to change [53].

The change of the magnetostriction coefficient is explained as follows [106]. When magnetization occurs in a ferromagnetic sample, first the domains tend to align themselves in the nearest easy axis corresponding to the stress or magnetic field direction. This alignment causes the bulk magnetization and bulk magnetostriction to increase. When loaded more, the domains align further in the exact direction of the stress of the applied magnetic field. Thus, the magnetization is increased but the magnetostriction decreases. If there is no stress acting with the applied magnetic field then the first step dominates. When tensile stress occurs with the applied magnetic field the alignment of domains to the nearest easy axis has already occurred due to the acting stress. Therefore, the magnetostriction increases more slowly and turns into a decreasing value much earlier (with lower magnetization **M**). With high stress, the magnetostriction decreases with increasing magnetization [106]. As a result, there is a reversal stress dependence with a high tensile stress region [74, 96, 105].

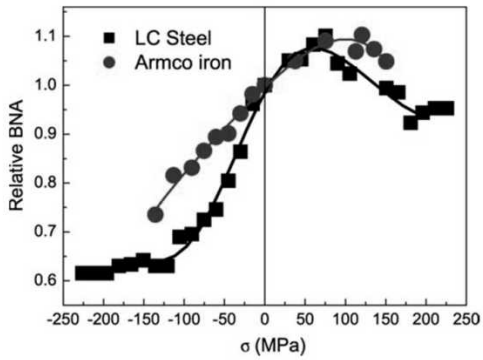

Figure 6. *Maximum amplitude of the BN response as a function of the applied stress for low carbon steel (LC steel: 0.07 C, 0.43 Si, 1.38 Mn, 0.01 P and 0.037 Al) and Armco iron (0.01 C, 0.1 Mn, 0.01 P, 0.008 S, 0.03 Cu and 0.006 N). [104]*

Magnetic properties may be modified by tensile stress in the following way: the 180° domain wall population is increased with increasing tensile stress [64] due to induced stress anisotropy [53]. In addition, 180° domain wall configurations can be reoriented, but it is also stated that some alignment occurs via the motion of 90° domain walls [57, 107]. Generally speaking, the pinning energies can be modified by stress [53].

Bending loading

Several studies have been carried out to study the effect of bending on BN phenomena [61, 93, 96, 97, 98, 108, 109]. In one variation of these bending tests the specimen acts as a cantilever. In the studies [93, 96, 98] made with this method, the specimens were mounted in such a way that the BN measurements could be carried out from both sides of the sample, from the surface under tension and from the opposite surface under compression. The bending moment was applied incrementally by increasing the mass on the free end of the cantilever. The BN measurements were performed with a low magnetizing frequency apparatus from opposite sides of the sample, thus results for compressive loading were also reported. [93, 96] However, to ensure constant stress over the bend area, the best way to perform a bending test is four-point bending. In four-point bending, the stress is constant between the two inner bending supports, whereas cantilever bending causes non-uniform stress in the sample surface.

During bending, both single-peak BN envelopes and multiple peak envelopes [97, 108] were registered. Multiple peaks were noticed in the compression of spheroidised cementite and tempered martensite samples [97]. Also, compression of hardened samples was noticed to produce double peaks [108]. The occurrence of double peaks in compression seems to be dependent on the composition and heat treatment of the samples [108]. Hardened and over-tempered steel samples were reported to produce a double peak in compression and high tensile strain [98]. Only one peak was noticed in the bending of standard tempered samples [98].

Barkhausen noise envelope features

Furthermore, it has been reported that tensile loading produces only one BN envelope peak [108, 110]. In contrast, during compressive loading several BN envelope peaks may appear [97, 104, 108, 110]. However, a double peak was observed after tension in an unloaded condition by studies of Gatelier-Rotha *et al.* [110] whereas only one peak was observed in the unloaded condition after compression. Besides the RMS value, the reciprocal of the BN peak amplitude was noticed to show a linear behaviour with respect to the applied tensile and compressive stress [65]. Earlier Garikepati *et al.* [80] had suggested that there is a relationship between the slope of an anhysteretic magnetization curve and stress. Their theory also suggested that the reciprocal value of anhysteretic susceptibility is linear with applied stress and that the dependence is much stronger in tensile stress. Further, Mierczak *et al.* [65] proved that the relationship of the reciprocal value of BN amplitude acts similarly to the reciprocal anhysteretic susceptibility. The trend was similar when considering the applied stress and also the residual stress. The assumptions are that both of these calculated values represent the same stage of the magnetization process, the steepest slope of the hysteresis loop.

Some BN studies concentrate on the sensitivity of BN to strain. The study of Stefanita *et al.* [77] investigated the behaviour of BN below the material yield strength in uniaxial tension. The peak height was observed to increase with increasing tensile stress [74]. In addition, an MBN energy parameter, referring to the area of the squared voltage pulse, was noticed to increase with increasing tensile stress [77], whereas, the peak width was also observed to increase with increasing tensile stress [65]. In contrast, Stewart *et al.* [74] noticed a decrease in the peak width with increasing tensile stress. The hysteresis loop has also been reported to become narrower due to increase in the differential susceptibility [72] with increasing tensile stress

[111] and to create an increased peak intensity emission [98]. Also the differential susceptibility was increased [72]. Thus the compressive stress was observed to change the peak position to larger values while the hysteresis loop becomes broader [74, 96, 104].

BN studies for surface residual stress determination

The BN method has been widely used to estimate the surface residual stresses (SRS) in many studies [89, 74, 112, 113]. Desvaux *et al.* [89] evaluated the SRS values with BN from aeronautic bearings after engine use. BN measurements were further validated with the X-ray diffraction method. While Gür *et al.* [112] evaluated the SRS from welded plates with the BN method with the help of a special calibration curve obtained from tensile and compressive loading. In addition Stewart *et al.* [74] and Yelbay *et al.* [113] used the BN method to determine residual stresses from welds. Yelbay *et al.* [113] used similar calibration curve as Gür *et al.* in their studies [112].

3.1.2. The effect of microstructure

The microstructure of the material determines the magnetic domain configuration and the pinning site distribution from the magnetic point of view. However, the magnetic domain size is not equal to the grain size, but has been referred to as proportional to the square root of the grain diameter [114]. Phase boundaries, grain boundaries and defects such as cracks or cavities that have different magnetic properties are pinning sites for the moving domain walls. In addition, interfaces between precipitates and the matrix and precipitates that have local stress fields around them can also hinder the domain wall motion [115]. It is well known that an increase in hardness that arises from an increase in lattice strain/dislocation density increases the resistance of the domain wall movement and consequently, reduces Barkhausen noise activity [115].

The magnetic BN method is sensitive to composition, phase variations and grain structure. Concequently, variations in these properties contribute to the observed BN signal. Many studies have been done to link microstructural features to BN behaviour as discussed below. Different features calculated from the BN envelope have been used to acquire information about the microstructural features. For example, peak height and position has been observed to vary according to the reduction of dislocation density and due to the pinning strengths towards the domain wall motion of obstacles [116]. In addition, different phases have distinct forms of BN envelopes. However, the extraction of individual effects is required and is possible only under certain conditions such as specially manufactured samples.

The heat treating of the steel and the subsequent transformation of austenite while cooling can be carried out in various ways to produce different microstructures. With similar carbon content, but performing the cooling from the austenite region, with different cooling rates, the microstructure can be altered. Also the carbon content influences the microstructure and as a result, the properties. As the isothermal transformation diagram presents, depending on the carbon content and the cooling rate of the steel, various phases can be obtained [117]. In the following, the effect of the various microstructural phases to the Barkhausen noise signal is explained.

Ferrite

In a ferrite structure the observed peak in the BN envelope is narrow and the peak appears at lower magnetic field strengths, as shown in Fig. 7. This phenomenon can be explained as follows: grain boundaries are the main pinning sites in the ferrite structure so the required

magnetic field to release domain walls from the pinning sites is low [73]. Thus, domain walls can move a longer distance in the ferrite phase before being pinned by obstacles, which in turn causes larger amplitude voltage pulses.

Pearlite

For a pearlite structure, the peak in the BN envelope is observed at higher magnetic field values than the peak from ferrite, as shown in Fig. 7. In a pearlite structure the pearlite colonies have a strong effect on the domain wall pinning. Studies of Saquet *et al.* [73] and Lo *et al.* [118] are consistent in stating that the cementite lamella direction has a bearing on the pinning strength. If the cementite lamellae were parallel to the domain wall they were more strongly pinned than lamellae perpendicular to the domain wall [118]. The increasing pearlite spacing was noticed to increase the BN amplitude monotonically and decrease the coercivity. The stronger pinning of domain walls was caused by the decreasing pearlite spacing leading to an increase in the cementite unit volume [118].

Martensite structure

Case-hardening processes such as carburizing produce a wear-resistant, strong layer consisting of martensite. During heat treatment, carbon is dissolved in the surface layer in a carbonaceous atmosphere at an austenitizing temperature followed by quenching. This results in a gradient of carbon content below the surface. This carbon gradient accompanies the gradient in hardness [119]. The structure of the martensite is tetragonal and this tetragonality forces the magnetization axis to be parallel to the c-axis in the martensite unit cell. Martensite structure is composed from small needles or packet laths. The micro-residual stresses in the martensite needles may also influence BN emission to some extent.

The magnetic BN signal obtained from a martensitic structure is notably lower than for ferrite and pearlite structures since domain walls are pinned due to high dislocation density [73, 119]. The peak of the martensite is also much broader than the peaks observed from other microstructures. These differences in the martensite BN envelope can be explained by the tetragonal structure of the martensite and the residual stresses in the martensite needles. The formation of compressive residual stresses in the martensite structure due to volume expansion must also be considered because they have an influence on BN [73]. Due to the small size of the martensite needles, the domain wall energy plays an important role, so the relative volume occupied by a wall is larger than in the other phases of steel [120].

Tempered martensite structure

Tempering is performed to brittle as-quenched martensite to improve ductility and to reduce the residual stresses caused by previous treatments such as quenching. A tempered martensite structure consists of carbides and ferrite. The carbides first precipitate as the tempering temperature is increased and at higher tempering temperatures the carbides coarsen and grow. During the magnetization process, in the tempered martensite structure the moving domain walls have to overcome the extra pinning sites generated by the carbide precipitates.

Normally, when steel is tempered, the first changes occur in the carbon atom arrangements [121] at temperatures from 25-100 °C [122]. The high supersaturation of the carbon in martensite along with the high mobility of interstitial carbon atoms makes certain that the carbon atoms rearrange themselves into dislocations and boundaries even at these low temperatures [121, 122].

When tempering high-carbon steels at temperatures of 100-200 °C, firstly the transition carbides, for example ε-carbide ($Fe_{2.4}C$), are precipitated [122]. Moreover, the carbon content of

the martensite matrix is decreased [121]. Epsilon (ε) carbides are observed as small (diameter less than 0.5 μm), evenly distributed carbides. Thus, they can be hard to detect even from scanning electron microscope micrographs taken with higher magnifications [122]. Transformation carbides are reported to array typically in linear clusters within the martensitic matrix [121]. They are stated to form on (100) planes of ferrite, which is also the easy magnetization axis. Therefore, they have been found to have only a minor pinning strength to domain wall motion and have been observed with increased BN emissions compared to solid solution high purity iron samples [110]. In addition, the width of the BN envelope has been observed to be larger than for solid solution samples [110].

At a temperature range of 200-350 °C the retained austenite is reported to decompose into a mixture of cementite and ferrite [122], which is called the second stage of tempering [121, 122]. Cementite carbides (Fe_3C) start to replace the transition carbides during the tempering temperature range of 250-350 °C [121]. The most likely sites for cementite nucleation are at the interfaces between the ε-carbides and the matrix [123]. Above 350 °C the carbides are coarsened and spheroidization takes place. It should be noted that Fe_3C can also precipitate directly and this is probable in the case of a material with high defect density. At higher tempering temperatures, the cementite carbides coarsen and grow at the expense of the ε-carbides. Besides, at a temperature range of 400-600 °C, the dislocation structure starts to recover, but the martensite lath-like structure is still maintained [122].

The cementite carbides are stated to have anisotropy and they are located on (110) planes in the matrix originating at a 54.74° angle between these planes and the easy axis of magnetization [110]. This produces a closure domain formation around the cementite carbides in the ferrite matrix. Cementite carbides have great influence on the BN emissions. Tempering, thus increases the BN activity compared to a martensite structure [73, 110].

Different changes in BN responses have been observed for martensite decomposition during tempering. In the studies of Saquet *et al.* [73], it was noticed that the BN emissions from a tempered martensite structure were transformed from low intensity high magnetic field martensite peaks into higher intensity BN peaks at low magnetic field strength when the tempering temperature was increased. This behaviour was due to the carbide precipitation that occurred. While tempering above 400 ºC, a strong increase in the amplitude of the BN peak was seen as the carbides started to spheroidize and the ferrite structure began to recrystallize [73].

Multiphase steels

The BN method has been utilized to study the relative amounts of phases present [124]. The method has been used to study the volume fraction of ferrite in ferrite-martensite and also ferrite-bainite steels. In particular, the peak position of the BN signal was sensitive to the volume fraction of the ferrite phase for both ferrite-martensite and ferrite-bainite steels. [124] Similar results were also obtained by Gür *et al.* [125] for ferrite-martensite steels. Also, Kaplan *et al.* [120] studied ferrite-martensite steels and noticed a decreasing RMS voltage trend as a function of increasing martensite volume fraction. This can be understood by considering the fact that martensite pins domain walls more effectively than ferrite.

Retained austenite

Retained austenite is observed to create non-magnetic (internal demagnetizing fields) areas that domain walls cannot overcome. The reason for this is that austenite is not ferromagnetic. This is why retained austenite has been observed to be a strong barrier to domain wall motion [75]. The retained austenite amount was observed to control the stress sensitivity of a 9Ni steel in the studies of Rautioaho *et al.* [126]. The maximum stress response was observed with the amount

of 3-5 % austenite whereas a decreased stress response was observed with high austenite contents [126]. The reason for this behavior is that retained austenite forms non-magnetic areas that domain walls are hard to overcome even in the presence of high tensile stress.

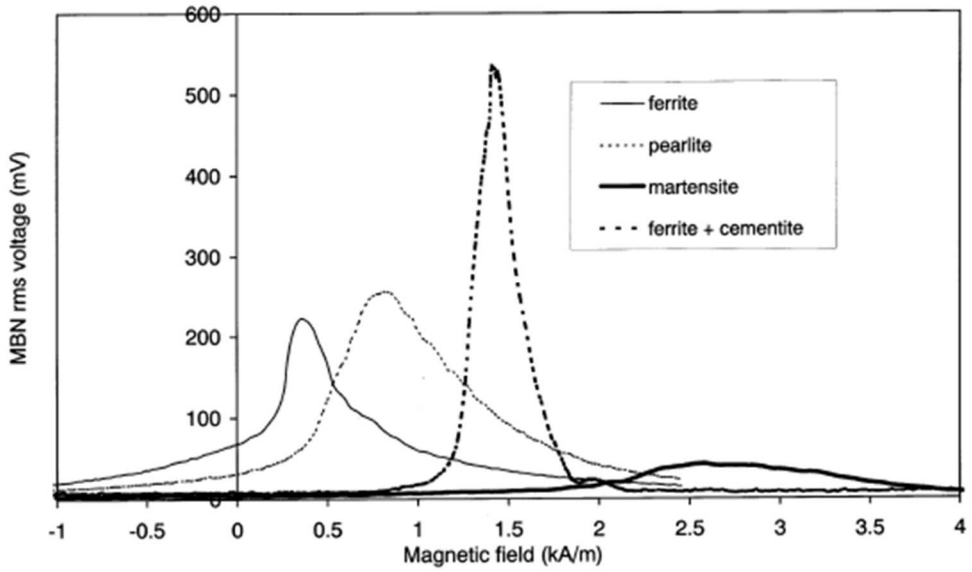

Figure 7. *The RMS value of the BN signal as a function of applied magnetic field with different microstructures [73].*

Grain size

Grain boundaries are commonly reported as active pinning sites for domain wall motion. Thus, the grain size has been said to be related to BN activity. The smaller grains provide to a larger number of grain boundaries creating more BN events of smaller amplitude [72]. The BN amplitude has been found to decrease when the grain size increases [110]. In contrast, Tiitto [127] observed the opposite behaviour, increasing BN amplitude with increasing grain size, at the beginning of the magnetization process. If the grain boundaries were the dominant pinning sites, one would expect BN amplitude to increase with increasing grain size as the mean free path increases. When this is not the case, other factors dominate the pinning of the domain walls.

4. UTILIZATION OF BARKHAUSEN NOISE METHOD

The magnetic Barkhausen noise method can be utilized in many applications such as quality control of heat treatments and quality control of grinding, as presented in the following section. Recent studies in particular have concentrated on the utilization of the BN method in the case-depth determination of hardened surfaces. In addition, some novel Barkhausen noise applications are introduced below.

4.1. Quality control of heat treatments

The case-hardening process is usually performed by carburizing case hardening, induction hardening or nitriding. These processes create surface layers with good wear and fatigue resistance, high hardness and high resistance against high surface pressures. The hardening effect of the surface in carburizing and nitriding is due to carbon or nitrogen diffusion into the

steel surface from a carbonaceous or nitrous atmosphere followed by a quench when the transformation of martensite occurs in the surface layer. This creates a hardness gradient and also compressive residual stresses within the sample surface [128]. Induction hardening is employed with an induction coil that creates eddy currents in a conductive material and this locally heats the component above the austenitization temperature. The martensite is formed within surface layer after a fast quench. Heat treatment parameters such as inductor coil frequency, time and power used can be varied to change the depth of the hardened layer produced [71].

The determination of case depth is one way to evaluate the composition gradients, microstructure gradients and also the quality of the hardening treatment. The detection of the case-hardened layer depth is normally done in a destructive manner by hardness depth profiling or from a cross-sectional sample by optical microscopy. Destructive case-depth evaluation can be done according to standards e.g. ISO 2639 and SFS-EN 10328 [129, 130]. The definitions for case-depth estimations obtained from different heat treatments are introduced below.

- For carburized case-hardened parts the hardness limit defining the case-hardness depth (CHD) is 550 HV (50 HRC) measured with $HV_{0.1}$, HV_1 or HV_5.
- For induction hardening components the case-hardness depth (Rht) is the distance from the surface where the hardness is 80 % of the surface hardness. Usually the value of 400 HV_1 is used (for surface hardness of 500 HV_1).
- For nitrided parts, the case-hardening depth (Nht) is the distance from the surface where the hardness is 50 HV_1 above the core hardness. [131]

Both optical microscope verification and micro-indentation procedures, are destructive in nature, time-consuming and require appropriate equipment to perform them in a factory environment. Thus, they are not fully applicable in modern factories with online process control and high productivity rates. However, these methods are suitable for verifying the findings of the non-destructive methods used in case-depth studies.

Magnetic non-destructive methods for case-depth determination

The detection of a hardened layer thickness by magnetic non-destructive methods has been studied widely in recent years. So far, no commercial systems based only on BN have been introduced to detect case-depths. The motivation for these measurements comes from the need for quality control in industry. The non-destructive detection of the hardened layer thickness is useful in the detection of the layer left for the re-grinding and verification of case-depths of hardening heat treatments. According to the present knowledge, case-depths can be accurately down to 1-2 mm by BN measurement.

Many studies [58, 59, 62, 132, 133, 134] that have been performed utilize the Barkhausen noise method in case-depth studies. The main approaches to the interpretation of the BN signal in case depth studies are listed below:

- Two peak behaviour of the BN envelope due to the soft core and hard case and the calculation of the ratios of these two peaks [21, 62, 132, 133, 135]
- Filtering of the BN signal to exclude the signal from the soft core [132, 133]
- Magnetic hysteresis loop parameter detection [58, 59]

However, many of the studies use a combination of these approaches. They are discussed in details in the following section.

Two-peak BN envelope studies

Two-peak behaviour, illustrated in Fig. 8, is expected when there are two different microstructural layers present within the BN skin depth range. The magnetization process is assumed to occur in two regions of different magnetic field strengths due to the presence of hard and soft phases. One of the peaks originates from the low hardness subsurface with lower magnetic field excitation and the peak at higher field strength originates from the hard case. It is well known that the core of the hardened specimen with a low hardness ferrite or ferrite-pearlite microstructure, described by low coercivity and high permeability, would be more easily magnetized with a lower magnetizing field. In contrast, the hard martensite case, having high coercivity and high remanence values, requires a stronger magnetic field to be magnetized [48].

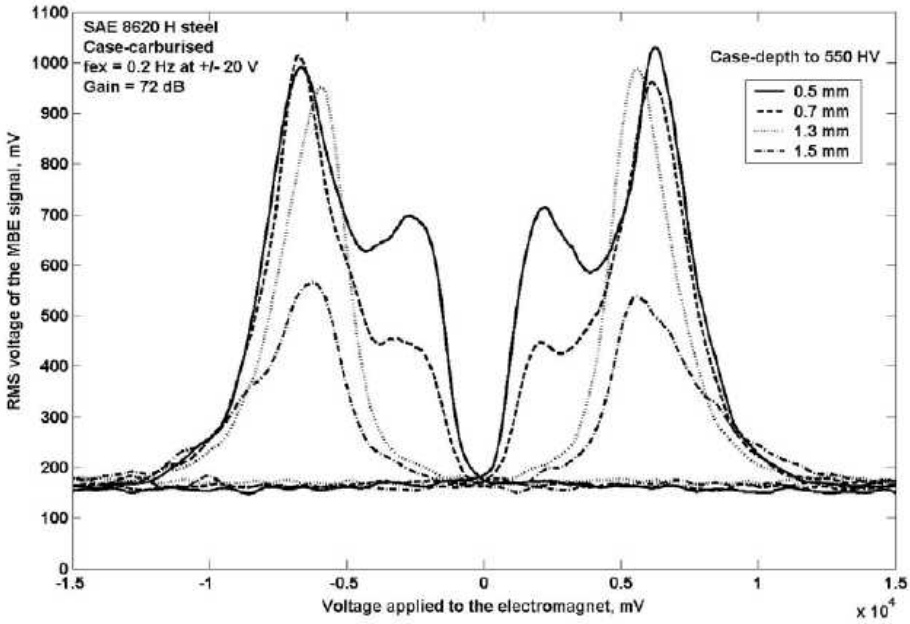

Figure 8. *An example of a two-peak BN envelope with different case-depth value samples [62].*

Many studies [62, 132, 133] have observed the occurrence of the two-peak BN envelope in case-depth studies. The two-peak feature has been found from both induction hardened sample BN envelopes [58, 59, 132, 134] and from case-carburized sample BN envelopes [59, 62].

A ratio of the two-peak heights, the ratio of the surface peak divided by the bulk peak, was observed to increase with increasing hardening depth in induction hardened samples to hardening depths of 4.5 mm [132]. Another study [134] concluded that the measurement limit was 1 mm for induction hardened samples. In addition to these systematic changes in the envelope, features of the BN signal could be used as indicators for the volume fractions of the ferrite and martensite phases [134]. Moorthy *et al.* have detected two-peak behaviour in many studies dealing with hardened steel samples that were measured by a laboratory-made low frequency BN equipment [61, 70, 135, 136]. For example Moorthy *et al.* [70] detected two-peak behaviour for differently tempered case-carburized steel samples having a case-depth value of 1 mm. The measuring frequency for these measurements was low, 4 Hz.

The assumption that two-peak behaviour is only observable with samples having smaller case-depth values has been proven in many studies [62, 134]. The measurements have shown that with an increasing case-depth value, the small peak formed with smaller magnetic field strength values gradually decreases and diminishes. This was proven by etching the case away and observing the peak behaviour changing in the same way compared to the shallower case-depths [62].

Besides the actual case-depth BN studies, many investigations have noticed double-peak behaviour [96, 104, 137] in the BN envelope. For example, a double-peak has emerged in compressive elastic and plastic loading [104]. It was assumed that in this case the double peak arose from two different types of pinning sites [104]. Also, a decarburized surface layer was found to produce a two-peak BN envelope [96, 137]. One explanation for this is to link these peaks to spike domains and their behaviour during the magnetization process. Sometimes the spike domains are generated in the specimen although it has been saturated. The reversal of the magnetic field creates nucleation of new domains and this makes new BN activity [137].

Case-depth studies with filtering of the BN signal

In most studies, many different methods for the determination and classification of the measured data have been used. Also, BN signal filtering has been studied [132, 133]. It is believed that the use of different filtering and frequency ranges used in the measurements may produce more detailed information about the microstructural gradients in the case-hardened samples. For example, several analysing filtering bandwidths and also the use of peak height ratios have been studied [132]. By determining the appropriate filtering, the two peaks could be distinguished. The highest filtering with 50 kHz diminishes the peak coming from the bulk material. This means that the optimal filtering range is essential so that no important information of the BN signal is lost.

In addition, a frequency range study has been performed [133] in order to find the best frequency band for case-depth estimation. A frequency spectrum with Fast Fourier Transformation (FFT) was recorded and the band was further divided into smaller ranges to find the appropriate one for signal analysis. The measured series contained two different carburised steel sample series with case depths varying from 100 µm to 1000 µm and three ion nitrided steel samples with case depths varying from 1 µm to 200 µm. Only one nitrided tool steel was found to have a two-peak behaviour in these studied conditions and due to this behaviour, the calculation of the ratio of the peaks could not be used [133].

Various studies [61, 70, 135, 136] made by Moorthy *et al.* during recent years have dealt with both high and low magnetizing frequency BN measurements. In many of their studies, they have detected a two-peak Barkhausen noise signal envelope from low frequency measurements. In one of their studies [70], various hardened and tempered steel samples were measured with both high and low frequencies to study the effect of different signal filtering techniques. The low frequency measurements revealed a two-peak envelope in which the different filtering ranges had more effect on the second peak arising from the higher magnetic field strengths.

Measurements of the magnetic hysteresis properties for case depth studies

Magnetic hysteresis loop properties have been used to study the case-depth measurement [58, 59, 60]. The coercivity and the hysteresis loss, referring to the area of the hysteresis loop, were found to increase while the case-depth increased [58]. Also, Kai *et al.* [60] concluded that coercivity increased with increasing hardening depth. In contrast, the maximum permeability [58] and relative permeability [60] were found to decrease as the case-depth increased. Kai *et*

al. [60] concluded that with a low measurement frequency, the difference of the magnetic properties dependent on case-depth and hardness was larger. This phenomenon can be explained by the fact that as the case-depth increases, more domain wall reversal occurs in the case consisting of martensite. Martensite is known to require quite a high magnetic field to unpin the domain walls and this contributes to the increase in coercivity and hysteresis loss values. The saturation magnetization value $\mathbf{M_s}$ was also found to correlate with case-depth values on both induction and carburized samples [59] and with hardened samples [60]. A change in the hardened layer thickness has an effect on the overall saturation magnetization and the case-depth can be determined by the calculation of the volume-weighed sum of the saturation magnetization of the core and case.

4.2. Quality control of grinding

As previously described, grinding burns compromise material properties and may lead to failures during the use of the ground pieces. Therefore, it is essential that damaged components can be detected in quality control. To ensure the surface integrity of a ground piece, many automatic or semiautomatic inspections with inspection machines are carried out to measure the tooth dimensions, profile and surface roughness after the grinding [8]. In addition any grinding burns can be detected by several methods. One possibility is destructive microhardness measurements. Microscopic inspection is also an effective way but unfortunately the destructive studies are not usable in industrial quality control. Additionally, the X-ray diffraction method can be used to non-destructively detect the residual stresses in the very near surface layer of the ground part e.g. [139].

The most common grinding burn detection technique used is the chemical nital etch procedure. This standardized [140] method is applicable for the detection of localized overheating in carburized case-hardened steels. The detection of grinding burns via nital etching is based on its sensitivity to surface hardness changes [8]. An etched surface with grinding burns demonstrates a colour change compared to a sound surface [8, 140]. The nital etch procedure requires awkward handling of the specimen to be tested in a container and cleaning. Also, the nital etch inspection is quite a slow method, hard to automate and the interpretation of the findings can be difficult. In addition, the nital etch might not reveal subsurface tensile residual stresses [141].

Besides the conventional chemical nital etch inspection and microhardness measurements described earlier, the non-destructive magnetic Barkhausen noise analysis method can also be utilized for grinding burn detection [6, 7, 142, 143, 145]. Barkhausen noise analysis can reveal the locally damaged surface containing an altered microstructure or residual stress state. There is a growing demand for non-destructive testing of steel components for detection of defects and residual stresses. The material characteristics affect the generated Barkhausen noise and the method can be used to detect the residual stress by controlling microstructure and to detect microstructural changes by a controlling residual stress level. The BN method is a fast and non-destructive way to examine components in quality control. Because the method can be automated, Barkhausen noise analysis is widely used in the gear manufacturing industry to control the quality of ground gears e.g. [20]. However, the method itself only produces relative results; these results need to be compared to a certain rejection limit. In addition, the method also needs calibration. These issues have already been discussed in the section on calibration of non-destructive measurements.

Several studies have been conducted to compare the BN method outcomes with observations from nital etching [142, 145]. For example, Dünck-Kerst [142] compared the nital etch results with the BN measurements of ground gears. The conclusion was that changes in the internal

stresses observed with BN occur mostly before the actual microstructural change leading to loss of hardness that could be located with nital etching. Thus the BN method can be used to observe changes occurring prior to changes detected with nital etching.

Also, several grinding parameter changes have been related to material property changes revealed by the measured BN characteristics. Parakka *et al.* [146] studied the effect of the grinding rate on the variation in the BN peak. The relation of the coolant flow and the BN peak and peak width was studied by Gupta *et al.* [143]. The BN peak was observed to change while decreasing the coolant flow to 25 % of the original amount [143]. Parakka *et al.* [147] studied the effect of coolant flow rate on the BN peak and peak width. Vashista *et al.* [148] studied the effect of wheel speed [148], work speed [148] and grinding downfeed [148, 149] on the magnetic responses and noticed e.g. that with an increase in wheel speed, work speed and grinding downfeed, the area under the BN amplitude spectrum increased. Klocke and Gorgels [29] worked on with the grinding parameters and noticed that the BN signal increases with increasing stock removal rate referring to an increase in the grinding wheel speed of the feed.

The relationship of the residual stress and BN outcome has also been studied for ground samples subjected to varying levels of grinding damage e.g. [136, 150]. The BN was found to increase with increasing tensile stress as expected [150]. However, some statistical fluctuations in the BN data were observed as a function of measured residual stress, which were explained by the fact that the microstructural changes affecting the BN signal were independent of the stress state [150]. Also, it should be noted that the measurement depth varies when comparing these high flow frequency measurement systems [141]. In general, only the high frequency BN measurement can be related to surface residual stress measurements occurring less than 20 µm below surface [115]. On the other hand, other studies concluded that high frequency BN does not show RS changes at depths more than 10 µm [136]. Klocke and Gorgels [29] investigated also the residual stress profiles produced by grinding samples and also from laser damaged samples. They concluded that the different thermal damage levels can be seen from the residual stress depth profiles [29].

4.3. Novel BN applications

The BN method has also been utilized in some novel areas in addition to these above mentioned well-known applications. New inspection targets for BN studies such as detection of decarburized layer thickness [137] or crack and flaw detection [151, 152, 153] have been investigated. The utilization of continuous magnetic Barkhausen noise for artificial groove detection was introduced by Franco and Padovese [154].

5. AIM OF THE PRESENT STUDY

During the manufacturing of hardened components, the fabrication of the material may cause changes in the material properties such as microstructure and surface residual stresses. Also, residual stresses may be created within the material due to inhomogeneous plastic deformation or thermal gradients during manufacturing. Stresses may be beneficial or detrimental to the component depending on the nature of the stresses (compressive or tensile). Characterization of these changes in quality control is a demanding task and generally destructive methods are not directly applicable due to their destructive nature and slow response. Barkhausen noise measurement is a promising non-destructive technique for analysing material properties low equipment cost and fast response.

The aim of this work was 1) to develop a methodology for detection of case-depths of hardened components with Barkhausen noise 2) to study the detection of grinding burns by the multiparameter Barkhausen noise method and to study the effect of various factors such as microstructural changes and different loading conditions on the Barkhausen noise signal in hardened steels used in wind turbine gears, 3) to make calibration samples to be used in the quality control of the Barkhausen noise method and 4) to study the stress response of tempered structures. The modelling of the BN signal used for the experimental results obtained here has been discussed elsewhere by Sorsa and Leiviskä, e.g. [155, 156].

The structure of the research topics and studied issues is presented in Fig. 9. The research was focused mainly on the manufacturing of artificial thermal damage to be used as test specimens in the BN measurements. The studies including the voltage sweep tests for case-depth measurements and stress vs. BN relation in different hardened materials were performed in order to attain a more profound insight into the BN method itself. This work is composed of six publications. The relationship between these publications and the research topic is presented in Fig. 9.

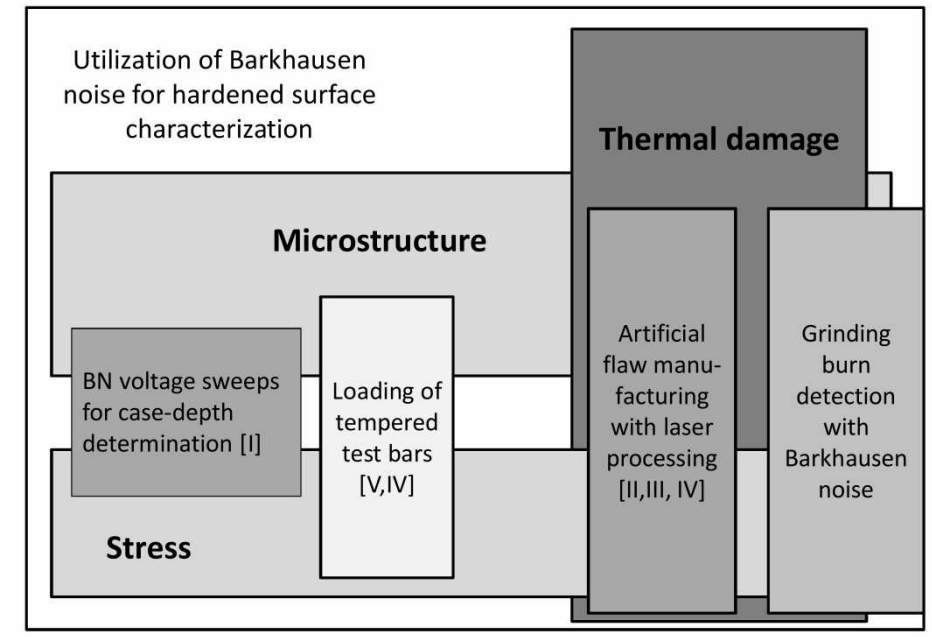

Figure 9. *The structure of the research work introducing the topics of the published papers.*

6. EXPERIMENTAL PROCEDURE

6.1. MATERIALS

The study concentrated on the characterization of hardened steel materials. Both carburizing case-hardened and induction-hardened samples were investigated. The materials studied were divided into three groups according to the field of research performed: case-depth samples, samples for artificial grinding burn detection and samples for loading and bending tests.

6.1.1. Samples for case-depth measurements (*Publication I*)

Hardened rod samples with a varying hardened layer thickness were prepared with induction heating and carburizing case hardening for case-depth detection with BN. For induction hardening, two steel grades, 34CrNiMo6 and 42CrMo4, were used. Steel grade 18CrNiMo7-6 was used for carburizing case hardening.

The length of all the rod-shaped induction-hardened samples was 300 mm and the diameter 45 mm. The samples were induction hardened to varying case-depths from 0.65 mm to 2.2 mm with material 34CrNiMo6 and from 0.35 mm to 1.9 mm with material 42CrMo4. Table 2 shows the chemical composition of the studied steels. Some of the induction-hardened samples, referred to as turned, were turned and finally ground to a smaller rod diameter of 39 mm in order to produce a shallower effective case-depth after the induction hardening. Five different sets of induction hardened samples were prepared. Table 3 presents a detailed description of the sample sets.

Table 2. *Chemical composition of the studied steels.*

Wt -%	C	Cr	Si	Mo	Mn	Ni	P	S	Ca	Cu	Fe
34CrNiMo6	0.36	1.36	0.28	0.17	0.71	1.31	0.024	0.029	-	-	bal
42CrMo4	0.41	1.07	0.31	0.17	0.73	-	0.017	0.03	0.0036	-	bal
18CrNiMo7-6	0.21	1.57	0.20	0.27	0.65	1.45	0.016	0.029	0.0044	0.18	bal

Table 3. *Description of the sample sets for case-depth determination with the BN method.*

	Set 1	Set 2	Set 3	Set 4	Set 5	Set 6
Hardening method	Induction hardening	Induction hardening	Induction hardening	Induction hardening	Carburizing case hardening	Induction hardening
Material	34CrNiMo6	34CrNiMo6	34CrNiMo6	42CrMo4	18CrNiMo7-6	34CrNiMo6, 42CrMo4
Hardening layer thickness variations [mm]	0.65-2.2	0.825-1.85	0.65-1.45	0.35-1.9	1.2-3.5	2.8, 2.9 (34CrNiMo6) 3, 4 (42CrMo4)
Sample manufacturer	Takoma Gears Oy, one-frequency machine	Takoma Gears Oy, multi-frequency machine	Bodycote Värmebehandling AB (Malmö, Sweden)	Takoma Gears Oy, one-frequency machine	Moventas Wind Oy (Karkkila and Jyväskylä)	Takoma Gears Oy

6.1.2. Samples for artificial grinding burn detection (*Publications II, III*)

The starting point for the preparation of samples for artificial grinding burn detection was that a controlled tempering with laser or induction processing was carried out to the already hardened steel surfaces. The prior state in all studied samples was a hardened surface, either by carburizing or induction hardening. The laser processing was applied to the samples to make tempered marks that simulate some softened areas in the otherwise hardened surface. Several experimental series of laser-processed and induction-processed samples were manufactured. The sample series contained hardened samples, both carburizing case-hardened and induction-

hardened and ground. Some samples were detached teeth from gears and a whole gear wheel was also processed. The details of the different sample categories are presented in Table 4. The sample series also contained powder metallurgically (PM) manufactured steel blocks and rectangular induction-hardened steel blocks. Table 5 shows the chemical composition of the studied steels. In addition, different surface conditions for laser processing such as ground, vibratory ground (VG) and a sand-blasted surface were studied for helical gear teeth samples. Fig. 10 shows the samples for the different laser-processed sample categories.

Table 4. *Details for the different sample categories prior the laser processing.*

	Set 1	**Set 2**	**Set 3**	**Set 4**	**Set 5**	**Set 6**
Sample name	Gear teeth	Planet gear	Planet gear teeth	Helical gear teeth	PM samples	Induction hardened samples
Figure	10 A1)	10 A2)	10 B)	10 C)	10 D)	10 E)
Hardening method prior laser processing	Carburizing case-hardening	Carburizing case-hardening	Carburizing case-hardening	Carburizing case-hardening	Hardened	Induction hardening
Material	18CrNiMo7-6	18CrNiMo7-6	18CrNiMo7-6	18CrNiMo7-6	S790	34CrNiMo6, 42CrMo4
Surface condition	Ground	Ground, vibratory ground (VG)	Ground	Ground, sand-blast	Ground	Ground

Table 5. *Chemical composition of the 18CrNiMo7-6, S790 (PM40), 34CrNiMo6 and 42CrMo4 steels used.*

Wt -%	**C**	**Cr**	**Mn**	**Mo**	**Si**	**V**	**W**	**Ni**	**Ca**	**Fe**
18CrNiMo7-6	0.17	1.65	0.56	0.32	0.19	<0.01	-	1.52	0.0044	bal
S790	1.3	4.2	0.3	5.0	0.5	3.0	6.3	-	-	bal
34CrNiMo6	0.36	1.36	0.71	0.17	0.024	-	-	1.31	-	bal
42CrMo4	0.41	1.07	0.73	0.17	0.31	-	-	-	0.0036	bal

All of the processed gear teeth samples were manufactured from case-hardened gear steel 18CrNiMo7-6 (EN 10084). The laser-processed samples were detached from a planet gear and from a smaller helical gear by water cutting. The gears were carburizing case-hardened, tempered at 180 °C and normally ground prior to water cutting. Grinding was performed with a gear tooth grinding machine with an aluminium oxide grinding wheel with proper cooling fluid prior to the water cutting.

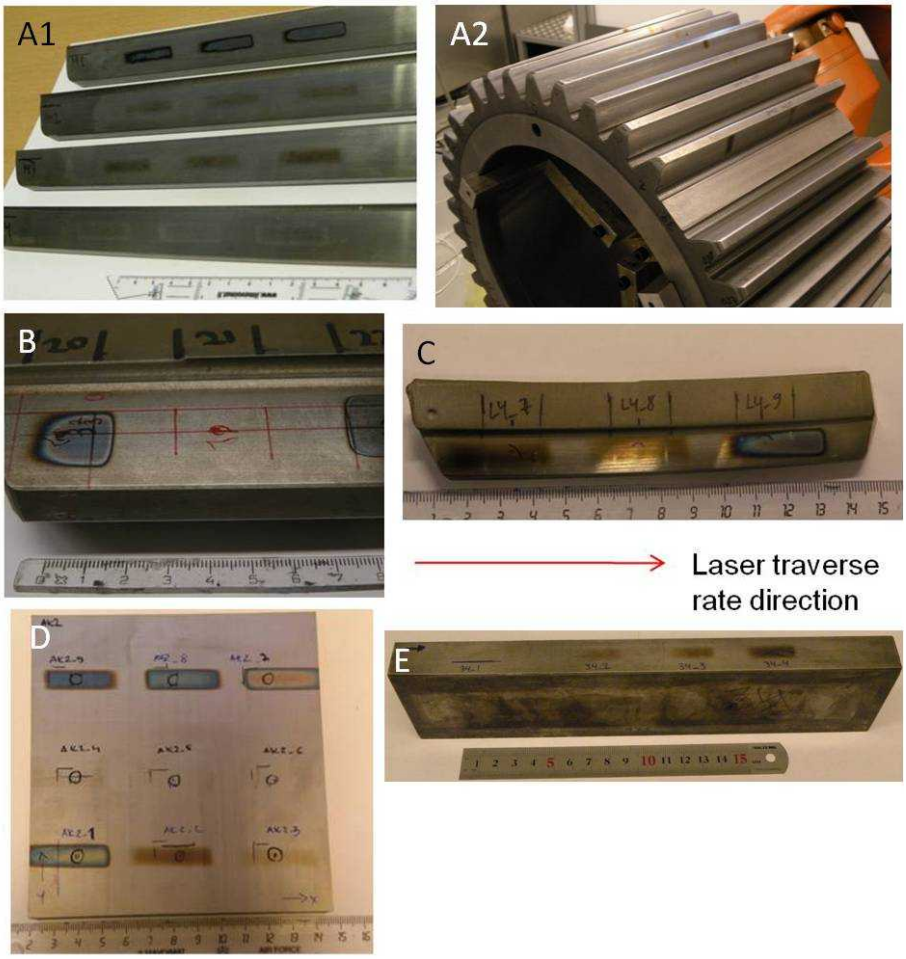

Figure 10. *The laser-processed samples; A1) detached gear teeth, A2) planet gear, B) detached planet gear teeth, C) detached helical gear teeth, D) PM sample block and E) induction hardened sample block. [III]*

Induction processing was performed on the planet gear teeth samples manufactured from case-hardened gear steel 18CrNiMo7-6 (EN 10084). The induction-heated teeth samples were detached from a planet gear.

6.1.3. Samples for stepwise loading and bending (*Publications V, VI*)

Two sets of samples were prepared for studying the effect of loading on BN responses.

1) The plate load test bars were machined from case-hardened steel 18CrNiMo7-6 (EN 10084). Table 6 presents the chemical composition of the studied steel. The test bars were rectangular with a length of 2400 mm and a width of 40 mm at the measuring point. The thickness of the test bars was 6 mm *(Publication V).*
2) The second set of samples was machined from RAEX400 low-alloy hot-rolled steel. Table 6 presents the chemical composition of the studied steel. The bending samples

were cut to a rectangular shape with a length of 300 mm, width of 30 mm and a thickness of 6 mm *(Publication VI).*

Table 6. *Chemical composition of the studied steels.*

Wt -%	C	Cr	Si	Mo	Mn	Ni	P	S	Ca	Cu	Fe
18CrNiMo7-6	0.21	1.57	0.20	0.27	0.65	1.45	0.016	0.029	0.0044	0.18	bal
RAEX400	0.14	0.9	0.2	-	1.2	-	-	-	-	-	bal

Heat treatments for the loaded samples

Both sample sets were first carburizing case-hardened and further tempered in order to modify the microstructural and residual stress state.

Carburizing case-hardening

1) Plate load test bars were carburizing case-hardened with 0.7 % carbon potential at 940 ºC for 20 hours after machining *(Publication V).*

2) The second set of samples were carburizing case-hardened in a vacuum chamber at 930 °C for 20 minutes to a case-hardening depth (CHD) of 0.8 mm. During the carburizing process the carbon potential of the furnace was adjusted to 0.8 %. The specimens were directly quenched in air. The hardening temperature of 930 °C was used to ensure a fully austenitic starting condition *(Publication VI).*

Tempering of the loaded samples

After the carburizing case-hardening, the samples were tempered in a tube furnace with different temperature-time combinations to modify the final microstructure and hardness. Table 7 shows the tempering procedure for set 1 samples. Two of the test bars, referred to as sand-blast, were first quenched into a salt bath then tempered and finally sand-blast. Table 8 shows the tempering procedure for set 2 samples.

Table 7. *The tempering procedures for the18CrNiMo7-6 samples.*

Procedure	Tempering temperature (ºC)	Tempering time (min)	Quench	Surface hardness (HV_1)
1.	180	90	Salt bath	710
2.	180	240	Air	680
3.	180	150	Air	700
4.	300	150	Air	600
5.	250	180	Air	620
6.	250	120	Air	650
7.	350	150	Air	560
8. sand-blast	180	90	Salt bath	720

Table 8. *The tempering procedures for RAEX400 samples.*

Procedure	Tempering temperature (°C)	Tempering time (min)	Quench	Surface hardness (HV_1)
Bulk sample	-	-	-	300
1.	180	60	Air	851
2.	160	60	Air	834
3.	200	60	Air	777
4.	225	60	Air	701
5.	275	60	Air	624
6.	300	60	Air	600
7.	250	30	Air	751
8.	275	30	Air	765
9.	300	30	Air	659
10.	630	150	Air	358

6.2. METHODS

At first the laser processing and induction processing used in this work to produce artificial flaws are introduced. Then, all the materials characterization and testing methods used in this work are explained.

6.2.1. Artificial flaw manufacturing

Laser processing *(Publications II, III, IV)*

Laser processing experiments were performed with a Nd:YAG (Yttrium aluminium garnet doped laser with neodymium ions) 4 kW Haas HL4006D lamp-pumped laser by heating up the tooth flank surface rapidly and allowing the component to cool freely in air. The wavelength of the Nd:YAG laser is 1.06 µm. The size of the top-hat profile laser beam on focus was roughly 8x12mm^2 in all experiments. The beam was moved along the sample surface for a distance of 20 mm. The laser optics distance from the surface of the laser-processed surface was 75 mm. The processing head and the laser beam were kept at 90° in relation to the tooth flank surface. Different laser processing directions on the tooth surface were studied: along the tooth surface, from the tip to the root or from the root to the tip. The studied laser processing directions are presented in Fig. 11. The laser processing arrangements for the two laser processing directions are presented in Fig. 12.

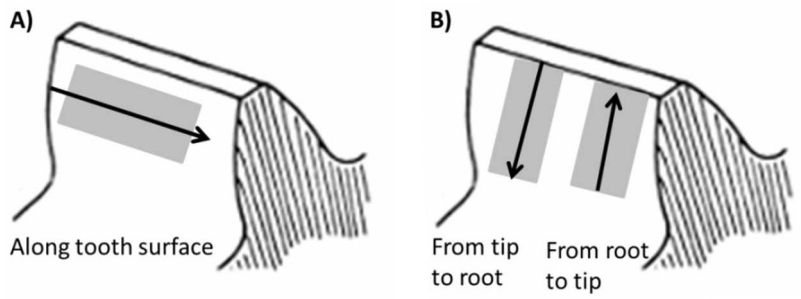

Figure 11. *Different laser processing arrangements on tooth surface. A) shows the laser processing direction along the tooth surface and B) shows laser processing directions from tip to root or from root to tip.*

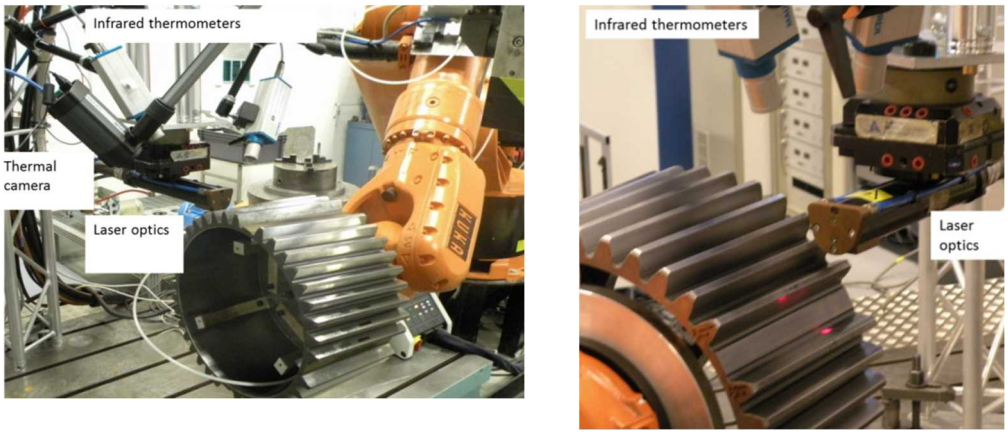

a) b)

Figure 12. *a) The planet gear in laser processing where the laser traverse rate direction is along the tooth axis, b) laser traverse rate direction along the tooth profile.*

Temperature measurements in laser processing (*Publications II, III, IV)*

The temperature of the laser beam irradiated area in laser processing was measured simultaneously with two infrared quotient thermometers Maurer KTR 2300-1 and Maurer QKTR 1075-1. These thermometers had different temperature measuring scales of 100-400 °C and 400-1100 °C, respectively. The temperature measuring frequency used was 0.125 seconds. The accuracy of the infrared thermometer was reported to be 1 % ± 1 °C by the device manufacturer [157] (*Publications II, III, IV).* In addition, a Flir A235 thermal camera was used together with infrared thermometers for surface temperature measurements for some helical gear samples and the PM samples *(Publication III).* The picture-capture frequency for the camera was 30 Hz and an emissivity value of 0.13 was used in the calculations for the samples. The emissivity value for the ground surface was provided by the device manufacturer. The accuracy of the thermal camera was reported to be ±2 % or ± 2 °C by the device manufacturer [158].

Induction heating for artificial grinding burn manufacturing (Publication II)

Induction heating was used to produce rapid thermal loads into the specimens, i.e. a varying degree of thermal damage was introduced. Temperature was controlled with temperature lacquers. Short interaction times for the surface heating processes were used in order to mimic the rapid heat production generated in grinding. Five different samples were heated with different target temperatures. The target temperatures of 200 °C, 300 °C, 400 °C and 500 °C were reached with a 1-second induction heating cycle and the target temperature of 600 °C was reached with a 3-second induction heating cycle. Each target temperature required a different heating time or heating power, so for each grinding burn mark a calibration power cycle was performed first. After the calibration power cycles, the actual burn marks were made on the teeth samples and the samples were allowed to cool freely in air after heating. The samples were manufactured by Trueflaw Inc.

6.2.2. Barkhausen noise measurements (*all publications*)

A Rollscan 300 Barkhausen noise analyser, manufactured by Stresstech Oy (Finland), was used to characterize all the studied samples. The BN measurements were recorded with MicroScan software, yielding different parameters calculated from the signal itself. The RMS value of the Barkhausen noise amplitude is commonly calculated from the signal. Table 9 introduces the measurement parameters for different sample categories. Normally, a magnetizing voltage of 4.3 vpp (voltage peak to peak) was used with a magnetizing frequency 125 Hz. In the analyses, the results were an average of 20 Barkhausen noise bursts filtered with a filter of 70-200 kHz. Each burst represents one half of the magnetizing cycle. For the case-depth samples, magnetizing frequency and voltage sweeps were performed with a various frequency and voltage parameters but the MicroScan measurements were performed with a frequency of 125 Hz and voltage of 7 vpp. Residual magnetism was measured from all the samples with a Residumeter II model EMUD2K meter manufactured by Electro-Matic Products Co. Electrical polishing using a Lectropol-5 apparatus, manufactured by Struers, with Struers A2 electrolyte, was performed on loaded sample sets prior to the BN measurements *(Publications V, VI)*. Uncertainties for the BN RMS measurements were assessed using an independent sample. The uncertainty was observed to be ± 6%.

Table 9. *Barkhausen noise measurement parameters for different sample categories.*

Sample categories		**Magnetizing frequency [Hz]**	**Magnetizing voltage [vpp]**	**Analysis frequency range [kHz]**	**Sensor**
Case-depth samples		20, 30, 60, ***125***	0-16, ***7***	70-200	S1-15-33-03, #5553
Samples for artificial grinding burn detection	PM-samples	30	4.3	70-200	S1-164-15-11, #5157
	Other samples	125	4.3	70-200	S1-164-15-11, #5157
Stepwise loaded and bend samples	Set 1: 18CrNiMo7-6	125	4.3	70-200	S1-164-15-11, #5157
	Set 2: RAEX400	125	8	70-200	S1-18-13-01, #4740

6.2.3. X-ray diffraction measurements (*all publications*)

Residual stress measurements

Residual stresses (RS) in all sample categories were measured with a portable Stresstech XStress 3000 X-ray residual stress diffractometer (XRD) (Stresstech Oy, Finland) introduced in Fig. 13 a). The system consisted of a goniometer, central unit and portable computer with the calculation program X3000.

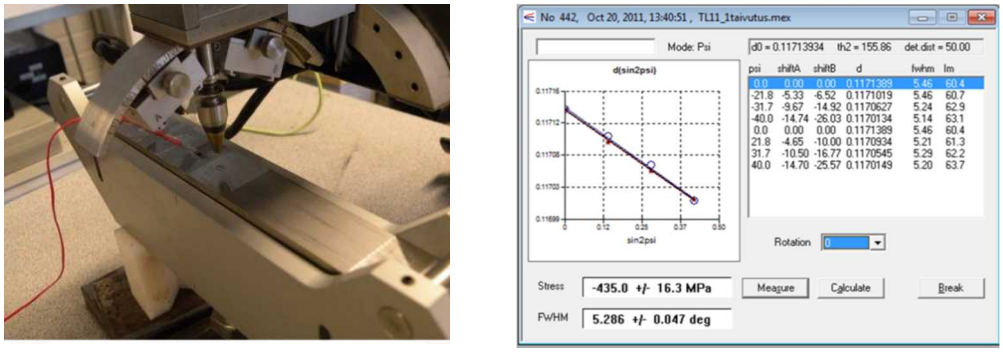

a) b)

Figure 13. *a) Bent sample under the X-ray diffraction XStress 3000 equipment. b) The slope of* $d/sin^2\psi$ *plot.*

The basis of residual stress measurement by X-ray diffraction methods is to measure the spacing of the lattice planes that are affected by the stress. Lattice plane spacing changes in the grains from a stress-free value to some new value that depends on the magnitude of the stress. The diffracted X-rays from the atoms of a crystal plane are amplified by each other and form a diffraction peak at the angles where the Bragg law, equation (7), is fulfilled. The Bragg law gives the conditions necessary for diffraction to occur and is the fundamental basis of the X-ray diffraction theory. Only the grains which fulfil the Bragg condition reflection, will contribute to the measured diffraction. Two or more scattered X-rays will be in phase and amplify each other only if the path difference is equal to a whole number of wavelengths which is defined in equation 1. The Bragg law may be written in the form [159]:

$$2d_{hkl}sin\theta = n\lambda \tag{7}$$

where d_{hkl} is the distance between hkl lattice planes, θ is the diffraction angle, λ is the wavelength of the X-ray radiation and n is an integer constant (1,2..). Strain obtained with X-ray diffraction will be the average strain acting in the sampled grains. Fig. 14 illustrates the diffraction of X-rays by the crystal lattice. The incident X-rays with a certain wavelength λ and at an angle θ are diffracted from those grains that fulfil the Bragg condition introduced in equation 7.

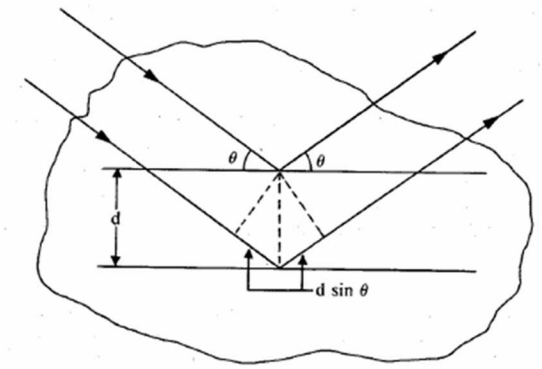

Figure 14. *Diffraction of X-rays by a crystal lattice [160].*

When stressed elastically, the lattice spacing of a crystalline material varies in relation to the orientation of the lattice planes and in relation to the stress direction. The elastic strain results in a change in the atomic lattice dimension and this dimension change can be measured by diffraction methods. With applied tensile stress, the lattice spacing will increase for the planes perpendicular to the direction of the applied stress and decrease for planes parallel to the direction of the applied tensile stress. The elastic strain of the crystal lattice can be calculated from the measured diffraction peak position when the lattice spacing in the stress-free condition d_o is known, as demonstrated by equation (8).

$$\varepsilon = \frac{d-d_0}{d_0} \tag{8}$$

where ε is the strain, d is the lattice spacing in the stressed specimen and d_o is the spacing from stress-free calibration powder. The obvious drawback of this approach is the need for calibration powder.

RS measurements were performed with the Chi method [161]. The principle of the measurement was that the interplanar lattice spacing of ferrite [211] plane can be calculated using the Bragg's law from the reflections from the 156° Bragg diffraction angle. The modified chi method is the most commonly used method of the X-ray diffraction technique with portable goniometer having detectors for stress determination. In the modified chi method, lattice spacing d of the sample is measured at different ψ tilts. Angle ψ is the angle between the normal of the sample and the normal of the diffracting plane. Normally four to six tilts are taken. The residual stress can be calculated with the elastic constants and the slope obtained from a plot of the lattice spacing d as a function of $\sin^2\psi$ that is introduced in Fig. 13 b). The stress can be calculated from the equation [162]

$$\sigma = \left(\frac{E}{1+\nu}\right) m \tag{9}$$

where σ is the stress in the measuring direction, E is the Young's modulus, ν is the Poisson's ratio and m is the slope obtained from the lattice spacing d vs. $\sin^2\psi$ curve. This technique for plane-stresses does not require the exact knowledge of the unstressed lattice spacing because the lattice spacing is a linear function of the $\sin^2\psi$. The interception of the zero value of $\sin^2\psi$ equals the unstressed lattice spacing. [163]

Inclined measurements were made at four different tilt angles. The measurements with the XStress 3000 stress analyser were conducted with a collimator of 3 mm, operated with 30 kV voltage, 6.7 mA current and CrKα radiation. CrKα radiation was selected as it gives a measuring depth of 5-6 μm [164]. Measurements from all the samples were done along the φ-directions of 0° and 90° corresponding to longitudinal and transverse directions in relation to sample surfaces. In addition to the residual stress values X-ray diffraction peak FWHM values were also determined.

The diffraction peak combines information of X-rays that are scattered from many individual atoms from different grains. A diffraction peak shift results from the change in lattice spacing over a uniform irradiated volume. Uniform microstresses and macrostresses have an influence on the lattice spacing and cause the shift of the diffraction lines to new 2θ positions [159]. X-ray diffraction peak broadening is detected when a non-uniform micro stress, caused by crystal defects such as dislocations and vacancies, produce local variation in the lattice spacing. Due to non-uniform microstresses, the lattice spacing is varying in adjoining regions of the grain area.

The observed peak is broadened because these regions in one grain with varying lattice spacing produce several diffraction lines at different 2θ values [159]. Peak broadening is associated with the martensite structure; in the hard martensite structure the FWHM value is higher. Peak broadening can be detected from the FWHM value calculated from the X-ray diffraction peak.

For the XRD residual stress measurements the instrument-operator uncertainty was observed to be ± 2 %. The uncertainty value was calculated from the repeated measurements as Fitzpatrick *et al.* suggested [162].

Retained austenite measurements *(Publication VI)*
Retained austenite measurement with CrKα radiation was performed on the hardened sample prior to tempering (VI) by the four-peak method with XRD by comparing the intensities of diffraction peaks arising from the different phases. The amount of retained austenite can be calculated from the integrated intensity ratio of two austenite lines ([200] at a diffraction angle of 80° and [220] at a diffraction angle of 130°) compared with the integrated intensity ratio of the ferrite lines ([211] at a diffraction angle of 106° and [200] at a diffraction angle of 156°).

6.2.4. Microstructural characterization

Optical and electron microscopes were used for the characterization of samples. The microscopes used in the study are described below.

Optical microscopes
Two optical microscope systems were used: Nikon Eclipse MA100 and Leica DM 2500 M (Leica Microsystems, Switzerland) in the examination of polished and etched microstructures (*Publications II, V).* Samples were prepared by grinding them with 320-4000 SiC papers and then by polishing with a 3µm diamond suspension. The etching procedure was performed with 4 % Nital (*Publications II, V).*

Scanning Electron Microscopes (SEM)
The structures of the samples were characterized using a scanning electron microscope (SEM, Philips XL30). The structures were analysed from etched metallographic cross-sectional samples. Samples were prepared by grinding them with 320-4000 SiC papers and then by polishing with a 3µm diamond suspension. The etching procedure was performed with 4 % Nital (*Publications II, V).* More detailed microstructure characterization was done using an ultra-high resolution field-emission scanning electron microscope (FESEM, Zeiss ULTRAplus). Metallographic cross-section samples were prepared using the same procedure as for SEM samples. The sample surfaces were cleaned with Emitech K1050X plasma cleaner prior to the microscope studies *(Publication III, V).*

Optical profilometer
The surface roughness of the laser-processed samples was characterized using the Wyko NT 1100 optical profiling system with a magnification of 2.5x. Vision software was used for data processing.

Surface roughness measurement device
Surface roughness was measured with a Mitotoyo SJ-301 device. The measurement length was 0.8 mm *(Publication III).*

6.2.5. Mechanical testing

Microhardness measurements

Hardness measurements were performed with a Duramin-A300 (Struers) hardness testing device with a load of 1 kg (RAEX400). A Matsuzawa MMT-X7 microhardness tester using indentation loads of 100 g and 1000 g was also utilized. The verification of the hardened layer thickness (*Publication I)* was performed with a hardness depth profile according to the standards [129, 130]. For induction-hardened samples, the value of the case-depth (Rht) is defined as the depth below the surface at which the Vicker's hardness value drops to 400 HV [130]. For carburizing case-hardened samples the case-hardening depth (CHD) is determined as the distance where hardness drops to 550 HV (50 HRC) measured with $HV_{0.1}$, HV_1 or HV_5 [129]. In addition, microhardness depth profiles were performed with an Anton Paar microhardness tester attached to a Philips XL30 scanning electron microscope using a load of 20 g *(Publications III, IV).*

Mechanical loading

Sample loading: bending (Publication VI)

Tempered samples were subjected to four-point symmetrical loading. A sample in the bending apparatus is shown in Fig. 15 a). In this four-point bending system, two load applicators, which are evenly spaced from the support, are used. Fig. 15 b) shows the load as a function of the sample position in four-point bending.

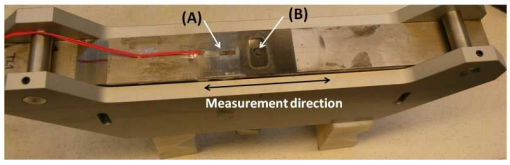

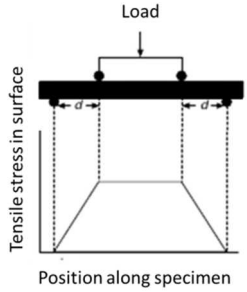

a) b)

Figure 15. *a) The experimental setup for bending. (A) indicates the location of the strain gage and (B) the location of the XRD stress and BN measurements. b) The load as a function of the position along the specimen surface. [IV]*

The load was applied to the specimen in increments by turning the adjustment screw manually with a fork spanner. After each load increment, the BN and surface residual stress measurements were carried out for each loading stage. After each load increment the specimen was unloaded before the next load increment. The measurements were performed in the purely elastic deformation range. The strain gage signal was recorded simultaneously with the bending and the strain was calculated with [165]

$$\varepsilon = \frac{2}{g}\frac{C}{Cv}u \qquad (10)$$

where the term C/C_v determines the calibration coefficient of the strain gage amplifier. C is the calibration output voltage value, C_v is the calibration voltage, u is the measured voltage and g is the gage factor. The measured voltage change due to the strain in the strain gage is Δu. In the tests, C was $2000 \cdot 10^{-6}$, C_v was 1 V and the gage factor g was either 2.11 or 2.08 depending on the strain gage series used. The stress on the surface was calculated with equation (11) from the measured strain gage readings. In (11) E is the Young's modulus, 204 GPa, for the studied steel.

$$\sigma = E\varepsilon \tag{11}$$

Sample loading: Uniaxial stepwise tensile and compression loading (Publication V, VI)

The plate load test samples from the 18CrNiMo7-6 material and from RAEX400 were used in the loading tests. A representative set of bending-tested specimens were loaded with a servo hydraulic material testing machine (*Publication VI).* The Instron 8800 testing equipment subjects the test-piece to a uniaxial elongation and the resultant load can be recorded. The test-pieces were rectangular in cross-section. The stress σ can be calculated by dividing the load F by the cross-sectional area A.

$$\sigma = \frac{F}{A} \tag{12}$$

The loading sequence is shown in Fig. 16 (*Publication VI).* During each loading step the load was kept constant while performing the BN measurements. The measurements were carried out at angles of 0° (LD) and 90° (TD) (*Publication VI)* and at angles of 0° (LD), 30°, 45°, 60° and 90° (TD) (*Publication V).* The load range varied from – 100 MPa to 250 MPa and was kept below the yield strength of the steel. The maximum compressive stress was limited because of the risk of buckling.

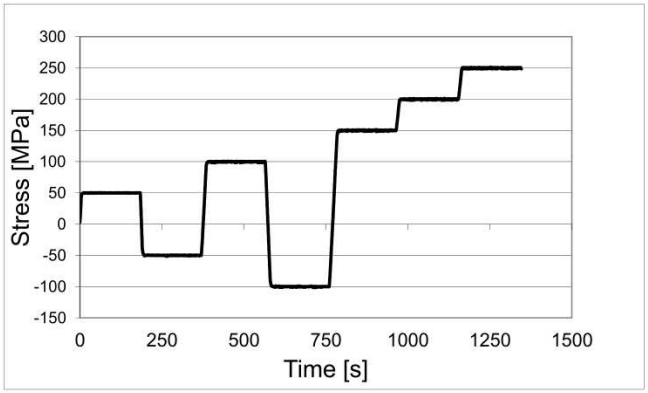

Figure 16. *The loading sequence for uniaxial stepwise tensile and compression loading with 180s holding time. (Publication VI)*

Strain measurements in bending and stepwise loading (Publication VI)

The strain measurements during the bending and uniaxial stepwise loading were performed with strain gages. They were mounted with epoxy on the test specimens in the longitudinal direction of the sample in order to measure the strain in the applied stress direction. The one-axial 5-mm-

long strain gages were manufactured by Kyowa. The model used was a KFG-5-120-C1-11L1M2R with gage factors of 2.11 or 2.08. The change in the resistance of the strain gage was measured with a quarter Wheatstone bridge that converts the resistance change to the relative voltage change. This signal was recorded and amplified with a Kyowa amplifier. The Kyowa amplifier was calibrated using the inner calibration operation of the equipment. The calibration of the setup was verified by tensile loading one sample with the servo-hydraulic materials testing device Instron 8800 (Instron).

7. RESULTS AND DISCUSSION

The aim of this study was to get more detailed information about Barkhausen noise when characterizing hardened surfaces, the effect of heat treatment, thermal damage and the effect of stress. The results and discussion chapter is divided into three sections, presenting the results of the different areas studied. Firstly, BN magnetizing voltage sweeps for case-depth determination are introduced. Secondly, the calibration samples for BN measurements are discussed. Finally, the effect of stresses on tempered surfaces is introduced. The characterization of samples in all cases was performed mainly by BN measurements, X-ray diffraction and destructive characterization methods. In the following section, the main results of the attached six publications are presented and discussed.

7.1. Barkhausen noise voltage sweeps for case-depth determination [*Publication I*]

Non-destructive case-depth determination is difficult and therefore development of a reliable method would have a high usage in the heat treatment industry. A new approach to the Barkhausen noise case-depth studies was taken by measuring magnetizing voltage sweeps (MVS) with a varying magnetizing frequency from hardened samples with Rollscan 300 equipment. The calculated slope of the MVS curve changed as the magnetizing voltage was increased, indicating an increase in the value of the applied magnetic field, as shown in Fig. 17 a). The slopes were calculated for each voltage sweep by fitting a first order polynomial to 25 consecutive data points. The MVS curve created this way can thus be correlated to the hysteresis curve and the slope value calculated from the MVS curve to the permeability or susceptibility value calculated from the hysteresis loop. Both of these values, permeability and susceptibility, characterize the magnetic behaviour of the material when the ferromagnetic specimen is exposed to a magnetic field. According to the literature, the reciprocal initial susceptibility has a linear behaviour with respect to the applied tensile stress [166]. The permeability calculated from the slope has been found to be influenced by the magnetic domain coupling and also by the domain density [167]. The magnetizing frequency value determines partly the depth from which the measured information comes [168]. Thus MVS performed with different frequencies can give information from different depths. The use of two different magnetizing frequencies in the MVS gave information about the compositional gradient layer influenced by the microstructural features and also about the residual stresses. The MVS behaviour showed a systematic change with respect to surface hardness and residual stress values. [I]

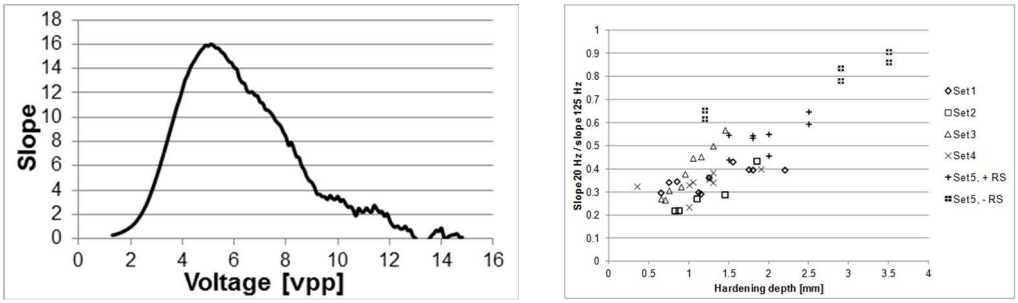

a) b)

Figure 17*. a) The slope calculated from MVS as a function of voltage. [I] b) The division of 20 Hz MVS slope with 125 Hz MVS slope studied sample sets 1-5. –RS denotes compressive residual stresses and +RS tensile residual stresses. [I]*

It was observed that no conclusions could be drawn from the MVS slope values carried out with one magnetizing frequency value in comparison with case-depths [I]. To analyse the sweeps, the maximum slope values were determined and compared to case-depths. Correlation coefficients between the case-depths and the refined slope information obtained with different magnetizing frequencies were calculated. The maximum correlation was found for the slope division for magnetizing frequencies of 20 Hz and 125 Hz, as given in Fig. 17 b). The slope ratio was correlated to the hardening depths of all sample sets, including both tensile and compressive residual stress of carburizing case-hardened samples. This frequency range was the widest frequency range studied, i.e. the measurement depth range was also the widest. In addition, higher correlations were observed if they were calculated only for one set at a time [I], as shown in Fig. 18 b) for set 3 samples.

Hardening heat treatments result in both a microstructural and a residual stress gradient in the surface layer of the hardened component [169]. This gradient also affects the magnetic properties and thus produces an observable gradient in the measured magnetic features. Many studies have discerned that hysteresis measurement features such as coercivity [58] and permeability [59] are dependent on the case-depth. The BN method could be more sensitive to changes in this gradient than the actual signals coming from the soft core and the hard case. Thus the division of the slopes created with two different magnetizing frequency values shows the magnetic gradient defining the hardening depth.

In order to utilize the information obtained about the relationship between the calculated slope and the hardening depth, the regression line together with the calculated upper and lower confidence limits was identified as shown in Fig. 18 a). The confidence interval can be used to indicate the reliability of the regression line. The confidence limits show the range where the identified line is located with a probability of 95 %. This means that, with certain measured slope division values, it is possible to estimate that the hardened layer thickness variations are within a range of certain limits with 95 % probability [I]. When one separate sample set, set 3 as shown in Fig. 18 b), was studied, this set was observed to create a precise correlation of the division between slope and the hardening depth [unpublished]. Set 3 samples were manufactured from the same material and with the same process device. In conclusion, even taking into account many different sample sets the MVS slope ratios led to high correlations, 0.86, when compared with the case-depth values [I].

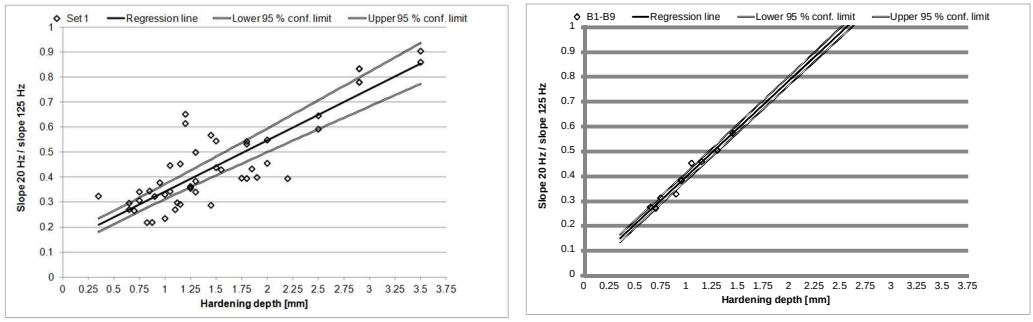

a) b)

Figure 18. *a) The 95 % confidence limits calculated for division of 20 Hz and 125 Hz slope for sample sets [I]. b) The 95 % confidence limits for sample set 3 [unpublished].*

Usually case-depth studies using the BN method rely on the two-peak behaviour of the BN signal envelope. However, in this study only a single peak envelope was observed with a commercial Rollscan 300 measurement device [I]. Different explanations for the observed two-peak behaviour have been introduced, e.g. a different pinning strength of the obstacles (or two phases [73]) are said to produce separate peaks. Thus similar data processing, e.g. studying the effect of two peak ratios, could not be analysed in this study because of the lack of the double peak.

Previous BN studies concerning case-depth measurements have concluded that the case-depth can be reliably estimated down to 1 mm [62]. However, the magnetizing frequencies used in this study are not low enough to produce a signal from the soft core of the hardened samples too, thus the data observed comes from the microstructural gradient of the case [I]. Here it was established that by studying magnetizing voltage sweeps it is possible to evaluate the compositional and microstructure gradients referring to case-depth values deeper, even down to 3 mm. Furthermore, it could be worth studying these same samples with some BN equipment similar to those used in two-peak studies. Thus the possible occurrence of double peaks could be detected.

7.2. Calibration samples for Barkhausen noise measurements [*Publications II, III, IV*]

The need for suitable calibration samples for grinding burn detection with BN measurements has emerged. Two possible methods, induction heating and laser processing, were studied, both of which create controlled thermal damage [II]. The sample sets consisted of hardened samples that were further processed by laser and induction to create a restricted tempering area where hardness values had been decreased and surface residual stress values had been changed compared to the original hardened surface. Laser processing was found to be a more suitable method for producing this kind of controlled thermal damage [II]. Therefore, the best laser processing layout, parameters and proper surface treatment for repeatable results were sought [III]. Laser processing has been used earlier [29, 30, 31] for creating thermal damage, but the studies did not concentrate on the actual laser processing itself.

The laser processing outcome can be evaluated by studying the BN responses, the RS and surface hardness measurements and also the obtained temperature profile [II, III]. The temperature profile can reveal if the laser absorption has changed during processing and verify the outcome and repeatability of the process itself.

7.2.1. Laser processing of calibration samples for BN

Laser parameters

Surface temperature control of laser processing can be done by adjusting the laser parameters: the beam power, laser traverse rate and diameter of the laser beam [33]. In this study, the laser input power and laser traverse rate were varied to obtain different surface temperatures. A central composite experimental design (CCD) was used to provide a series of different parameter combinations with a small number of experiments. First the upper and lower limits for both varied features were determined. For example the laser input power was varied between 520 W and 1310 W and the traverse rates between 3 mm/s and 14 mm/s for helical detached teeth samples [II]. It was noticed that both of these varying features need to be optimized to avoid excess surface heating and re-hardening of the microstructure or considerable changes in the tensile residual stresses leading to the saturation of the BN signal [II]. Klocke and Goergels [29] found in their studies a similar phenomenon in that the BN level increased as a function of increasing laser power, but after a certain threshold, in this case an input power of 1500 W, the BN response started to decrease due to the re-hardening phenomena. Fig. 19 presents a framework for optimal laser processing parameters for ground planet gear wheel teeth with the laser direction along the tooth surface. For these particular samples the optimal laser power was observed to be 950-1000 W and the optimal laser traverse rate for achieving meaningful changes in the RMS results was from 5 mm/s to 9 mm/s. For these optimal laser parameters, the compressive residual stress stage was observed to have changed into tensile residual stress after heating of above temperature 300 °C [II]. It was noticed that even a surface temperature of 300-400 °C would change the RMS value meaningfully. Too high a temperature can cause the residual stress change to become too large and create a decrease in the BN signal. Thus the temperature range of 300-400 °C produced sufficient variation in the samples. The limits of the laser parameters were noticed to be different in each separate case when the surface appearance changed, e.g. the vibratory ground surface with a matte appearance was noticed to require lower laser input power values for similar surface temperatures to the ground surface [III].

The different laser traverse rates produce different heat interaction times in the heating zone, thus a longer interaction time provides an opportunity to produce more changes in the microstructural and residual stress state than a shorter interaction time. When heating to higher temperatures, the residual compressive stresses relax and turn into tensile stresses. Simultaneously hardness decreases. Both these factors facilitate the movement of the domain walls under lower magnetizing values.

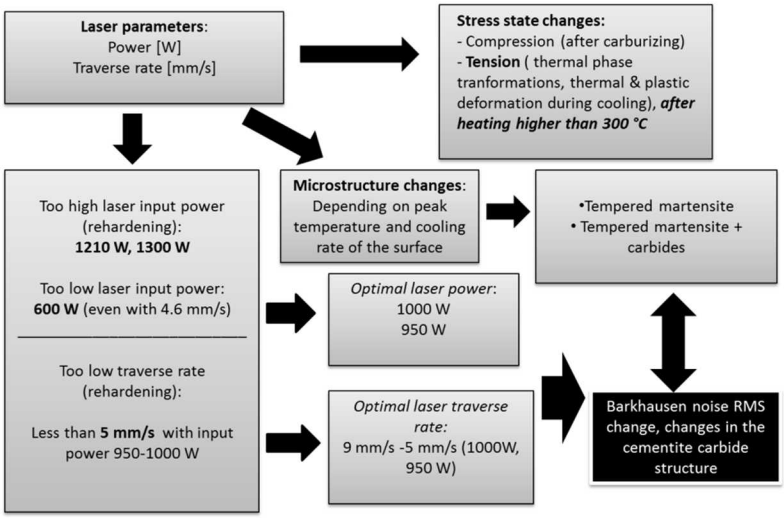

Figure 19. *The chart of optimal laser parameters for a ground planet gear surface with the laser direction along the tooth surface.*

As introduced in the Methods section in Fig. 11, different laser processing layouts with different laser optics traverse directions were studied. The laser traverse direction along the tooth surface [II] produced laser marks at the halfway point of the tooth profile. The temperature profiles showed that laser processing in this direction in ground helical tooth samples produced an even temperature distribution [III]. In addition, the processed area was uniformly thick, so theoretically there should not be changes in the heat conduction behaviour of this laser mark area.

The laser processing direction along the tooth profile needed more adjustment of the laser head, because if the laser hits the edges of the samples (the tip of the tooth or bottom of the tooth), a change occurred in the absorption and the surface temperature was observed to change [unpublished]. In addition, the curved surface may create some changes in the trajectory of the laser head that has an influence on the incident angle between the laser and the surface. This causes changes in the absorption behaviour as the Brewster angle, giving the highest local absorptance levels, is not always used or met [32]. For the case of the laser traverse direction along the tooth surface, the angle and distance of the laser head could be kept equal more precisely due to the geometry of the tooth.

Repeatability of the laser processing

Repeatability of laser processing is said to be good as long as the absorption of the laser beam by the surface is constant. It was noticed, e.g. from the temperature profiles, that changes such as darker grooves in the ground surface produced different absorption condition in the laser beam. Therefore, a surface treatment that makes the surface uniform looking and less reflective would be useful for reliable laser processing.

Temperature measurement results

Two methods were used to measure the surface temperature: a thermal camera and an infrared (IR) quotient thermometer [III]. The disadvantage for the utilization of the thermal camera is that the emissivity of the surface needs to be known in advance. The IR quotient thermometer was calibrated with a heated sample and a thermocouple. The exact determination of emissivity for the thermal camera was difficult [III] because the emissivity coefficient is also a function of

the temperature. In addition, the temperature measurements carried out with the thermal camera were noticed to have decreased temperature values in comparison with those obtained with the IR quotient thermometer [III]. This IR quotient thermometer was observed to be more suitable for temperature measurements in laser processing due to the easier calibration procedure and the fact that exact emissivity coefficient of the surface is not needed. [III]

Different studied samples

Several experimental series of laser-processed samples were manufactured and studied. In addition, the effect of the surface condition on laser processing was observed. The sample sets consisted of hardened samples that were further processed by laser processing to create a restricted tempering area where the hardness values had been decreased and the surface residual stress values had been changed compared to the original hardened surface. All other studied materials were steel grades used in gear manufacturing apart from powder metallurgically manufactured S790. Different sample geometries were studied: detached teeth from gears (helical gear and planet gear) and whole planet gear teeth. In addition flat hardened samples were studied [III]. The sample shape mainly affects the programming of the trajectory of the laser head optics. The sample geometry was also noticed to affect the usability of the process, for the laser direction from tip to root or from root to tip laser processing could be performed only on a whole gear if the tooth next to the processed one was removed [unpublished]. Laser processing was applicable for all the studied materials [III]. However, the parameters need to be optimized according to the sample surface and its absorption of the laser beam.

The effect of surface condition to laser processing

Laser absorption into a sample surface depends on many factors e.g. surface roughness and oxide layers [32]. One of the aims in this study was to find a suitable surface finish for laser processing. The optimum calibration sample is similar to the one that is normally measured, thus a ground surface was first used to demonstrate the laser processing method [II]. As is generally known, the reflectivity of metals is known to be high, meaning that little of the incident light is absorbed by the material [32]. As a result, some tests reducing the surface reflectivity with sandblasting and vibratory grinding were carried out [III].

Grinding of gears results typically in a surface with an arithmetic average roughness height value (Ra) of about 0.8 µm. Thus, the ground surface can be considered as optically smooth to a Nd:YAG laser used with a wavelength of 1.06 µm [32]. In addition, the Nd:YAG laser beam was considered to be circularly polarized and thus the beam was symmetrical in relation to the optical axis.

Bommi *et al.* [40] worked on the surface modification of steel surfaces prior to laser hardening. They used sand-blasted and black painted surfaces on laser hardening and noticed that the sand-blasted surface produced a better laser processing outcome. However, their study cannot be compared directly with the experiments done in this work because the surface temperatures in hardening are much higher than in laser tempering [40].

The topographies of these laser-processed surfaces were studied by FESEM and an optical profilometer; the images from the FESEM studies are presented in Fig. 20. The surface roughness values obtained with the optical profilometer for ground, vibratory ground, mildly sand-blasted and roughly sand-blasted teeth pieces were: 0.8, 0.6, 1.2 and 1.6 µm, respectively. The ground surface was observed to have the largest surface directionality due to the grinding wheel marks. Sandblasting and vibratory grinding, on the other hand, produced a more random surface appearance with deep scratches.

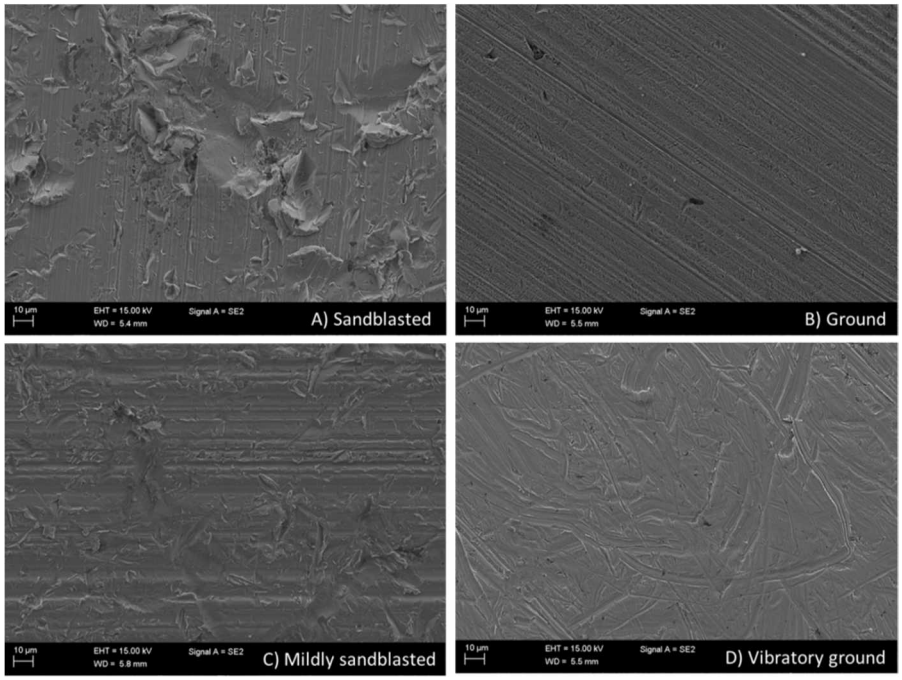

Figure 20. *FESEM micrographs of different surface treatments prior to laser processing, A) sandblasted, B) ground, C) mildly sandblasted and D) vibratory ground. [III]*

Vibratory grinding was found to create more changes (mechanical deformation) to the tooth tip area in the case of a whole gear. This more extensive deformation was noticed to cause an increased temperature in the tip area when using the laser direction along the tooth profile [II]. The ground surface did not exhibit similar altered temperature behaviour [II].

BN features vs. temperature

The goal for laser processing was to produce a surface temperature that causes observable changes in the RMS value compared to RMS values measured in the original hardened state. The change in the measured values was calculated by subtracting the value prior to treatment from the value after the treatment. Fig. 21 presents the relationship between changes in the RMS value and changes in the residual stress value as a function of the treatment temperature for induction- and laser-heated samples [II]. The laser-processed samples were divided into two groups, ground planet gear and ground helical gear samples, referring to the size of the samples. It can be seen that the change in the RMS value increased substantially with temperatures over 300 °C for the planet gear samples and helical gear samples. A surface temperature increase up to 300-400 °C for planet gear samples was enough to produce meaningful changes compared to the original RMS values. Thus, the laser processing parameters can be chosen in a way that the temperature is limited to 400 °C to produce meaningful changes.

The saturation and decrease of the BN signal as a function of the RS of the helical gear samples can be seen in Fig. 22 a). For the helical gear samples, a residual stress change of 900 MPa from the pre-treatment value of -600 MPa to +300 MPa was observed to cause the BN signal to saturate. When heated further, rehardening occurs as seen in the decreased RMS values. A similar decrease and saturation of BN signal with applied high tensile stress has been found in other studies [74, 105]. This complicated phenomenon can be explained in many ways according to Cullity [53]. The main factor influencing this behaviour is the fact that tensile

stress affects the magnetostrictive coefficient, making it negative and thus influencing the BN amplitude. Both the applied magnetic field strength and applied stress induce the magnetostriction to change. [53]

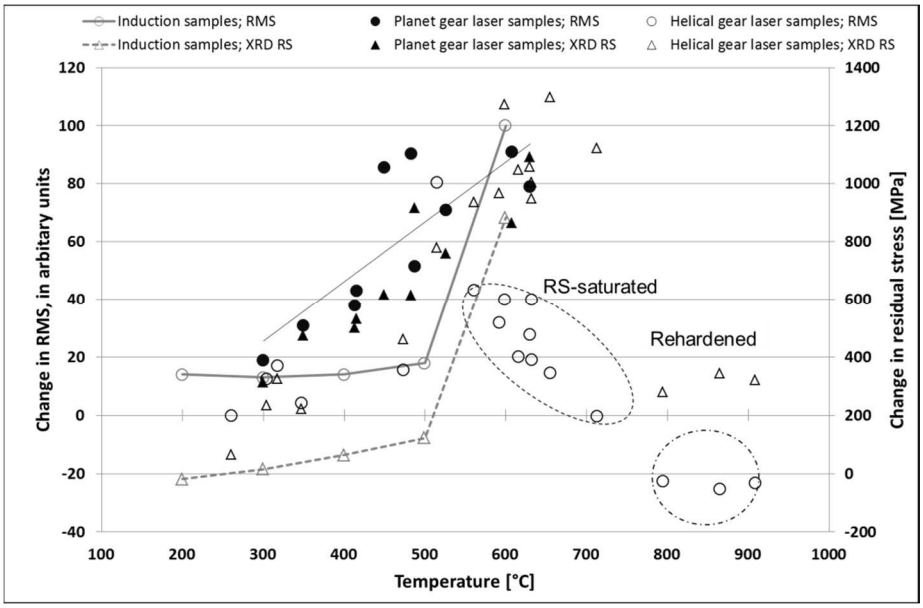

Figure 21. *The relation between the change in RMS, surface temperature and change in residual stress for induction samples, planet gear and helical gear laser samples as a function of heating temperature [II]. The residual stress saturated and rehardened samples are marked separately.*

Several parameters extracted from the BN signal can be used to characterize the magnetic response to changed microstructure and stress, among which the peak position, which was also studied in the case of laser-processed samples. The peak position value was noticed to decrease as a function of increasing surface temperature above 350 °C while the peak position value was more or less constant for samples heated up to 300 °C [II]. This constant value means that similar magnetizing current values can overcome the obstacles i.e. the pinning strength of the pinning sites in laser-processing does not change until the surface temperature of 350 °C. This could stand for the fact that, in this case, the dislocations are the only obstacles for domain wall motion and residual stress remains compressive.

Moorthy *et al.* [70, 75] have studied the effect of tempering on the BN peak position value. In these studies concerning increased tempering temperature and different tempering times, the peak position value was found to decrease as the temperature increased. In addition, a peak position increase was found in over-tempered samples [55]. However, these studies [55, 70, 75] cannot be compared directly because laser processing produces only short heating and the interaction time is short so there is no time for diffusion-based changes in the microstructure to occur as they can with longer tempering times.

Residual stress changes

An important part of the evaluation of laser processing is the residual stress measurement from the sample surface. The change in residual stress was measured in two perpendicular directions,

namely along the tooth axis (the same measurement direction as in the BN measurements) and along the tooth profile. The change in residual stress was calculated by subtracting the value prior to treatment from the value after treatment. The residual stress values prior to laser processing were observed to be somewhat different in the two measured directions; the correlation coefficient describing the relation of two variables, was from 0.2 to 0.51 in all sample categories, meaning that there were notable variations in the measured RS values prior to the laser processing [III]. However, after laser processing, the correlation coefficient for the changes in residual stresses was from 0.73 to 0.98 in all the studied sample categories. This means that laser processing produced uniform changes in RS values in both measured directions. In addition, the absolute residual stress values measured after laser processing for the two different directions produced correlation coefficients of 0.94-0.99 depending on the sample category, except for samples that were laser-processed along the tooth profile, which had a correlation of 0.58. This low correlation indicates that laser processing along the tooth profile produced an uneven distribution of measured RS values in two perpendicular measurement directions [III]. Fig. 22 a) presents the relationship between the surface residual stress and RMS for planet and helical gear samples, laser-processed in the direction along the tooth profile in absolute values. The relationship between the residual stress and temperature is presented in Fig. 22 b). The relationship between RMS and residual stress is linear for both studied sample sets. The residual stress values increased with an increasing RMS value. In addition there was some more scatter in the RMS values for helical gear samples.

Balart *et al.* [15] studied the effect of grinding temperature on the residual stresses of four different hardened steels. For example, for steel grade En31 the critical temperature for producing tensile residual stresses in the surface layer was 200 °C [15]. For the studied planet and helical gear samples, tensile stresses were generated in the surface layer at 300 °C for planet gear samples whereas helical gear samples needed a higher temperature, over 400 °C. This difference might be due to the different pre-treatment residual stress levels. The pre-treatment RS values of the helical gear samples varied between -500 and -600 MPa whereas the planet gear samples RS values varied between -300 and -400 MPa. Also the effect of mechanical loading in the grinding can be one reason for the difference. In addition, the temperature range of the two infrared quotient thermometers changed at 400 °C.

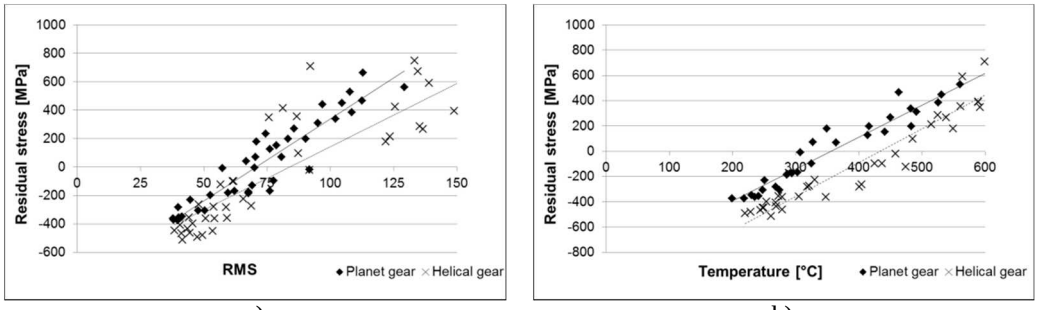

a) b)

Figure 22. *a) The relation in absolute values between the surface residual stress and RMS for planet and helical gear samples laser-processed in the direction along the tooth profile. [Unpublished] b) The relation between the residual stress and temperature in laser-processing for planet and helical gear samples laser-processed in the direction along the tooth profile. [Unpublished]*

Response surfaces were identified by mapping the results of the laser-processed planet gear samples for qualitative analysis as presented in Fig. 23. Modelling of residual stress changes

[IV] showed that the response surface of the change in residual stresses as a function of temperature and laser power was almost linear for the laser-processed planet gear samples. In addition, the quantitative analysis of the residual stresses showed that the correlation of the predicted and measured residual stresses is 0.956 [IV]. This means that the residual stresses created in laser-processing could be predicted by samples having a similar response to laser-processing.

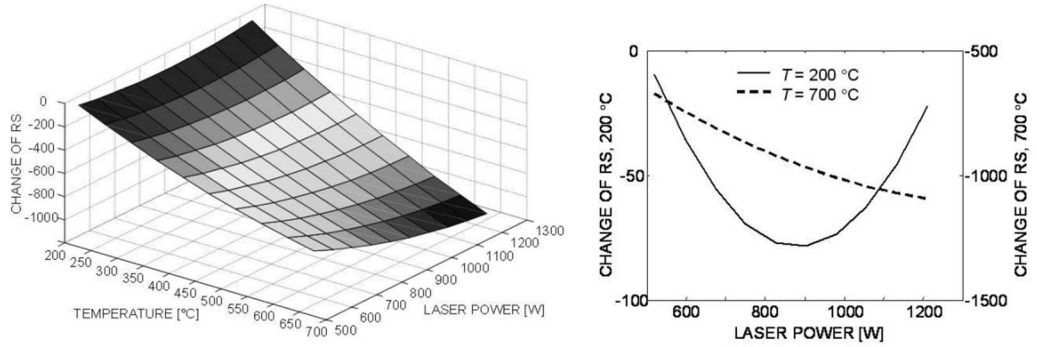

a) b)

Figure 23. *a) Response surface of the change in residual stress as a function of temperature and laser power. [IV] b) Close up from curves at temperatures of 200 °C and 700 °C.*

Microstructural changes

Scanning electron micrographs taken from six laser-processed planet gear samples are shown in Fig. 24. The reference sample was carburizing case-hardened and tempered steel with a surface hardness of 660 HV_1, residual stress of -320 MPa and BN RMS of 42. The reference sample microstructure was verified as martensite. The temperatures from 307 °C to 416 °C produce structures that can be detected with RMS values of up to 83. Laser processing produces a short heating and cooling cycle with just 1.5-2.4 s cooling from the peak temperature to a temperature of 100 °C. Therefore, the changes that can be seen in the micrographs are minor and ε-carbides, which are formed in the temperature range of 100-200 °C, and are so small that they cannot be verified in these pictures.

In general, laser processing did not produce significant changes in the microstructures shown in Fig. 24. The diffusion of carbon is limited to short distances with high heating rates; the calculated estimation of carbon diffusion in a ferrite material is only 0.2-0.5 µm at heating rates of 1500 °C/s to 400 °C [170]. The short and fast heating e.g. in laser processing limits the carbon diffusion into carbides. The changes occurring with such high heating rates in laser processing, 430 °C/s calculated from the laser parameters used of 760 W and 13 mm/s laser traverse rate, are mainly due to the recovery of the structure due to dislocation motion.

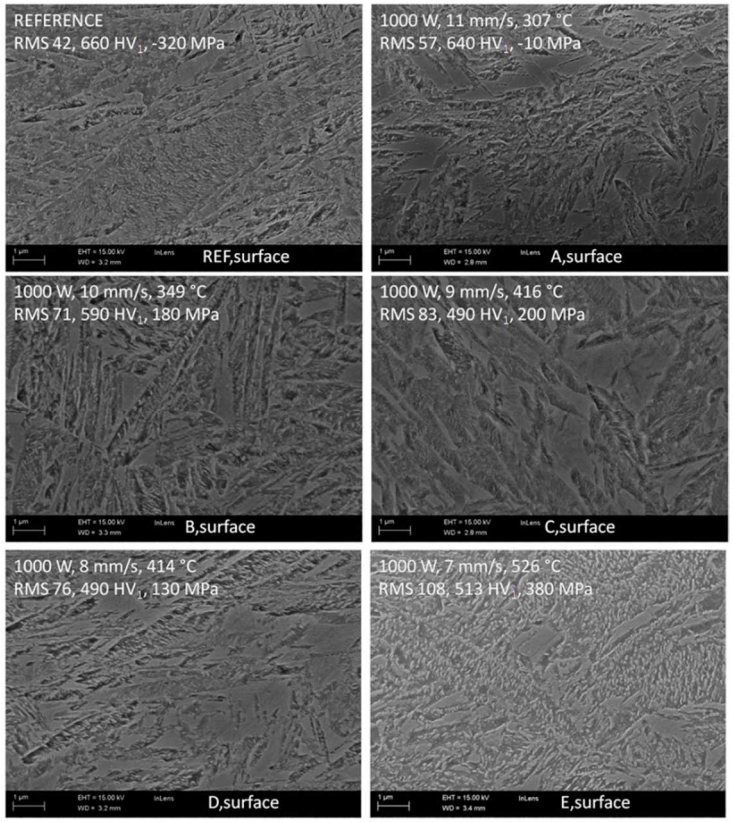

Figure 24. *SEM-micrographs of reference sample and laser-processed planet gear samples with 1000 W laser input power and varying traverse rates [171].*

Hardness changes

The changes in hardness due to laser processing were studied by means of surface hardness measurements and cross-sectional hardness depth profiles. It was noticed that surface hardness values affected more than the hardness profile values [III]. With a constant laser power value, a smaller traverse rate produced a larger decrease in surface hardness values [III]. Correlation coefficients calculated for the measured RMS and surface hardness values after laser processing were from 0.77 to 0.94 within studied sample categories. This indicates that the RMS values have a good correlation with the measured surface hardness values [III].

Laser processing produces quite an intense heat distribution in the surface and the size of the laser beam used affects the intensity of the thermal damage. Thus, the resulting laser-produced hardness and residual stress profiles may be sharper than those caused by actual grinding burn.

Long-time durability of laser-processed calibration blocks

A series of periodic BN and RS measurements were performed to confirm possible long-term changes occurring in laser-processed samples. The BN and RS measurements were carried out multiple times during a longer measurement period of 6 to 12 months. Two sample categories were used in these studies: PM laser-processed samples and one set of helical gear teeth samples as shown in Table 10. The PM samples were measured first after laser processing and then after 6 months' time. The helical gear samples were measured after laser processing and after 12 months' time. Both of the studied categories produced a 1-2 % change in the measured

RMS values. This minor change may be due to normal measurement deviation. The measured RS changes in both categories were larger, from 7.5 to 11 %. The measurement depth in RS measurements is much smaller than in RMS measurements and therefore likely that the changes occur more in the surface of the specimen than in the interior structure, due to normal changes by time-dependent plastic deformation on a microscopic scale.

Table 10. Percentage changes in RMS and RS values [unpublished].

Sample	Percentage change in RMS value	Max. Percentage change in RMS value	Percentage change in RS values, y-dir	Percentage change in RS values, x-dir
AK1, 6 months	1.2	3.9	7.5	7.5
AK2, 6 months	2.2	7.6	8	11
Helical gear samples, 12 months	2.0	6.4	9	-

Studies concerning the time dependence of the laser-processed sample BN measurements indicated that no major changes were observed in RMS values during a timescale of 6 or 12 months. However, the RS measurements revealed some changes. The issue of time-dependent changes should be considered when determining the optimal utilization time for calibration samples. Temperature changes could be one contributing factor for RS changes so keeping calibration blocks at constant temperature may be beneficial.

The usage of laser-processed calibration samples requires that the laser marks be manufactured in a way that the BN sensor detects the altered mark. In addition the position of the BN sensor does not have to be exactly in the same location, i.e. the laser mark has homogeneous properties for a wider area [III].

7.2.2. Induction heating of calibration samples for BN

Induction heating produced a significantly increased RMS value only for samples heated up to 600 °C [II] as shown in Fig. 21. In addition, only the highest temperature, 600 °C, produced changes in the BN peak position and surface residual stress values. The highest temperature heating was performed with a 3 s treatment time whereas the lower temperatures were treated with a 1 s treatment time. One problem in the induction heating was that the shorter heating time was too short to produce any meaningful changes [II]. The heating had occurred only in a thin surface layer where a temperature lacquer was used to verify the surface temperature. Considering these results, the induction hardening method cannot be used as such to produce thermal damage for BN calibration purposes as it is not well controlled and tends to cause microstructural changes which do not characterize practical grinding burns.

7.3. Barkhausen noise and stress relationship in tempered samples [*Publications V, VI*]

Microstructural studies of tempered samples

Two series of samples were hardened and further tempered with different temperature-time combinations to modify the final microstructure and hardness. Set 1 samples, with plate test bars manufactured from 18CrNiMo7-6, were tempered with a temperature varying from 180 to 350 °C with durations of 90–240 min. Set 2 samples, with plate test bars manufactured from RAEX400, were tempered with a temperature varying from 160-300 °C with durations of 30–

60 min. Set 1 tempering times were notably longer than those for set 2. Fig. 25 presents SEM micrographs taken from set 1 tempered plate specimens.

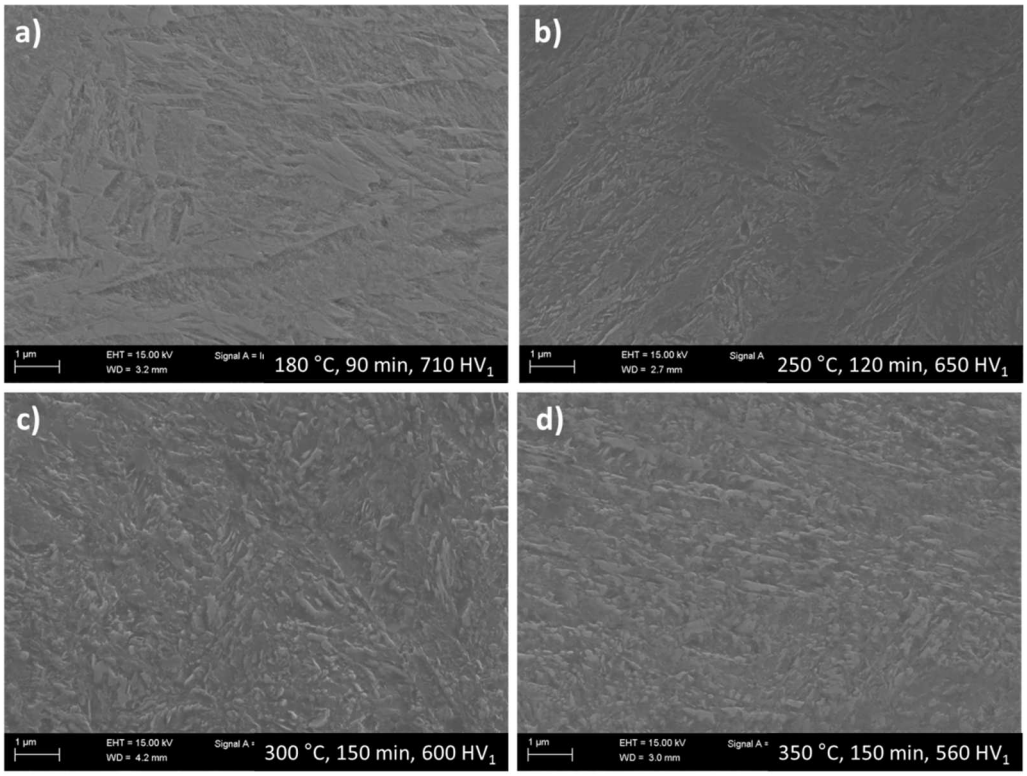

Figure 25. *SEM micrographs from tempered 18CrNiMo7-6 samples; a) martensite tempered at 180 °C for 90 min, b) martensite tempered at 250 °C for 120 min, c) martensite tempered at 300 °C for 150 min and d) martensite tempered at 350 °C for 150 min. [unpublished]*

In total, eight different hardness levels were achieved in the tempering. The surface hardness variation was from 560 HV_1 to 720 HV_1. Fig. 25 shows some of the tempered samples. Explicit microstructural changes had taken place mainly in the samples where the hardness had decreased down to 650 HV_1 or less. The microstructure in all the samples can be verified to be tempered martensite. The tempering promoted the change of the martensite structure into ferrite with carbides. As seen in Figs. 25. b), c) and d), carbon precipitation into carbides had taken place.

The SEM micrographs for sample set 2 manufactured from RAEX400 are presented in Fig. 26. The tempering at 180 °C for 1 h produced only a slightly tempered martensite structure (Fig. 26 b). In contrast, a tempering temperature of 300 °C produced a structure of tempered martensite (in c) and d)), where the martensite lath structure had already changed. Compared to the untempered sample, the microstructure in samples tempered at 300 °C had changed drastically. The carbon in martensite had diffused into carbide precipitates. The transformed area with carbide precipitates can be clearly seen in Fig. 26 b) where an arrow indicates the carbide region. These carbide regions may be due to compositional differences in the material. Similar regions were observed in all of the studied samples near the surface area. In this sample, the changed grain structure consisting of carbides was found to extend down to a distance of 50 µm

from the sample surface. More detailed information on the structure can be seen in Fig. 27, taken with a higher magnification from an untempered martensite sample (Fig. 27 a), a sample tempered at 300 °C for 30 min (Fig. 27 b), a sample tempered at 300 °C for 30 min (Fig. 27 c) and a stress relief annealed sample at 630 °C for 150 min (Fig. 27 d). As seen in Fig. 27. b) and c), carbon precipitation resulting in carbides had taken place. For example, in Fig. 27 d) a fine martensite structure with carbides arrayed in linear clusters within the matrix can be seen. In the stress relief annealed sample (Fig. 27 d) carbon dissolution from the martensite matrix had taken place to form carbides in the lath boundaries. Even though the tempering durations were shorter for sample set 2, the changes in the microstructure are more visible for this sample set. In conclusion, the martensite lath structure changed to a finer lath structure that was more evident in sample set 2 manufactured from RAEX400.

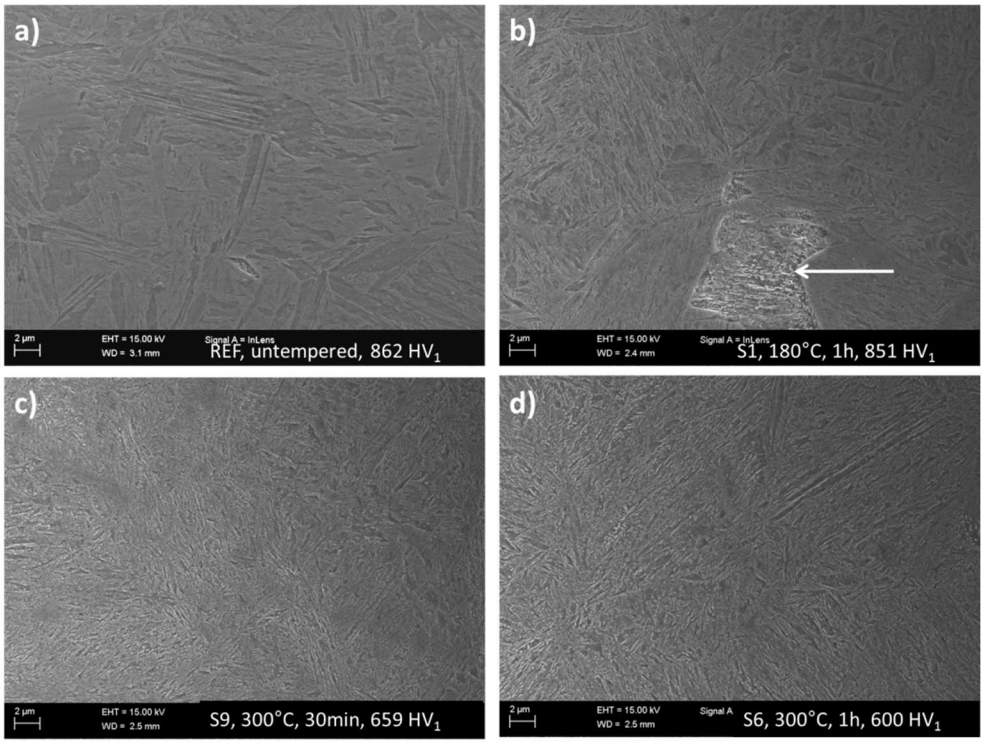

Figure 26. *SEM micrographs of RAEX400 sample series showing a) untempered martensite structure, b) martensite tempered at 180 °C for 1 h, an arrow indicating the carbide region, c) 300 °C for 30 minutes and d) 300 °C for 1 h for RAEX400 steel. [unpublished]*

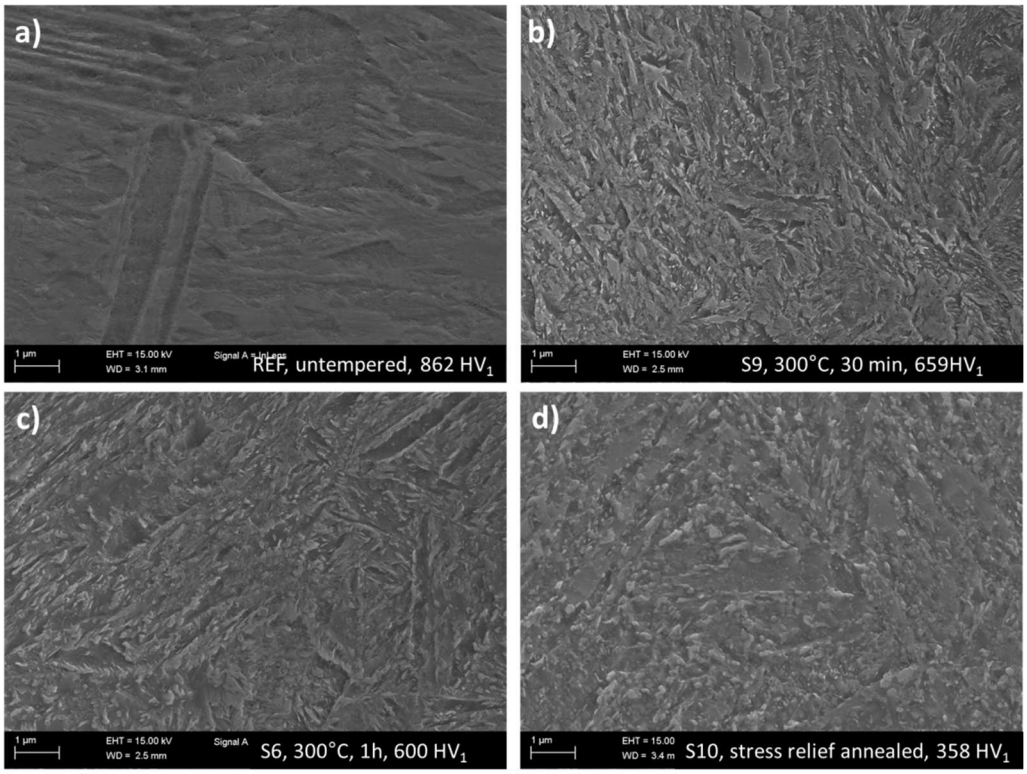

Figure 27. *Higher magnification SEM micrographs a) untempered martensite structure [Publication VI], b) tempered martensite at 300 °C for 30 min [unpublished], c) tempered martensite at 300 °C for 1 h taken 50 µm distance from the sample surface [Publication VI], d) stress relief annealed at 630 °C for 150 min [unpublished].*

Characterization of tempered samples with BN and XRD prior to loading

The microstructural features that affect dislocation motion also influence domain wall motion [53]. This means that, in general, in hard specimens the BN peak height and RMS are lower than in softer materials. Furthermore, in hard materials the BN peak is expected to be located at higher BN measurement magnetization values. The reason for this is that, in hard materials higher magnetization in BN measurements is required to detach the domain walls from the pinning sites i.e. in hard materials the pinning sites are stronger. The effect of microstructure on the BN phenomenon can be illustrated by studying the relationship between the surface hardness and the RMS value. Fig. 28 illustrates the relationship of the surface hardness and residual stress to the BN RMS for both studied sample sets. Fig. 28 shows that the measured initial values of surface hardness for both sample sets, after tempering but prior to loading, have a linear relationship with the RMS value. The decreasing surface hardness produces increased RMS. Linear behaviour can also be discovered when comparing residual stresses and RMS. These observed relationships with BN RMS are in accordance with the literature e.g. [75]. A higher compressive residual stress produces smaller RMS values. The 18CrNiMo7-6 samples were observed to have decreased compressive residual stress values compared to the RAEX400 samples. This can be explained by the longer tempering times used for the 18CrNiMo7-6 samples. Additionally, other differences in the composition and in the microstructure may influence this. The sand-blast samples in sample set 1 had higher compressive residual stress values than the other bars in this category, accompanied by a lower BN value. It is worth

mentioning that the BN measurements were conducted with different BN sensors and different measurement parameters to these two sample sets.

For sample set 1, the peak height value was observed to carry similar information to that of the RMS value for tempered plate samples prior to loading [V]. Fig. 28 shows the BN FWHM and peak position as a function of the surface hardness value for both studied sample sets prior to loading. The peak position value as a function of hardness did not show any meaningful changes for the 18CrNiMo7-6 samples. One explanation for this might be that in this case-hardened material, the nature of the obstacles pinning the domain wall motion remains similar despite the varying hardness. The number of hindrances affecting domain wall motion, however, changes causing an alteration in the RMS and peak height values as a function of hardness [V]. However, there was a decreasing linear relationship between the peak position and the surface hardness values for the RAEX400 samples. This relationship is inconsistent with literature findings [75, 172]. This RAEX400 sample set exhibited larger variation in the residual stress values whereas the change in the RS for the 18CrNiMo7-6 set was minimal and thus might be the reason why it did not affect the peak position values. For both sample series, the FWHM corresponding to the BN peak width was observed to be unchanged as a function of surface hardness, as shown in Fig. 29. The FWHM is related to the homogeneity of the distribution of hindrances and thus it can be concluded that distribution was homogeneous because there were no observable changes. A peak position study was made by Davut and Gür on tempered test bars where the peak position was noticed to shift to lower magnetic field values due to tempering [55]. However, the tempering between 200-300 °C did not affect the peak or peak position values significantly [55].

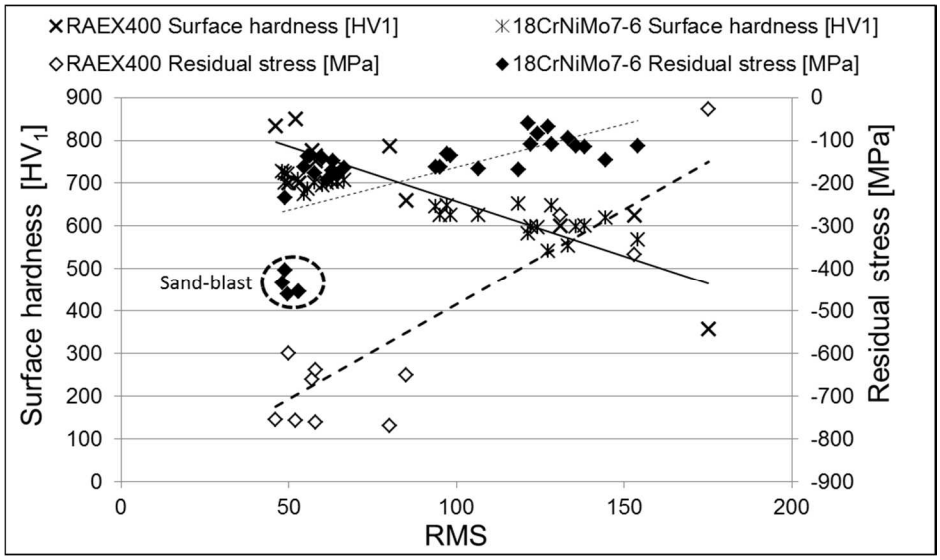

Figure 28. *Surface hardness and residual stress as a function of the RMS BN value for both tempered sample sets. [unpublished]*

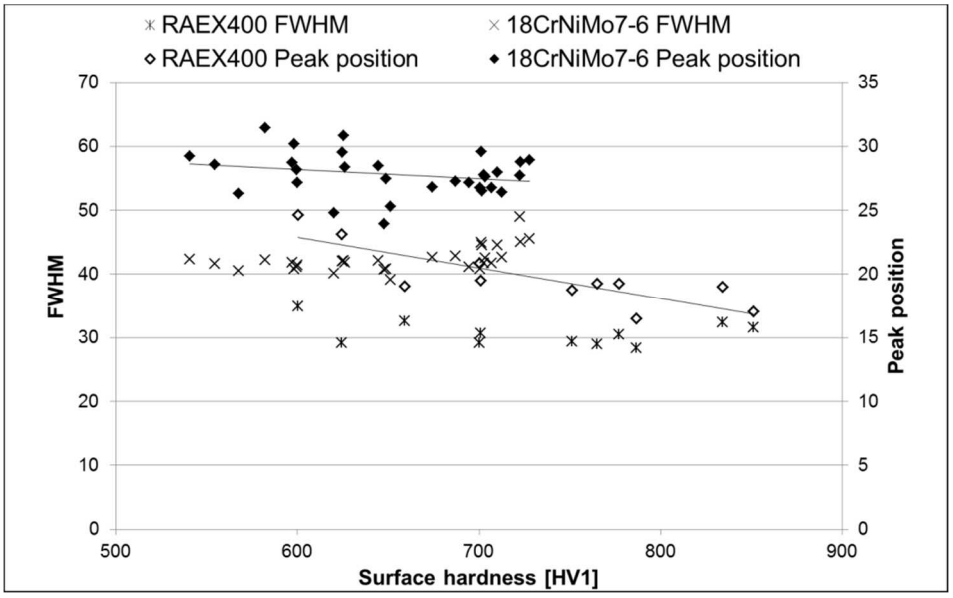

Figure 29. *BN FWHM and peak position as a function of the surface hardness value for both tempered sample sets. [partly unpublished]*

Loading of tempered samples

Stepwise tensile and compressive loading

The loading for tempered specimens was performed in tensile and compressive loading and bend loading. In uniaxial tensile testing for both studied sample series, the RMS of the Barkhausen noise increased in the loading direction under the applied tensile stress. Under compressive stress the BN RMS decreased in the loading direction [V, VI]. The results of the uniaxial stepwise loading performed simultaneously with BN measurements are presented in Fig. 30. It was impossible to carry out XRD RS measurements during loading and thus a computational value referred to as the real stress is introduced here. The real stress value takes into account the residual stress value of the unloaded sample and is calculated by adding it to the applied external stress value. Fig. 30 shows that there is a relationship between the BN RMS values and the real stress value for both studied sample categories. For the 18CrNiMo7-6 set of samples the calculated real stress values are smaller than for RAEX400 due to the differences in the RS values prior to loading. As expected, based on the literature [91], the RMS value increased with increasing tensile stress. The RMS value behaved linearly as a function of real stress when each of the samples was studied individually. However, the overall relationship shows two distinct regions where the strength of the RMS vs. real stress relationship varied. The RMS values for the softer test bars grew exponentially with respect to the applied stress, whereas the RMS values for the harder test bars were linear. After tempering above 275 °C (RAEX400 samples S5 and S6) and above 250 °C (18CrNiMo7-6 samples Bars 4-7), a distinct change occurs in the stress versus measured BN behaviour. The hardness values of 680 HV_1 and 660 HV_1 were the limits for the linear behaviour for 18CrNiMo7-6 and RAEX400, respectively. This change in the slope and increased BN RMS values clearly indicated some significant change in the microstructural state due to tempering. Possible carbide formation in the material could be one explanation. This behaviour might be due to cementite carbide formation above 200 °C. Below this temperature only epsilon carbides grow. Carbon from the martensite structure diffuses into carbides and decreases the dislocation density, leading to

lower residual stresses that pin the domain wall motion thus creating a higher BN signal. Tempering reduced the dislocation density, and also lowered the required magnetic field needed to overcome the obstacles [V, VI].

The RMS values for the 18CrNiMo7-6 sample set were also measured for the transverse and 45° direction compared to the loading direction. The non-linear stress response of the softer samples was only observable for the loading direction [V].

BN amplitude was not saturated in the two load test bar series at the values of the applied stress in stepwise loading. The saturation is typically observed at higher compressive and tensile stresses than those used in this study [V, VI].

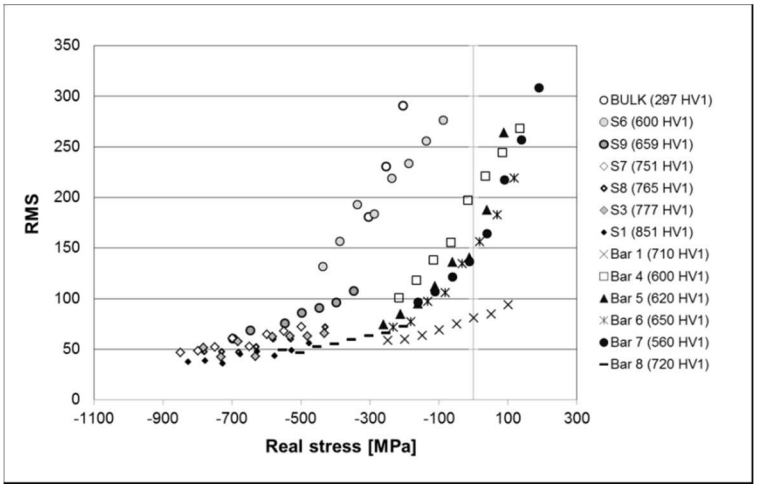

Figure 30. *Calculated real stress values as a function of RMS value for stepwise loaded 18CrNiMo7-6 and RAEX400 samples. BN measurement direction is the same as the loading direction. [Combined from V, VI]*

Fig. 31 displays the directional angle diagram of the RMS value under applied stress in 18CrNiMo7-6 test bars 1 (710 HV_1), 5 (600 HV_1) and 7 (560 HV_1). The diagram clearly indicates the anisotropical behaviour of the test bars with different hardness conditions under the applied compressive and tensile stress. [V].

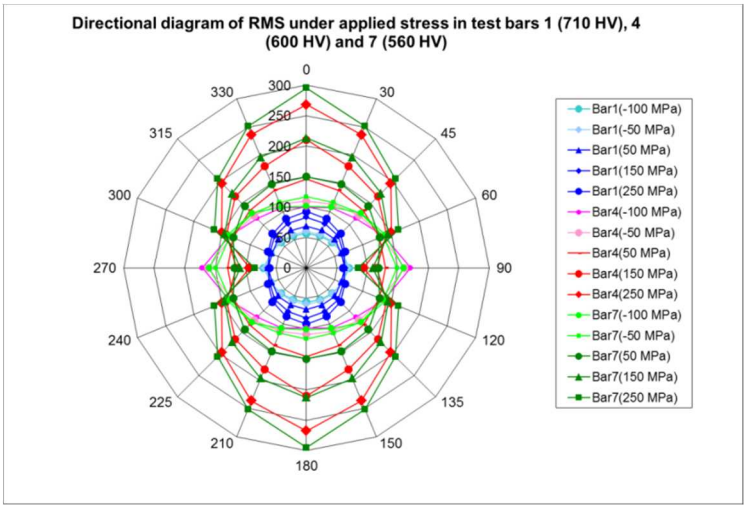

Figure 31. *Directional diagram of RMS under applied stress in 18CrNiMo7-6 test bars 1 (710 HV_1), 5 (600 HV_1) and 7 (560 HV_1) [V].*

Bending

In the bending tests loading was incrementally applied to RAEX400 samples in the purely elastic deformation region. During the bending, the stresses were measured by the X-ray diffraction method simultaneously with the loading. It is worthwhile mentioning that the BN method is sensitive only to residual stresses close to the surface. The measurement depth of the XRD method is less than the measurement depth of BN [163, 164]. BN measurements were also performed while the specimen was loaded to obtain information about the BN vs. stress relationship. The relationship of the measured RMS as a function of the measured stress by XRD in bending was consistent with previously reported results on the stress vs. BN behaviour of samples with different hardness states [97]. The steel samples with high hardness showed only minor loading-imposed changes in the BN root mean square values of voltage amplitude (RMS) values. In addition the BN signal was almost saturated in the region with the high compressive stress of about -800 MPa on the tensile loaded side.

The results reveal the linear behaviour of the reciprocal RMS value in the measured XRD stress range of -800 MPa to -200 MPa, as shown in Fig. 32. For the soft bulk sample and for the stress relieved sample S10, the behaviour was not linear. The studies of Mierczak *et al.* [65] reported the reciprocal value of BN peak amplitude to have a linear relationship to the applied stress and also to the measured surface residual stress values. This phenomenon was observed by applying different tensile stresses to one carburized sample. Similar behaviour was also observed with variously ground carburized samples with different residual stresses. This phenomenon was explained by the BN peak amplitude vs. stress behaviour corresponding to the relationship between stress and the slope of the anhysteretic magnetization curve [80]. Garikepati *et al.* [80] suggested that there is a relationship between the slope of the anhysteretic magnetization curve and stress. Their [80] theory also suggests that the reciprocal value of the anhysteretic susceptibility behaves linearly with the applied stress and that the dependence is much stronger under tension. Furthermore, Mierczak *et al.* [65] proved that the reciprocal value of the BN peak amplitude behaves similarly to the reciprocal anhysteretic susceptibility. The trend was similar in terms of the applied stress and the residual stress [65]. The assumptions were that both of these features represent the same stage of the magnetization process corresponding to

the steepest slope. Another suggestion was that the rate of change of the magnetization was proportional to the BN activity.

The results of the reciprocal RMS values as a function of the measured residual stress presented in Fig. 32, suggested that there was a linear relationship between the reciprocal RMS and the applied stress measured with XRD and strain gages. However, it was noticed that the strength of the relationship depended on the surface hardness. The harder samples with a surface hardness value of over 800 HV_1 did not show a meaningful change in RMS values when the measured compressive residual stress decreased from -800 MPa to -550 MPa. Hardness with increased dislocation density in the martensite produced a strong hindrance to the moving domain walls. To analyse the influence of hardness, regression lines were identified for the test series. Examples of these regression lines are given in Fig. 32. As shown in the figure, the harder sample series produced a steeper regression line. For the harder samples (e.g. S1 and S2) the slope value was from $-4 \cdot 10^{-5}$ to $-3 \cdot 10^{-5}$ 1/RMS whereas for the samples with a hardness of 650-700 HV_1 the slope value was $-2 \cdot 10^{-5}$ 1/RMS. The soft samples had slope values of $-1 \cdot 10^{-5}$ 1/RMS. The studies of Garikepati *et al.* [80] and Mierczak *et al.* [65] did not consider the effect of hardness on stress sensitivity.

It is stated in the literature [91] that high dislocation density has an influence on domain wall mobility. Different inclusions and precipitates such as carbides also act as hindering elements to the domain walls. It can be expected that the size and distribution of the carbides is the major parameter that affects observed BN behaviour. Microstructural observations showed that carbides had formed in the martensite and were quite small in the studied samples as shown in Fig. 27 c). The changes in the RMS vs. stress relationship were thus justified by the changes in the microstructure. [VI]

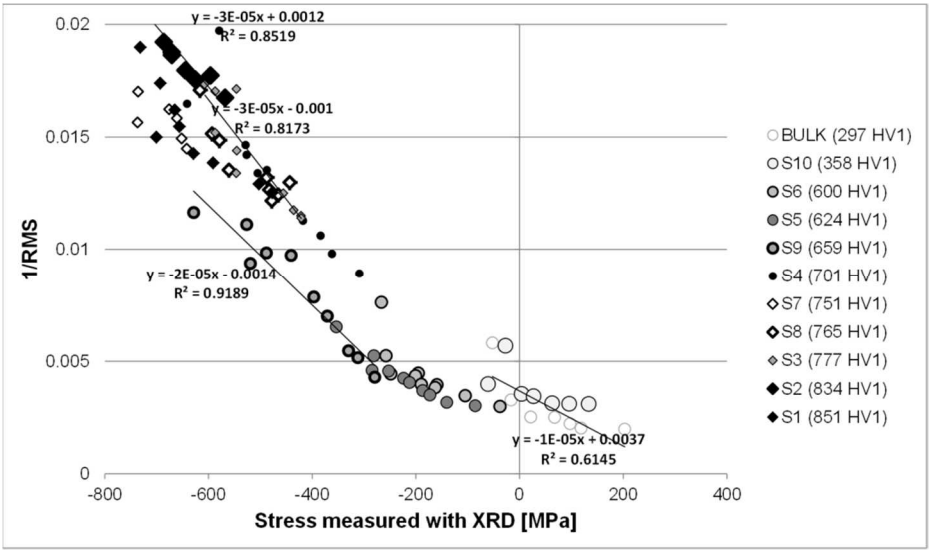

Figure 32. *The reciprocal RMS values for different samples of RAEX400 series as a function of the measured XRD stress values in bending [VI].*

8. CONCLUDING REMARKS AND SUGGESTIONS FOR FUTURE WORK

The aims of this work were to develop a methodology for the detection of the case-depths of hardened components with Barkhausen noise, to study the detection of grinding burns with a multiparameter Barkhausen noise method and to study the effect of various factors such as microstructural changes and different loading conditions on the Barkhausen noise signal. The aim was also to produce calibration samples to be used in the quality control of the Barkhausen noise method and to study the stress response of tempered structures.

In general, non-destructive evaluation is performed to gain confidence in the structural integrity of components. The lack of a standardized calibration procedure for the Barkhausen noise method hinders the possible wider utilization of the procedure. Moreover, one important research area of Barkhausen noise development is the case-depth measurements of hardened components.

1) Barkhausen noise voltage sweeps for case-depth determination

The previous BN studies concerning case-depth measurements have shown that the case-depth can be reliably estimated down to 1 mm. Here it was established that by studying magnetizing voltage sweeps it is possible to evaluate the compositional and microstructural gradients referring to case-depth values deeper, even down to 3 mm. The ratio of two different MVS slopes at different frequencies was noticed to correspond well to the case-depth value of hardened components. The results were obtained from a broad group of samples prepared with different hardening methods. The tested series in this study contained only a small set of actual gear teeth samples. The future challenge for the utilization of this method is to increase the accuracy and confidence of the method. For this reason, the utilization of voltage sweeps should be carried out for a wider variety of the actual gear components manufactured from different materials with varying case-depth values.

2) Calibration samples for Barkhausen noise measurements

Two methods were used for creating controlled thermal damage to hardened surfaces. Laser processing was found to create controllable changes in the surface layer whereas induction heating did not produce as well-defined changes in the measured parameters. With the present knowledge of the laser processing as a flaw manufacturing method, it is possible to produce thermal damage i.e. notable and controllable changes in the stress and hardness states. However, the appearance of the metal surface was observed to have a significant effect on the laser processing outcome. For future consideration the surface quality needs to be made more uniform by testing different surface conditions to find the most suitable one for laser processing. Laser processing needs to be optimised for each case individually. The detailed laser parameters should first be tested according to the specimen surface condition, surface appearance and specimen geometry. One solution to improve the laser process further is a use of the temperature controlled laser. In the future, this aspect should be one of the focuses of research.

Furthermore the detailed characterization of the laser-processed samples by transmission electron microscope (TEM) studies would provide information about the detailed

microstructural changes and in addition about the changes in the dislocation structure could be observed.

3) Barkhausen noise and stress relationship in tempered samples

Interpretation of the Barkhausen noise vs. stress response has proven to be challenging. In the loading experiments applied to two different series of hardened and tempered samples, the stress sensitivity of the RMS value was noticed to depend on the surface hardness of the specimen. The steel samples with high hardness showed only minor loading-imposed changes in the BN root mean square values of voltage amplitude (RMS) values due to loading. The RMS values for the softer test bars grew exponentially in relation to applied stress, whereas the RMS values for the harder test bars were linear. After tempering above 275 °C for RAEX400 samples and above 250 °C for 18CrNiMo7-6 samples, a distinct change from linear to exponential behaviour occurs in the stress versus measured BN behaviour.

In bending, the results of the reciprocal RMS values as a function of the measured residual stress suggest that there is a linear relationship between the reciprocal RMS and the applied stress measured with XRD and strain gages. However, it was observed that the strength of the relationship depends on the surface hardness.

Recommendation for future work here includes the detailed microstructural characterization of the tempered samples. Transmission electron microscopy (TEM) studies would provide information about the details of the microstructural changes and in addition the dislocation structure changes could be observed.

REFERENCES

[1] P. J. Shull, Nondestructive EvaluationTheory, Techniques, and Applications, CRC Press, 2002.

[2] G. Dobmann, M. Kröning, W. Theiner, H. Willems, U. Fiedler, Nondestructive characterization of materials (ultrasonic and micromagnetic techniques) for strength and toughness prediction and the detection of early creep damage, *Nuclear Engineering and Design*, 157 (1992) 137-158.

[3] http://www.ndt-ed.org/EducationResources/CommunityCollege/Radiography/AdvancedTechniques/Real_Time_Radiography/ProcedureDevelopment%20ASME%20Code.htm (17.6.2012).

[4] T. Astrom, From Fifteen to Two Hundred NDT-methods in Fifty Years, Proceedings of the 17th World Conference on Nondestructive Testing, 25-28 Oct 2008, Shanghai, China.

[5] J. Lu, Handbook of Measurement of residual stresses, Society for experimental Mechanics Inc., The Fairmont Press Inc, 1996.

[6] B. Karpuschewski, O. Bleicher, M. Beutner, Surface integrity inspection on gears using Barkhausen noise analysis, *Procedia Engineering*, 19 (2011) 162-171.

[7] A. S. Wojtas, L. Suominen, B. A. Shaw, J. T. Evans, Detection of Thermal Damage IN Steel Components After Grinding Using the Magnetic Barkhausen Noise Method, *NDT.net*, 3(9) (1998).

[8] J. R. Davis (Ed), Gear Materials, Properties, and Manufacture. ASM International, Materials Park, OH. 2005.

[9] ASM Handbooks Online, Volume 5, Thermal Aspects of Surface Finishing Processes, Introduction, ASM International (17.6.2012).

[10] J. Grum, A review of the influence of grinding conditions on resulting residual stresses after induction surface hardening and grinding, *Journal of Materials Processing Technology* 114 (2001) 212-226.

[11] S. Malkin, Grinding technology: Theory and Applications of Machining with Abrasives. Chichester Horwood, 1989.

[12] ASM Handbooks Online, Volume 9, Metallography and Microstructures, Martensitic Structures, Tempering of Martensite, ASM International (22.8.2007).

[13] L. P. Tarasov (Ed.), Machining- Theory and Practice. American Society for Metals, 1950.

[14] J. Paulo Davim (Ed.), Surface Integrity in Machining, Springer, 2010.

[15] M. J. Balart, A. Bouzina, L. Edwards, M.E. Fitzpatrick, The onset of tensile residual stresses in grinding of hardened steels, *Materials Science and Engineering A*, 367 (2004) 132-142.

[16] http://www.ndt-ed.org/EducationResources/CommunityCollege/Ultrasonics/CalibrationMeth/calibrationmethods.htm (19.3.2012).

[17] SFS-EN ISO 7963, Non-destructive testing. Ultrasonic testing. Specification for calibration block No.2. Suomen Standardoimisliitto SFS, Helsinki, Finland, 2010.

[18] http://www.olympus-ims.com/en/ultrasonic-transducers/testblocks (19.3.2012).

[19] http://www.ndt-ed.org/EducationResources/CommunityCollege/Radiography/cc_rad_index.htm (17.6.2012).

[20] R. Kvist, P. Lundin, The mastering and calibration procedure of Barkhausen noise measurements of camshafts at Scania heavy engine manufacturing, Proceedings of the 9th International Conference on Barkhausen Noise and Micromagnetic Testing, 27-30 June 2011, Hejniche, Czech Republic.

[21] V.S. Augutis , Z. Nakutis, R. Ramanauskas, Advances of Barkhausen Emission Measurement. *IEEE Transactions on instrumentation and measurement*, 58(2) (2009) 337-341.

[22] P. E. Mix, Introduction to Nondestructive Testing: A Training Guide, Second edition, John Wiley & Sons, 2005.

[23] http://www.ndt-ed.org/EducationResources/CommunityCollege/Other%20Methods/RFT/RFT_Cal.htm (17.6.2012)

[24] S. Santa-aho, Characterization of gear grinding burns by multiparameter Barkhausen noise measurements, Master of Science Thesis, Tampere University of Technology, Tampere, Finland, 2008.

[25] M. Kemppainen , I. Virkkunen, Crack Characteristics and Their Importance to NDE, *Journal of Nondestructive Evaluation*, 30(3) (2011) 143-157.

[26] I. Virkkunen, Thermal Fatigue of Austenitic and Duplex Stainless Steels. Acta Polytechnica Scandinavica, Mechanical Engineering Series No. 154, Espoo, 2001, http://lib.tkk.fi/Diss/2001/isbn9512256878/

[27] M. Kemppainen, Realistic Artificial Flaws for NDE Qualification – A Novel Manufacturing Method Based on Thermal Fatigue. Mechanical Engineering Series, Espoo, 2006, http://lib.tkk.fi/Diss/2006/isbn9512282631/

[28] B. Helifa, A. Oulhadj, A. Benbelghit, I.K. Lefkaier, F. Boubenider, D. Boutassouna, Detection and measurement of surface cracks in ferromagnetic materials using eddy current testing. *NDT&E International*, 39 (2006) 384-390.

[29] F. Klocke, C. Gorgels, Influence of the Process on the Material Properties in Gear Profile Grinding and its Detection using Barkhausen Noise Analysis, Proceedings of the 5th International Conference on Barkhausen Noise and Micromagnetic Testing, 2-3 June 2005, Petten, The Netherlands.

[30] F. Klocke, C. Gorgels, J. Reimann, Influence of Grinding Burn on the Load Carrying Capacity of Parts under Rolling Stress, Proceedings of the 7th International Conference on Barkhausen Noise and Micromagnetic Testing, 15-16 July 2009, Aachen, Germany.

[31] G. V. Lomaev, E. V. Kharanzhevskii, Testing of Laser-quenched Layers with the Help of Barkhausen noise. *Russian Journal of Nondestructive Testing*, 36(9) (2000) 631-639.

[32] J. F. Ready, D.F. Farson (Eds.), LIA Handbook of Laser Materials Processing, Laser Institute of America, Magnolia Publishing, Inc. 2001.

[33] X.F. Wang, X.D. Lu, G.N. Chen, Sh G. Hu, Y.P. Su, Research on the temperature field in laser hardening, *Optics & Laser Technology*, 38 (2006) 8-13.

[34] D. Bergström, J. Powell, A.F.H. Kaplan, The absorptance of steels to Nd:YLF and Nd:YAG laser light at room temperature. *Applied Surface Science*, 253 (2007) 5017-5028.

[35] H. Kwon, W.-K. Baek, M.-S. Kim, W.-S., Shin, J. J., Yoh, Temperature-dependent absorptance of painted aluminum, stainless steel 304, and titanium for 1.07 μm and 10.6 μm laser beams. *Optics and Lasers in Engineering*, 50(2) (2012) 114-121.

[36] K.C.A. Crane, R.K. Garnsworthy, L.E.S Mathias, Ablation of materials subjected to laser radiation and highspeed gas flows, *Journal of Applied Physics* 51(11) (1980) 5954-5961.

[37] H. Pantsar, Models for diode laser transformation hardening of steels. Acta Universitatis Lappeenrantaensis 204, 2005.

[38] T. Burakowski, T. Wierzchon, Surface Engineering of Metals, Principles, Equipment, Technologies. CRC Press. 1999.

[39] H. Kwon, J. Yoh, Polarized reflectance of aluminium and nickel to 532, 355 and 266 nm Nd:YAG laser beams for varying surface finish. *Optics & Laser Technology*, 44 (2012) 1823-1828.

[40] V. C. Bommi, M. K. Mohan, S. Prakash, Surface modification of martensitic stainless steel using metal working CO_2 laser, International Symposium of Research Students on Materials Science and Engineering, December 20-22, 2004, Chennai, India, 12p.

[41] R. L. Murty, Precision Engineering in Manufacturing. New Age International. 2005.

[42] http://www.sfs.fi (17.6.2012).

[43] C. Waites, M. Bièth, A Comparison of European Guidelines for Inspection Qualification, NDT.net, 7(8), 2002, Proceedings of the 3rd International Conference on NDE in Relation to Structural Integrity for Nuclear and Pressurized Components, Nov 14-16, 2001, Seville, Spain, http://www.ndt.net/article/v07n08/waites/waites.htm

[44] M. Bièth, European Standardization Methodology for Qualification of Non-Destructive Tests, NDT.net, 7(8), 2002, Proceedings of the 3rd International Conference on NDE in Relation to Structural Integrity for Nuclear and Pressurized Components, Nov 14-16, 2001, Seville, Spain, http://www.ndt.net/article/v07n08/bieth/bieth.htm

[45] C. Waites, J. Whittle, The current status of performance demonstration and evaluation developments, NDT.net, 3(7), 1998, Proceedings of the 7th ECNDT, Copenhagen, 26-29 May 1998.

[46] B. Denkena, F. Stimpel. REmBRAnt - Development of a Guideline for BN Inspections in Gear Manufacturing. Proceedings of the 5th International Conference on Barkhausen Noise and Micromagnetic Testing, 2-3 June 2005, Petten, The Netherlands.

[47] R.M. Bozorth, Ferromagnetism, Van Nostrand Company Inc. 1951.

[48] S. Chikazumi, Physics of Magnetism, John Wiley & Sons, Inc. 1964.

[49] G. Dobmann, NDT for stress measurements in components, K.H.J. Busxhow (Ed.) et al. Encyclopedia of materials: science & technology, Oxford, Elsevier (2001) 5971-5976.

[50] C.-G. Stefanita, Surface Magnetic Barkhausen Noise Response to Plastic Yield of Steel, Thesis, 1999.

[51] http://www.ndt-ed.org/EducationResources/CommunittCollege/Other%20Methods/AE/AE_BarkhausenTechniques.htm (17.6.2012).

[52] J. Harris, W. Benenson, H. Stöcker, Handbook of physics, Springer, 2002.

[53] B.D. Cullity, Introduction to magnetic materials, Addison-Wesley Publishing Company, 1972.

[54] D.C. Jiles, Recent advances and future directions in magnetic materials, *Acta Materialia*, 51 (2003) 5907-5939.

[55] K. Davut, G.H. Gür, Monitoring the Microstructural Changes During Tempering of Quenched SAE 5140 steel by Magnetic Barkhausen noise, *Journal of Nondestructive Evaluation*, 26 (2007) 107-113.

[56] D. O'Sullivan, M. Cottrell, D.A. Tanner, I. Mészáros, Characterisation of ferritic stainless steel by Barkhausen techniques. *NDT&E International*, 37 (2004) 489-496.

[57] J. M. Makar, B.K. Tanner, The effect of plastic deformation and residual stress on the permeability and magnetostriction of steels, *Journal of Magnetism and Magnetic Materials*, 222 (2000) 291-304.

[58] C. C. H. Lo, E. R. Kinser, Y. Melikhov, D. C. Jiles, Magnetic non-destructive characterization of case depth in surface-hardened steel components. In: D.O. Thompson, D.E. Chimenti (Eds.) Review of Progress in Quantitative non-destructive evaluation 25B, AIP Conference Proceedings, 820 (2006) 1253-1260.

[59] C. Zhang, N. Bowler, C. Lo, Magnetic characterization of surface-hardened steel, *Journal of Magnetism and Magnetic Materials*, 321 (2009) 3878-3887.

[60] Y. Kai, Y. Tsuchida, M. Enokizono, Numerical analysis for non-destructive evaluation of hardening steel taking into accound measured magnetic properties depending on depth. Electromagnetic Nondestructive Evaluation, Takahashi, S. and Kikuchi, H. (Eds.), IOS Press, Amsterdam, 2007.

[61] V. Moorthy, B.A. Shaw, P. Hopkins, Surface and subsurface stress evolution in case-carburised steel using high and low frequency magnetic barkhausen emission measurements. *Journal of Magnetism and Magnetic Materials*, 299(2) (2006) 363-375.

[62] V. Moorthy, B.A. Shaw, K. Brimble, Testing of Case Depth in Case carburized steels using Magnetic Barkhausen Emission technique. *Materials Evaluation*, 62(5) (2004) 523-527.

[63] V. Moorthy, B.A. Shaw, P. Hopkins, Magnetic Barkhausen emission technique for detecting the overstressing during bending fatigue in case-carburised En36 steel, *NDT&E International*, 38 (2005) 159–166.

[64] T.W. Krause, A. Pattantyus, D.L. Atherton, Investigation of Strain Dependent Magnetic Barkhausen Noise in Steel, *IEEE Transactions on magnetics*, 31(6) (1995) 3376-3378.

[65] L. Mierczak, D.C. Jiles, G. Fantoni, A New Method for Evaluation of Mechanical Stress Using the Reciprocal Amplitude of Magnetic Barkhausen Noise. *IEEE Transactions on Magnetism*, 47(2) (2011) 459-465.

[66] C. H. Gür, I. Cam, Comparison of magnetic Barkhausen noise and ultrasonic velocity measurements for microstructure evaluation of SAE 1040 and SAE 4140 steels, *Materials Characterization*, 58 (2007) 447-454.

[67] A. Flammini, D. Marioli, E.Sardini, A.Taroni, Robust Estimation of Magnetic Barkhausen Noise Based on a Numerical Approach, *IEEE Transactions on Instrumentation and Measurement*, 51(6) (2002) 1283-1288.

[68] M. Lindgren, T. Lepistö, On the stress vs. Barkhausen noise relation in a duplex stainless steel, *NDT&E International*, 37 (2004) 403-410.

[69] J. Grum, B. Pecnik. Calibration of various sensor units by using different parameters of the magnetic Barkhausen noise, 16th WCNDT 2004- World Conference on NDT, Aug 30-Sep 3, 2004, Montreal Canada

[70] V. Moorthy, B. A. Shaw, J. T. Evans, Evaluation of tempering induced changes in the hardness profile of case-carburised EN36 steel using magnetic Barkhausen noise analysis, *NDT&E International*, 36 (2003) 43-49.

[71] R.E. Haimbauch, Practical Induction Heat Treating. ASM International, Ohio USA. 2001.

[72] D.C. Jiles, Dynamics of domain magnetization and the Barkhausen effect *Chechoslovak Journal of Physics*, 50(8) (2000) 893-924.

[73] O. Saquet, Barkhausen noise from plain carbon steels: analysis of the influence of microstructure, *Materials Science and Engineering A*, 269 (1999) 73-82.

[74] D.M. Stewart, K.J. Stevens, A.B. Kaiser Magnetic Barkhausen noise analysis of stress in steel, *Current Applied Physics*, 4 (2004) 308-311.

[75] V. Moorthy, S. Vaidyanathan, K. Laha, T. Jayakumar, K. Bhanu Sankara Rao, B. Raj, Evaluation of microstructures in 2.25Cr-1Mo and 9Cr-1Mo steel weldments using magnetic Barkhausen noise, *Materials Science and Engineering A*, 231 (1997) 98-104.

[76] R. Volkers, The influence of dislocations on magnetic properties in steel- Magnetisation curve and magnetic Barkhausen effect in relation to deformation and recovery in C-Mn and IF steel, Thesis, 2008.

[77] C.-G. Stefanita, D.L. Atherton, L. Clapham, Plastic versus elastic deformation effect on magnetic Barkhausen noise in steel, *Acta Materialia*, 48 (2000) 3545-3551.

[78] A. Mitra, M.R. Govindaraju, D.C. Jiles, Influence of microstructure on micromagnetic Barkhausen emissions in AISI 4140 steel, *IEEE Transactions on magnetics*, 31(6) (1995) 4053-4055.

[79] H.C. Kim, K.H. Lee, C.G. Kim, D.G. Hwang, Barkhausen noise in ferromagnetic metallic glass Fe40Ni38Mo4B18. *Journal of Applied Physics* 72 (1992) 3626-3633.

[80] P. Garikepati, T.T. Chang, D.C. Jiles, Theory of Ferromagnetic Hysteresis: Evaluation of Stress from Hysteresis Curves, *IEEE Transactions on Magnetism*, 24(6) (1988) 2922-2924.

[81] V. Moorthy, S. Vaidyanathan, T. Jayakumar, B. Raj, On the influence of tempered microstructures on magnetic Barkhausen emission in ferritic steels, *Philosophical Magazine A*, 77(6) (1998) 1499-1514.

[82] C. D'Amato, C. Verdu, X. Kleber, G. Regheere, A. Vincent, Characterization of Austempered Ductile Iron Through Barkhausen Noise Measurements, *Journal of Nondestructive Evaluation*, 22(4) (2003) 127-139.

[83] A. Mitra, Z.J. Chen, F. Laabs, D.C. Jiles, Micromagnetic Barkhausen emissions in 2.25 wt% Cr-1 wt% Mo steel subjected to creep, *Philosophical Magazine A*, 75(3) (1997) 847-859.

[84] J. Chen, B.J. Zhang, D. Shu, X.Zhou, W.Wang, X. Qi, Improvement of stress testing performance using Barkhausen noise sensor, *Sensors and Actuators A: Physical*, 168 (2011) 51-57.

[85] M. Vashista, S. Paul, Novel processing of Barkhausen noise signal for assessment of residual stress in surface ground components exhibiting poor magnetic response, *Journal of Magnetism and Magnetic Materials*, 323 (2011) 2579-2584.

[86] B. Zhu, M. J. Johnson, C.C. H. Lo, D.C. Jiles, Multifunctional Magnetic Barkhausen Emission Measurement System, *IEEE Transactions on magnetics*, 37(3) (2001) 1095-1099.

[87] S. Yamaura, Y. Furuya, T. Watanabe, The effect of grain boundary microstructure on Barkhausen noise in ferromagnetic materials, *Acta Materialia*, 49 (2001) 3019-3027.

[88] P. Zerovnik, J. Grum, G. Zerovnik, Determination of Hardness and Residual-Stress Variations in Hardened Surface Layers With Magnetic Barkhausen Noise, *IEEE Transactions on magnetics*, 46 (3) (2010) 899-904.

[89] S. Desvaux, M. Duquennoy, J. Gualandri, M. Ourak, The evaluation of surface residual stress in aeronautic bearings using the Barkhausen noise effect, *NDT&E International*, 37 (2004) 9-17.

[90] C. Jagadish, L. Clapham, D.L. Atherton, The Effect of Stress and Magnetic Field Orientation on Surface Barkhausen Noise in Pipeline Steel, IEEE Transactions on Magnetics, 26(1) (1990) 262-265.

[91] D.C. Jiles, Introduction to Magnetism and Magnetic Materials, Chapman and Hall, 1991.

[92] M. Lindgren, T. Lepistö, Application of a novel type Barkhausen noise sensor to continuous fatigue monitoring, *NDT&E International*, 33 (2000) 423-428.

[93] T. R. Hyde, J. T. Evans, B. A. Shaw, Effect of Stress and Heat Treatment on Magnetic Barkhausen Emission in Case Carburized Steels, *Materials Evaluation*, 58(8) (2000) 985-990.

[94] M. Lindgren, T. Lepistö, Effect of prestraining on Barkhausen noise vs. stress relation. *NDT&E International*, 34(5) (2001) 337-344.

[95] C.G. Stefanita, L. Clapham, D.L. Atherton, Subtle changes in magnetic Barkhausen noise before the macroscopic elastic limit, *Journal of Materials Science*, 35 (2000) 2675-2681.

[96] M. Blaow, J.T. Evans, B.A. Shaw The effect of microstructure and applied stress on magnetic Barkhausen emission in induction hardened steel, *Journal of Materials Science*, 42(12) (2007) 4364-4371.

[97] M. Blaow, J.T. Evans, B.A. Shaw, Magnetic Barkhausen noise: the influence of microstructure and deformation in bending, *Acta Materialia*, 53 (2005) 279-287.

[98] B.A. Shaw, J.T. Evans, M. Blaow, Magnetic Barkhausen Noise: the Influence of Microstructure, Deformation in Bending and Residual Stresses in Low Alloy Steel, Proceedings of the 5th International Conference on Barkhausen Noise and Micromagnetic Testing, 2-3 June 2005, Petten, The Netherlands.

[99] T.W. Krause, L. Clapham, A. Pattantyus, D.L. Atherton, Investigation of the stress-dependent magnetic easy axis in steel using magnetic Barkhausen noise, *Journal of Applied Physics*, 79(8) (1996) 4242-4252.

[100] V. Vengrinovich, D. Dmitrovich, Bi-axial stress quantitative evaluation with Barkhausen noise: the past and perspectives, Proceedings of the 17th World Conference on Nondestructive Testing, 25-28 October 2008, Shanghai, China.

[101] D.J. Buttle, V. Moorthy, B. Shaw, Measurement Good Practice Guide No.88, Determination of Residual Stresses by Magnetic Methods, National Physical Laboratory.

[102] T.H. Courtney, Mechanical Behavior of Materials, Second edition, McGraw-Hill, New York, 1999.

[103] A.J. Birkett, W.D. Corner, B.K. Tanner, S.M. Thompson, Influence of plastic deformation on Barkhausen power spectra in steels, *Journal of Physics D: Applied Physics*, 22(8) (1989) 1240-1242.

[104] X. Kleber, A. Vincent, On the role of residual internal stresses and dislocations on Barkhausen noise in plastically deformed steel, *NDT&E International*, 37 (2004) 439–445.

[105] J. Anglada-Rivera, L.R. Padovese, J. Capó-Sánchez, Magnetic Barkhausen Noise and hysteresis loop in commercial carbon steel: influence of applied tensile stress and grain size. *Journal of Magnetism and Magnetic Materials*, 231 (2001) 299-306.

[106] K.J. Stevens, Stress dependence of ferromagnetic hysteresis loops for two grades of steel. *NDT&E International*, 33(2) (2000) 111-121.

[107] R. Rautioaho, P. Karjalainen, M. Moilanen, Stress response of Barkhausen noise in a tempered C-Mn steel, *Journal of Magnetism and Magnetic Materials*, 68 (1987) 314-320.

[108] M. Blaow, J.T. Evans, B.A. Shaw BA Effect of deformation in bending on magnetic Barkhausen noise in low alloy steel, *Materials Science and Engineering A*, 386 (2004) 74-80.

[109] F. Jerabek, C. Scheer, New Approach in Analyzing Barkhausen Noise to Separate Changes in Stress and Hardness in 100Cr6 and 16MnCr5 Steel, Proceedings of the 7th International Conference on Barkhausen Noise and Micromagnetic Testing, 15-16 July 2009, Germany.

[110] C. Gatelier-Rothea, J. Chicos, R. Fougeres, P. Fleischmann, Characterization of pure iron and (130 p.p.m.) carbon-iron binary alloy by Barkhausen noise measurements: study of the influence of stress and microstructure, *Acta Materialia* 46(14) (1998) 4873-4882.

[111] M.J. Sablik, B. Augustyniak, The effect of mechanical stress on a Barkhausen noise signal integrated across a cycle of ramped magnetic field, *Journal of Applied Physics*, 79 (1996) 963-972.

[112] C. Gür, H. Yelbay, I. Cam, Prediction of Surface Residual Stresses in Butt-Welded Steel Plates by Magnetic Barkhausen Noise Analysis, 10th European Conferfence on Non-Destructive Testing, June 7-11 2010, Moscow, Russia.

[113] H.I. Yelbay, I. Cam, C.H. Gür, Non-destructive determination of residual stress state in steel weldments by Magnetic Barkhausen Noise technique, *NDT&E International*, 43 (2010) 29-33.

[114] J. Degauque, B. Astie, Evolution of the Configuration of Magnetic Domains Interacting with Structural Defects in High Purity Iron, *Physica Status Solidi (A)*, 74(1) (1982) 201-210.

[115] V. Moorthy, S. Vaidyanathan, T. Jayakumar, R. Raj, Microstructural characterization of quenched and tempered 0.2% carbon steel using magnetic Barkhausen noise analysis, *Journal of Magnetism and Magnetic Materials*, 171 (1997) 179-189.

[116] J. Kameda, R. Ranjan, Nondestructive evaluation of steels using acoustic and magnetic Barkhausen signals- I: Effect of carbide precipitation and hardness, *Acta Metallurgica*, 35(7) (1987) 1515-1526.

[117] A.K. Rakhit, Heat Treatment of Gears, A Practical Guide for Engineers, ASM International, 2000.

[118] C.C.H. Lo, C.B. Scruby, G.D.W. Smith, Dependences of magnetic Barkhausen emission and magnetoacoustic emission on the microstructure of pearlitic steel, *Philosophical Magazine*, 84(18) (2004) 1821-1839.

[119] J.R. Davis (Ed), Surface Hardening of Steels: Understanding the Basics. ASM International, Materials Park, OH. 2002.

[120] M. Kaplan , C.H. Gür , M. Erdogan, Characterization of Dual-Phase Steels Using Magnetic Barkhausen Noise Technique, *Journal of Nondestructive Evaluation*, 26 (2007) 79–87.

[121] G. Krauss, Tempering of Martensite, Encyclopedia of Materials: Science and Technology (Second edition), 2001, 9093-9097.

[122] D.A. Porter, K.E. Easterling, Phase Transformations in Metals and Alloys, Second edition, Nelson Thornes. 1992.

[123] R. Honeycombe, H.K.D.H. Bhadeshia, Steels, Microstuctures and properties, Second edition, Edward Arnold. 1995.

[124] X. Kleber, A. Hug-Amalric, J. Merlin, Evaluation of the Proportion of Phases and Mechanical Strength of Two-Phase Steels Using Barkhausen Noise Measurements: Application to Commercial Dual-Phase Steel, *Metallurgical and Materials Transactions A*, 39(6) (2008) 1308-1318.

[125] C.H. Gür, M. Ozer, M. Erdogan, Investigation of the Variations in Microstructure and Mechanical Properties of Dual-Matrix Ductile Iron by Magnetic Barkhausen Noise Analysis, *Research in Nondestructive Evaluation*, 19(1) (2008) 44-60.

[126] R. Rautioaho, P. Karjalainen, M. Moilanen, Stress response of Barkhausen noise and coercive force in 9Ni steel, *Journal of Magnetism and Magnetic Materials*, 68 (1987) 321-327.

[127] S. Tiitto, On the influence of microstructure on magnetization transitions in steel, Acta Polytechnica Scandinavica. *Applied Physics Series*, No. 119, 1977.

[128] G.E. Totten (Ed.), Steel Heat Treatment: Metallurgy and Technologies. Deklor, New York, 1997.

[129] SFS-EN ISO 2639. Steels. Determination and verification of the depth of carburized and hardened cases. 2002.

[130] SFS-EN 10328. Iron and steel. Determination of the conventional depth of hardening after surface heating. 2005.

[131] P. Bucan, Repeatable, Reproducible Preparation and Hardness Depth Measurement of Surface Hardened Steels, Industrial Heating Magazine, Internet: http://www.vacaero.com/News-Info-From-Industrial-Heating-Magazine/News-Info-From-Industrial-Heating-Magazine/Repeatable-Reproducible-Preparation-and-Hardness-Depth-Measurement-of-Surface-Hardened-Steels.html (14.8.2011)

[132] G. Bach, K. Goebbels, W.A. Theiner, Characterizatio of Hardening Depth by Barkhausen Noise Measurements, *Materials Evaluation*, 46 (1988) 1576-1580.

[133] M. Dubois, M. Fiset, Evaluation of case depth on steels by Barkhausen noise measurements, *Materials Science and Technology*, 11(3) (1995) 264-267.

[134] S. Vaidyanathan, V. Moorthy, T. Jayakumar, B. Raj, Evaluation of induction hardened case depth through microstructural characterization using magnetic Barkhausen emission technique, *Materials Science and Technology*, 16 (2000) 202-208.

[135] V. Moorthy, B.A. Shaw, Magnetic Barkhausen Emission Measurements for Evaluation of Depth of Grinding Damage. Proceedings of the 7th International Conference on Barkhausen Noise and Micromagnetic Testing. 15-16 July, 2009, Aachen, Germany.

[136] V. Moorthy, B.A. Shaw, P. Mountford, P. Hopkins, Magnetic Barkhausen emission technique for evaluation of residual stress alteration by grinding in case-carburised En36 steel, *Acta Materialia*, 53 (2005) 4997-5006.

[137] O. Stupakov, O. Perevertov, I. Tomas, B. Skrbek, Evaluation of surface decarburization depth by magnetic Barkhausen noise technique. *Journal of Magnetism and Magnetic Materials*, 323(12) (2011) 1692-1697.

[138] C.-G. Stefanita, From Bulk to Nano, The Many Sides of Magnetism, Springer Series in Materials Science, 2008.

[139] J.E. Wyatt, J.T. Berry, A new technique for the determination of superficial residual stresses with machining and other manufacturing processes, *Journal of Materials Processing Technology*, 171 (2006) 132-140.

[140] ISO14104:1995 Gears- Surface temper etch inspection after grinding, 1995.

[141] P. Prevey. X-ray Diffraction Residual Stress Techniques, Metals Handbook: Ninth Edition, Vol. 10, ed. K. Mills, Metals Park, OH: American Society for Metals, 1986, pp. 380-392.

[142] K. Dünck-Kerst, Using the Barkhausen Noise for Process Optimisation and Process Control – An Example for the Production of Gears, Proceedings of the 7th International Conference on Barkhausen Noise and Micromagnetic Testing, 15-16 July 2009, Aachen, Germany.

[143] H. Gupta, M. Zhang, A.P. Parakka, Barkhausen effect in ground steels. *Acta Materialia*, 45(5) (1997) 1917-1921.

[144] H.K. Tönshoff, B. Karpuschewski, C. Regent, Process Monitoring in Grinding Using Micromagnetic Techniques, *The International Journal of Advanced Manufacturing Technology*, 15 (1999) 694-698.

[145] B.-R. Höhn, P. Oster, T. Tobie, S. Scgwienbacher, P. Koller, Indicating Grinding Burn on Gears- Comparison and Evaluation of Different Testing Methods, Proceedings of the 7th International Conference on Barkhausen Noise and Micromagnetic Testing, 15-16 July 2009, Aachen, Germany.

[146] A.P. Parakka, J. Batey, D.C. Jiles, M. Zang, H. Gupta, Effect of surface mechanical changes on magnetic Barkhausen emissions, IEEE Transactions on Magnetics, 33(5) (1997) 4026-4028.

[147] A.P. Parakka, D.C. Jiles, H. Gupta, S. Jalics, Effects of surface condition on Barkhausen emissions from steel, *Journal of Applied Physics*, 79(8) (1996) 6045-6046.

[148] M. Vashista, S. Paul, Prediction of Residual Stress Using Micro-Magnetic Properties in High Speed Grinding, Proceedings of the 8th International Conference on Barkhausen Noise and Micromagnetic Testing, 11-12 February 2010, Kalpakkam, India.

[149] M. Vashista, S. Kumar, A. Ghosh, S. Paul, Surface Integrity in Grinding Medium Carbon Steel with Miniature Electroplated Monolayer cBN Wheel, *Journal of Materials Engineering and Performance*, 19(9) (2010) 1248-1255.

[150] H.D. Allison, R.W. Hendricks, Correlation of Barkhausen Noise Signal and X-ray Residual Stress Determination in Grinding-Burned 52100 Steel, in: Ericsson, T.; Odén, M., and Andersson, A., eds. Fifth International Conference on Residual Stresses; 1997 Jun 16-1997 Jun 18; Linköping, Sweden. Linköping, Sweden: Linkopings Universitet; (1998), pp. 640-645.

[151] G. Donzella, L. Solazzi, Use of Barkhausen Noise for Crack Closure Measurements, Proceedings of the 5th International Conference on Barkhausen Noise and Micromagnetic Testing, 2-3 June 2005, Petten, The Netherlands.

[152] H.N. Singh, K.C. Sahoo, Crack Growth Characterization Using Barkhausen Noise Measurement, Proceedings of the 5th International Conference on Barkhausen Noise and Micromagnetic Testing, 2-3 June 2005, Petten, The Netherlands.

[153] J. Blachnio, The Effect of a Dislocation Microstructure of the Martensite Steel on the Barkhausen Noise Level, Proceedings of the 5th International Conference on Barkhausen Noise and Micromagnetic Testing, 2-3 June 2005, Petten, The Netherlands.

[154] F.A. Franco, L.R. Padovese, NDT flaw mapping of steel surfaces by continuous magnetic Barkhausen noise: Volumetric flaw detection case, *NDT&E International*, 42 (2009) 721-728.

[155] A. Sorsa, K. Leiviskä, Feature Selection From Barkhausen Noise Data Using Genetic Algorithms with Cross-Validation, Adaptive and Natural Computing Algorithms, *Lecture Notes in Computer Science*, 5495 (2009), 213-222.

[156] A. Sorsa, K. Leiviskä, Comparison of feature selection methods applied to Barkhausen noise data set, 18th IFAC World Congress, August 28-September 2, 2011, Milano, Italy.

[157] http://www.maurer-ir-de (12.6.2012).

[158] http://flir.custhelp.com/app/answers/detail/a_id/221/~/accuracy-specification-of-flir-cameras (12.6.2012).

[159] B.D. Cullity, Elements of X-ray Diffraction, Second edition, Addison-Wesley Publishing Company Inc, 1978.

[160] J.S. Blakemore, Solid State Physics, Second edition, Cambridge University Press, 1985.

[161] SFS-EN 15305, Non-destructive Testing- Test Method for Residual Stress analysis by X -ray Diffraction. Suomen Standardoimisliitto SFS, 2008.

[162] M.E. Fitzpatrick, A.T. Fry, P. Holdway, L. Kandil, J. Shackleton, L. Suominen, Measurement Good Practice Guide No. 52, Determination of Residual Stresses by X-ray Diffraction- Issue 2, Crown, 2005.

[163] P. Prevey. Current applications of X-ray diffraction residual stress measurement, Developments in Materials Characterization Technologies, eds. G.F. Van der Voort and J.J. Friel, Materials Park, OH: American Society of Metals, 1996, pp. 103-110.

[164] V. Hauk, Structural and Residual Stress Analysis by Nondestructive Methods, Elsevier, 1997.

[165] K. Hoffmann, An Introduction to Measurements using Strain Gages, Hottinger Baldwin Messtechnik GmbH, Darmstadt, 1989.

[166] D.C. Jiles, The Effect of Stress on Magnetic Barkhausen Activity in Ferromagnetic Steels. *IEEE Transactions on Magnetics*, 25(5) (1989) 3455-3457.

[167] D.C. Jiles, D.L. Atherton, Theory of ferromagnetic hysteresis. *Journal of Magnetism and Magnetic Materials*, 61(1986) 48-60.

[168] J.T. Wilson, G.Y. Tian, V. Moorthy, B.A. Shaw, Magneto-Acoustic Emission and Magnetic Barkhausen Emission for Case Depth Measurement in En36 Gear Steel. *IEEE Transactions on Magnetics*, 45(1) (2009) 177-183.

[169] M. Blaow, J.T. Evans, B.A. Shaw, Effect of hardness and composition gradients on Barkhausen emission in case hardened steel, *Journal of Magnetism and Magnetic Materials*, 306 (2006) 153-159.

[170] T. Saarinen, unpublished PhD thesis, 2012.

[171] S. Santa-aho, A. Sorsa, M. Vippola, J. Latokartano, M. Lindgren, T. Lepistö, Laser produced grinding burns for Barkhausen noise measurement result validation, Abstracts of Papers, The seventh International Conference on Condition Monitoring and Machinery Failure Prevention Techniques, 22-24 June 2010, Ettington Chase, Stratford-upon-Avon, England.

[172] K. Davut, S. Bayramoglu, G. Gürer, C.H. Gür, Non-Destructive Characterisation of Spheroidised Aisi 1060 Steel by Magnetic Barkhausen Noise Measurements, Proceedings of the 6th International Conference on Barkhausen Noise and Micromagnetic Testing, 9-10 July 2007, Valenciennes, France.

APPENDIX: ORIGINAL PUBLICATIONS

Publication I

Suvi Santa-aho, Minnamari Vippola, Aki Sorsa, Kauko Leiviskä, Mari Lindgren and Toivo Lepistö

Utilization of Barkhausen noise magnetizing sweeps for case-depth detection from hardened steel

NDT&E International 52 (2012) 95-102.

Publication II

Suvi Santa-aho, Minnamari Vippola, Aki Sorsa, Jyrki Latokartano, Mari Lindgren, Kauko Leiviskä and Toivo Lepistö

Development of Barkhausen noise calibration blocks for reliable grinding burn detection

Journal of Materials Processing Technology 212(2) (2012) 408-416.

Publication III

Suvi Santa-aho, Minnamari Vippola, Aki Sorsa, Mari Lindgren, Jyrki Latokartano, Kauko Leiviskä and Toivo Lepistö

Optimized laser processing of calibration blocks for reliable Barkhausen noise based grinding burn detection method

Journal of Materials Processing Technology 212(11) (2012) 2282-2293.

Publication IV

Aki Sorsa, Kauko Leiviskä, Suvi Santa-aho, Minnamari Vippola, Toivo Lepistö

A study on laser-processed grinding burn simulation and analysis based on Barkhausen noise measurement

Insight 52(6) (2010) 293-297.

Publication V

Suvi Santa-aho, Minnamari Vippola, Toivo Lepistö and Mari Lindgren

Characterisation of case-hardened gear steel by multiparameter Barkhausen noise measurements

Insight 51(4) (2009) 212-216.

Publication VI

Suvi Santa-aho, Minnamari Vippola, Tuomo Saarinen, Matti Isakov, Aki Sorsa, Mari Lindgren, Kauko Leiviskä and Toivo Lepistö

Barkhausen noise characterisation during elastic bending and tensile-compression loading of case-hardened and tempered samples

Journal of Materials Science 47 (2012) 6420-6428.

Tampereen teknillinen yliopisto
PL 527
33101 Tampere

Tampere University of Technology
P.O.B. 527
FI-33101 Tampere, Finland

ISBN 978-952-15-2926-9
ISSN 1459-2045